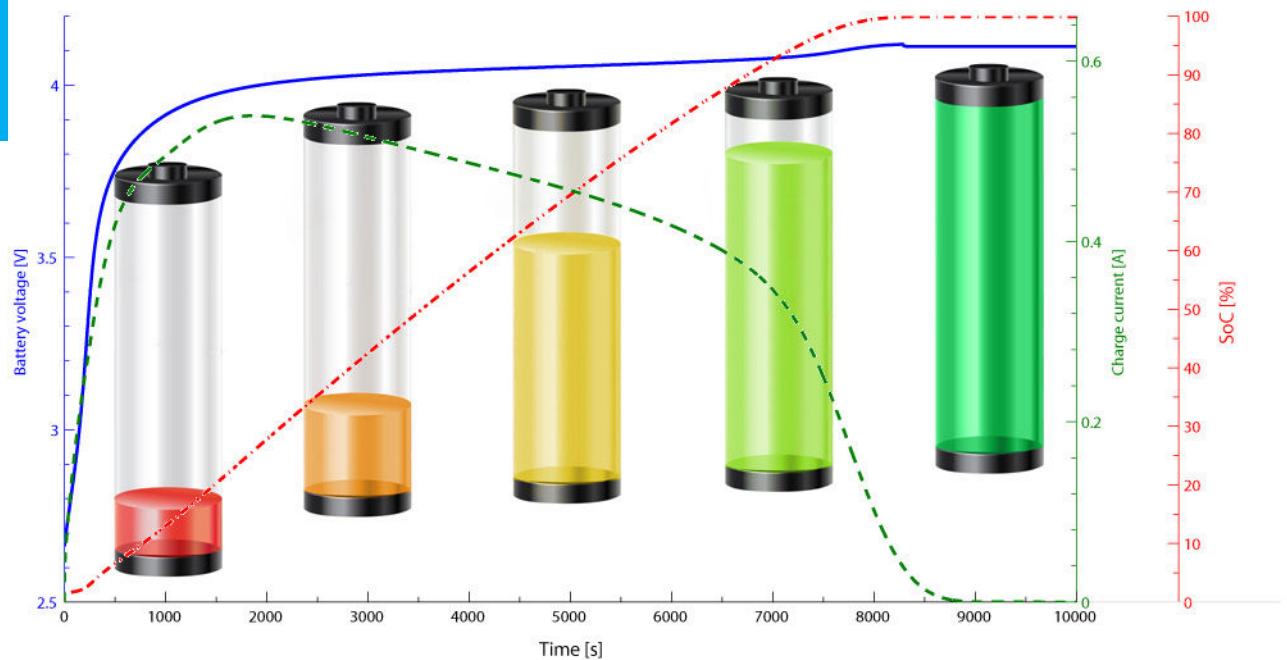


Li-Ion Charger for Implantable Devices

Selection of optimal charge algorithm and implementation

R.C. van Dongen

Master of Science Thesis



Li-Ion Charger for Implantable Devices

Selection of optimal charge algorithm and implementation

by

R.C. van Dongen

MASTER OF SCIENCE THESIS

For the degree of Master of Science in BioMedical Engineering,
Biomedical Instrumentation at Delft University of Technology

Supervisors:

Dr.ir. Wouter A. Serdijn
Senad Hiseni MSc

Thesis committee

Dr.ir. Wouter A. Serdijn
Dr. E.M. Kelder
Dr.ir. H. Polinder
M.N. van Dongen MSc

December 7, 2012

Faculty of Electrical Engineering, Mathematics and Computer Science
Delft University of Technology

LI-ION CHARGER FOR IMPLANTABLE DEVICES
Copyright © 2012 R.C. van Dongen
Biomedical Electronics Group, Electronics Research Laboratory
Faculty of Electrical Engineering, Mathematics and Computer Science
Delft University of Technology
All rights reserved.



Abstract

Deep Brain Stimulation (DBS) is a method for treating diseases like Parkinson's Disease (PD) and various other movement disorders. An Implantable Pulse Generator (IPG) is placed in the chest and wires are run through the neck to provide electrical pulses to a certain target in the brain via an electrode. Results with this treatment are good but today's stimulators are bulky and last only three to five years. Furthermore the electrode and pulse generator are often placed in two different surgeries.

The device should be miniaturized so that it can be placed in the skull while inserting the electrode. This reduces the number of placement surgeries and eliminates lead failures. The size of the device is dominated by the battery volume, however no compromises on battery life can be made since battery replacement requires, again, surgery. Switching to a rechargeable Lithium-Ion battery that can be recharged through the skin is a way to reduce battery size without compromising the lifetime of the device.

Lithium-Ion batteries are, however, delicate devices and should be charged and discharged with care. The classic method to ensuring safe charging of these types of batteries is the Constant Current Constant Voltage (CCCV) method. Here a fixed current is pushed into the battery until the battery reaches its maximum voltage. After this the voltage is kept constant and the current slowly decreases to a small fraction of the initial current.

Although this method ensures safe and complete charging of Lithium Ion (Li-Ion) batteries it also has some downsides. The abrupt switch from constant current to a constant voltage might introduce stability issues. Furthermore, characteristics of a battery vary depending on their state of charge and this is not taken into account by this algorithm.

In this research a possible new algorithm that smoothly regulates charge current is investigated. It turns out that this algorithm is slightly less efficient and slower than the classical CCCV method. The best method to charge the battery of an implantable device is via the CCCV method.

An implementation of this method is proposed where both Constant Current (CC) and Constant Voltage (CV) phases are controlled by the same control loop and the transition between the two phases is a smooth hyperbolic tangent function. An inductively powered system was

designed that reaches an average efficiency, in circuit simulation, of 87.36% from antenna output to battery. For this implementation, the rectifier is the only part in series with the inductive link and the battery. The efficiency is therefore mostly limited by the diodes used for the AC to DC rectifier.

An prototype of the designed system was built and the correct operation of the system was verified by wirelessly charging a 160mAh Li-Ion battery. The results of the performed measurements showed that the inductive link had a poor power transfer efficiency. Mismatch between the resonance capacitor value and coil inductances caused the resonance frequency to deviate from the desired value. The efficiency of the charger was, as expected, mostly determined by losses in the rectifier.

Further research should be done in optimization of the inductive link to provide good efficiency even when the device is poorly aligned with the charger. Furthermore the parameters of the system should be tuned to a medical grade battery and the possibility of combining the power transfer with data communication can be investigated.

Table of Contents

Abstract	i
Preface	xiii
Acknowledgments	xv
Dedication	xvii
1 Introduction	1
2 Batteries, types and terminology	7
2-1 Introduction	7
2-2 Terminology	7
2-2-1 Ampere Hour (Ah)	7
2-2-2 C rate	8
2-2-3 State of Charge (SoC)	8
2-2-4 State of Health (SoH)	9
2-2-5 Depth of Discharge (DoD)	9
2-2-6 Cycle life	9
2-2-7 Shelf life	9
2-2-8 Over- and under-potential	10
2-3 Primary cells	10
2-4 Secondary cells	11
2-5 Modeling of batteries	12
2-6 Aging of batteries	14
2-6-1 Operating voltage	15
2-6-2 Operating temperature	16
2-6-3 Charge and discharge rates	16
2-6-4 Depth of Discharge (DoD)	17
2-7 Conclusion	18

3	Using batteries, Charging and Discharging	19
3-1	Introduction	19
3-2	Battery use profile	19
3-2-1	Discharge scenario	19
3-2-2	Charge scenario	21
3-3	Charge algorithms	23
3-3-1	Constant Current Constant Voltage (CCCV) charging	23
3-3-2	Multi-stage Constant Current (CC) charging	25
3-3-3	Build-in Resistance Compensated (BRC) charging	25
3-3-4	Pulse topping charging	26
3-3-5	Float charging	27
3-3-6	Ion relaxation charging	28
3-3-7	Ion relaxation charging with negative pulse	29
3-3-8	Boostcharging	29
3-4	Conclusion	31
4	Selection of charge algorithm	33
4-1	Introduction	33
4-2	Proposed new algorithm, Smooth Charging	34
4-3	Simulation setup	34
4-3-1	CCCV simulation	35
4-3-2	Smooth charging simulation	36
4-4	Simulation results	37
4-4-1	Charging time	37
4-4-2	Power consumption and over-potential	40
4-4-3	Expected implementation complexity and cost	42
4-5	Conclusion	44
5	System overview of charger	45
5-1	Introduction	45
5-2	Inductive link	46
5-3	Switched mode current regulation	49
5-4	Control	50
5-4-1	Hyperbolic tangent function	50
5-4-2	End of charge voltage reference	50
5-5	Simulation result	51
5-5-1	Charge curve	52
5-5-2	Power consumption	53
5-5-3	System efficiency	53
5-6	Conclusion	54

6	Hardware implementation	57
6-1	Introduction	57
6-2	Inductive link	58
6-2-1	Primary side	59
6-2-2	Secondary side	59
6-3	Current regulation switch	60
6-4	Rectifier topology	60
6-4-1	Diode rectifier	60
6-4-2	MOS rectifier	61
6-4-3	MOS diode hybrid rectifier	62
6-5	Control loop	62
6-5-1	Bipolar Junction Transistor (BJT)	63
6-5-2	MOS transistor	64
6-6	Voltage sensing	66
6-7	Current sensing	66
6-8	Pulse-width Modulation (PWM) generator	67
6-9	Simulation results	67
6-9-1	Charge curve	67
6-9-2	System efficiency	68
6-10	Conclusion	72
7	Practical tests setup using discrete components	75
7-1	Introduction	75
7-2	The prototype	76
7-2-1	Inductive link	76
7-2-2	Control PCB	78
7-2-3	Test battery	81
7-3	Measurement setup	82
7-3-1	CCCV charge	83
7-3-2	CC discharge	83
7-3-3	Hyperbolic tangent charge	83
7-3-4	System efficiency measurements	84
7-4	CCCV charge and CC discharge results	84
7-4-1	Charge and discharge time	84
7-4-2	Battery charge efficiency	85
7-5	Hyperbolic tangent charge and CC discharge results	86
7-5-1	Charge and discharge time	86
7-5-2	Battery charge efficiency	87
7-6	Overall system efficiency	88
7-6-1	Link efficiency	88
7-6-2	Charger efficiency	89
7-7	Conclusion	91

8 Conclusion and Recommendations	93
8-1 Conclusion	93
8-2 Project goals and contributions	96
8-3 Recommendations	97
8-3-1 Additional features	97
8-3-2 Characteristics of the battery	98
8-3-3 Inductive link improvements	98
8-3-4 Charger improvements	99
A Frequently used primary cells	101
A-1 Lithium-Manganese Dioxide (Li-MnO ₂)	101
A-2 Lithium-Iodine (Li-I ₂)	102
A-3 Comparison	103
B Frequently used secondary cells	105
B-1 Lithium cobalt oxide (Li-CoO ₂)	105
B-2 Comparison	106
Bibliography	107
Glossary	113
List of Acronyms	113
List of Symbols	113
Index	115

List of Figures

1-1	Slice of the brain with basal ganglia.	2
1-2	IPG and connecting leads in a patient.	3
1-3	Picture of an IPG cut open.	4
2-1	Typical discharge curve used for SoC calculation.	8
2-2	Cycle life of EaglePicher Lithium-Ion family.	10
2-3	Transport of lithium ions in a rechargeable battery.	12
2-4	Equivalent circuit of a lithium battery.	13
2-5	U-shaped impedance curve of Li-ion cell.	14
2-6	Equivalent circuit of a lithium battery with non-linear resistor.	14
2-7	Left, battery stored at 100% SoC. Right, battery stored at 50% SoC.	15
2-8	High Energy cells designed for satellites.	17
3-1	Example of an stimulation pattern.	20
3-2	Hand held charge scenario.	21
3-3	Pillow based charge scenario.	23
3-4	Simulation of Constant Current Constant Voltage Charging of a lithium battery.	24
3-5	Five Constant Current steps Charging of a lithium battery.	25
3-6	Build in Resistance Compensated Charging of a lithium battery.	26
3-7	Topping of a battery with current pulses.	27
3-8	Pulse pattern of a microbattery charged with incrementing pulses.	28
3-9	Pulse pattern of a microbattery charged with negative pulses.	29
3-10	Simulation of the boost charge algorithm.	30
3-11	Overview of discussed charge algorithms.	32
4-1	Charging of Li-ion cell according to the smooth charging algorithm.	35

4-2	Simplified schematic of Simulink model of the CCCV charge algorithm.	36
4-3	Simplified schematic of Simulink model of the smooth charge algorithm.	36
4-4	Results of Simulink simulation of the CCCV charge algorithm.	37
4-5	Results of Simulink simulation of the smooth charge algorithm.	38
4-6	Current profiles of the CCCV and Smooth charge algorithms.	39
4-7	Current profiles of the CCCV and Smooth charge algorithms verses the State of Charge.	40
4-8	a. Overpotential over charge cycle. b. Energy lost due to overpotential.	42
5-1	Schematic system overview of proposed charger.	46
5-2	Schematic system overview of existing implementation.	46
5-3	Transformer model and equivalent circuit of inductive link.	47
5-4	Hyperbolic tangent function for charge current control.	51
5-5	Charge curve of proposed charge system simulated in Matlab/Simulink.	52
5-6	Decrease in power delivered by the source once link is short-circuited.	53
5-7	Power consumption of proposed charge system over a full charge cycle simulated in Matlab/Simulink.	55
5-8	Link efficiency and charger efficiency of proposed charge system over a full charge cycle simulated in Matlab/Simulink.	56
6-1	Full bridge rectifier composed of Schottky diodes.	61
6-2	Full bridge rectifier composed of MOS transistors.	61
6-3	Full bridge rectifier composed of MOS transistors and diodes.	62
6-4	Temperature dependency of the hyperbolic tangent function.	64
6-5	Charge curve of proposed charge system simulated in Cadence Virtuoso Analog Design Environment.	68
6-6	Power consumption of proposed charge system over a full charge cycle simulated in Cadence Virtuoso Analog Design Environment.	69
6-7	Link efficiency and charger efficiency of proposed charge system over a full charge cycle simulated in Cadence Virtuoso Analog Design Environment.	70
6-8	Current through one of the rectifier diodes.	72
6-9	Current flow through substrate of rectifier diodes and switches.	73
7-1	Primary coil mounted on a acrylate support structure	76
7-2	Secondary coil mounted on a acrylate support structure	77
7-3	Primary and secondary coil mounted on a acrylate support structure, which form the inductive link	78
7-4	Printed Circuit Board of prototype.	79
7-5	Measurement result of the hyperbolic tangent control loop	80
7-6	Lithium Ion battery under test	82
7-7	Source unit and measurement equipment used for testing the prototype	85
7-8	Charge profile of the test battery when charging according to the CCCV method.	86

7-9	Discharge profile of the test battery when discharging with a constant current after CCCV charge.	87
7-10	Charge profile of the test battery when charging with the prototype PCB.	88
7-11	Discharge profile of the test battery when discharging with a constant current after charging with the prototype PCB.	89
7-12	Measurement of link voltage and current.	91

List of Tables

4-1	Comparison of charge time in seconds of CCCV and smooth charging algorithm .	39
4-2	Parameters of battery overpotential model for different temperatures	41
6-1	Component values for calculation of the link operating frequency.	58
7-1	Component values of the inductive link.	78
A-1	Data of primary lithium cells	103
B-1	Data of secondary lithium cobalt oxide cell	106

Preface

Since its development in the 1960's and FDA approval in 2002 [1] DBS has been used for treatment of Parkinson's disease. Also various other movement disorders like essential tremor and even psychiatric disorders, such as Tourette's syndrome and obsessive compulsive disorder, can be treated using DBS [2]. Until now the focus has been on the elderly population but also children as young as eight years might benefit from DBS [3].

Although the patients benefit a lot from DBS therapy, the current systems are far from perfect. The systems are too bulky to fit in the skull. Therefore they need to be implanted in the chest and connected with a long extension wire. Often the stimulation electrode and pulse generator are placed in two different surgeries. Besides these problems the current battery lifetime is only about three to five years [1] resulting in frequent battery-replacement surgeries each with risk of complications and infections.

The Biomedical Electronics group of the TU Delft has done quite some research in reducing the power consumption of neurostimulators and increasing the flexibility and effectiveness of the systems. The power needed to stimulate tissue however, still remains high making the device power-hungry. This led to the idea that making the stimulator rechargeable could help in reducing the size and at the same time prolonging the lifetime.

Today rechargeable stimulators already exist and they indeed surpass the five year lifetime of the non-rechargeable systems. For example the Eon, an IPG that is produced by Advanced Neuromodulation Systems Inc, can operate for at least seven years at high stimulation settings [4]. Due to these promising results and ongoing improvements in the field of batteries this looked like an interesting field to focus our attention on. After getting more acquainted with the rechargeable IPG it turned out that we could improve the charge algorithm and circuitry. In this thesis this best available algorithm will be selected and a circuit implementation will be presented.

Acknowledgments

I would like to thank my supervisor, Dr.ir. Wouter A. Serdijn, for his assistance during the forming of the project, design and writing of this thesis. My daily supervisor, Senad Hiseni MSc, I would like to thank for his help in getting me acquainted with the Cadence simulation environment as well as the regular use of his coffee card.

All the other Ph.D. students, M.Sc. students and employees of the Biomedical Electronics Group I would like to thank for the general support in the form of lunches, coffee breaks and various other social gatherings. Tim Velzeboer I would like to thank for sacrificing his own cell-phone to provide me with a lithium battery that could be used for building a test-setup of the designed circuit.

Special thanks goes out to the student society ETV for providing an relaxing environment to over think the challenges that came up during this project. The opportunity to organize and participate in the Sunrise Study Tour is an good example of such an challenging activity. Frequent meetings and an four week during trip halfway the project proved to be both relaxing and motivating.

Delft, University of Technology
December 7, 2012

R.C. van Dongen

“Man is only man at the surface. Remove the skin, dissect, and immediately you come to machinery. ”

— *Paul Valery*

Chapter 1

Introduction

Parkinson's Disease (PD) is the second most common neurodegenerative disorder. It is affecting about 1% of all people over the age of 50 [5] and 3% of people over the age of 65 [6] which comes down to more than one million patients in the US alone [7]. In the Netherlands, 29490 patients consulted an neurologist in the year 2007/2008 and were diagnosed with parkinsonism [8].

The disease is named after James Parkinson who lived from 1755 to 1824 and is considered to be the father of the disease. His essay *An Essay on the Shaking Palsy*, that he published in 1817, started the lively discussion and numerous publications on PD. The essay was based on six patients of which three were only seen from a distance or casually met on the street.

Despite this small number of patients Parkinson managed to give an accurate description of symptoms and already realized that it was a disease of long duration and significant disabilities. Although he made a clear and accurate description of the PD tremor (and its difference from other tremors) he also described a case of the disease that manifested without this characteristic tremor [7].

The cause of symptoms like resting tremor, rigidity, postural instability and a narrow based and shuffling gait lies deeply hidden in the brain. Degeneration of the substantia nigra, an subpart of the basal ganglia of the Central Nervous System (CNS), results in a shortage of the neurotransmitter Dopamine. In Figure 1-1 the location of the basal ganglia with the substantia nigra is indicated in a slice of the brain.

Due to the lack of Dopamine, the basal ganglia motor loop, a feedback loop that is responsible for initiating movement, can no longer function properly. The traditional treatment for PD is therefore based on complementing the lacking Dopamine with L-3,4-dihydroxyphenylalanine better known as Levodopa, or L-dopa for short. This substance allows the remaining braincells in the substantia nigra to produce more Dopamine and restore the normal concentration of the neurotransmitter.

60 years after the discovery of L-dopa it was finally approved by the United States Food and Drug Administration for use in PD in 1970 [5, 9]. Even today L-dopa still forms the

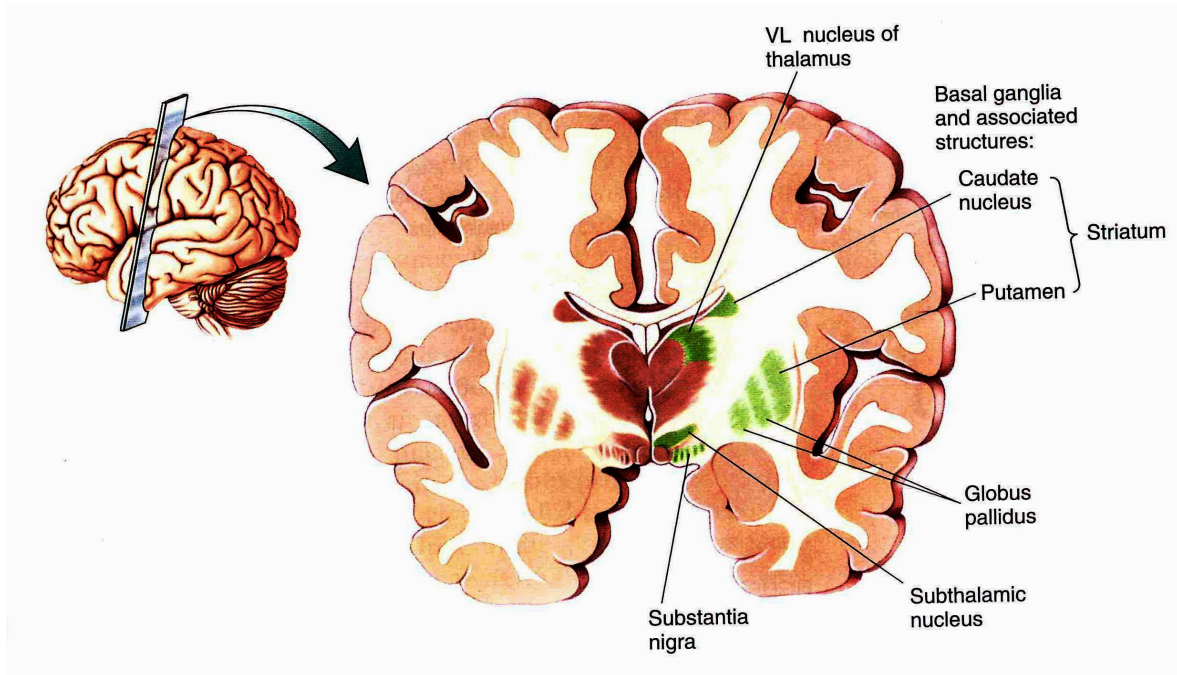


Figure 1-1: Slice of the brain with basal ganglia. Picture courtesy of M.F. Bear [5]

cornerstone for treatment of PD but there are some drawbacks. Patients treated with L-dopa for a long term suffer from what is referred to as the “long-term Levodopa syndrome”.

After a decade of medication nearly 90% suffers from motor fluctuations and neuropsychiatric disturbances are frequent. Patients have long “off-periods” were the symptoms are severe and shorter and shorter “on-periods” were the medication is effective. This decreasing effectiveness of the treatment might be because of the progress of PD but also because L-dopa is potentially toxic to the remaining braincells [9].

If medication fails to relief the symptoms of PD, surgery may be considered. By lesioning certain hyperactive targets in the brain, the balance in the motor loop can be restored, even with an reduced level of dopamine. Results of these types of surgery are fairly good and in general patients score 50% better in the Unified Parkinson’s Disease Rating Scale (UPDRS) test, for 2 years after surgery [10].

Complications are rare but surgeons need to be absolutely confident about the location and size of the lesion they are introducing in the brain. Today, most medical centers use micro-electrode recordings or electrical trial stimulations to verify the target and test the possible effect of the surgery. One can imagine that continued electrical stimulation can have comparable effects as lesion surgery and indeed this is the case.

In the 1980s, during thalamic lesioning surgery, it was observed that low frequency stimulation increased tremor while stimulation above 100Hz decreased it. Today continued stimulation with 135 to 185Hz pulses of 60 to 120 μ s long and an amplitude of 1V to 3V is typically used as a treatment [9]. This type of treatment is referred to as Deep Brain Stimulation (DBS) and has largely replaced other surgical procedures.

DBS is done by implanting an Implantable Pulse Generator (IPG) in the chest near the

collarbone. Small leads that run through the neck then connect the IPG to an electrode that is inserted in the target. For some severe cases, stimulation at multiple locations is required. As shown in Figure 1-2, two stimulators each with their own lead and electrode, can be placed to achieve bilateral stimulation.

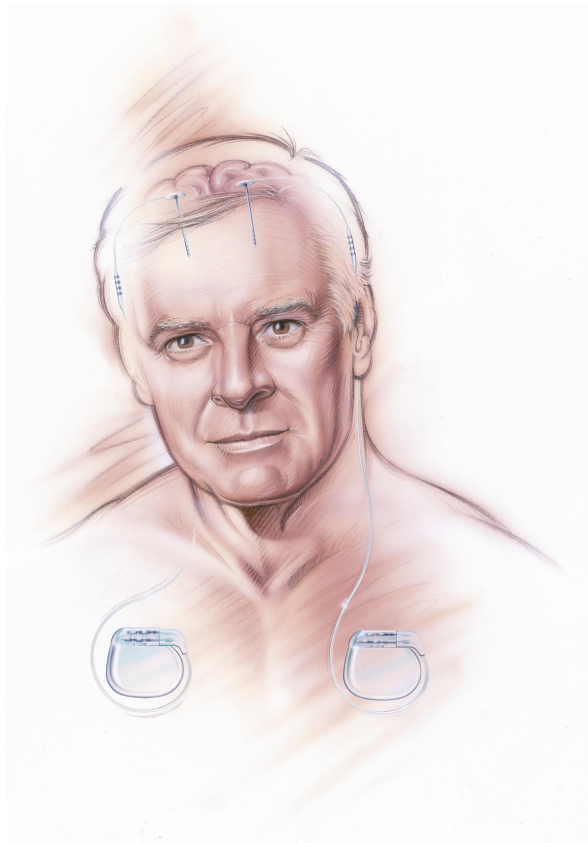


Figure 1-2: IPG and connecting leads in a patient. Picture courtesy of Medtronic, Inc.

Although DBS is an effective treatment for PD and various other movement disorders it is still far from perfect. Current devices need battery replacement within three to five years [1] depending on the stimulation settings. Since surgery is needed for battery replacement, each replacement comes with new risks of infections and complications. There is even a severe case where the DBS therapy was finally changed to a permanent lesion because there were four battery replacements needed in five years [9].

Another fragile part of the system is the extension wire that connects the IPG to the electrode. Especially during rough neck movements the lead can fracture or connections can be broken. In this case a surgery is needed to replace the wire. Even in first installation of the system the extension wire and IPG are often placed in a second operation to give the patient some time to recover from the electrode placement. Of course this operation comes with new risks of infections and complications.

To reduce the number of failures (due to wire breakage) and the number of surgeries, as well as ecstastic, there is a wish for size reduction. If miniaturization can be achieved, the electrode and IPG might both be placed inside the skull during the same surgery. Neurosurgeon D. De

Ridder states that, in order to be able to place the stimulator inside the skull, the size need to be reduced to about two stacked €2 coins (2.2cm^3).

An existing stimulator fabricated by Medtronic is over 17 times the desired size with an volume of 39cm^3 [11]. As depicted in Figure 1-3, the battery consumes most of the available space inside existing IPGs. Usually a non-rechargeable lithium battery that powers the device for years is used. Since patients as young as eight years can get a stimulator implanted [3], we can make no compromise on the battery lifetime. Still, miniaturization can be achieved by replacing the non-rechargeable battery with a smaller size battery that can be recharged transcutaneously.



Figure 1-3: Picture of an IPG cut open. The battery consumes roughly half the total volume

Already rechargeable stimulators with a smaller size and long lifetime are available. A good example is Medtronic's Aactiva RC with an expected lifetime of nine years and an volume of 22cm^3 [12]. Although this is an improvement over the non-rechargeable stimulator, some patients experience problems while coupling the charger to the device. Even a special vest to hold the charger in place is not always effective so that patients have to lie down and align the recharging device by hand in order to maintain good contact [13].

In this project the design of the charger system is reconsidered in order to improve patient comfort and prolonging battery life. A new charge system is designed with the following aspects in mind:

- The design needs to ensure *long battery life* and charge the battery safely. There should be no risk of damaging the device due to, for example, overcharging of the battery.

Furthermore the number of possible battery cycles should be maximized in order to extend the lifetime of the device.

- The design needs to be highly *energy efficient* so that most of the available energy is stored in the battery. Even when the coupling of the device with the charger is weak, it should be possible to charge the battery. especially when the available energy is limited it is crucial not to waste it in the charge circuit but instead store it in the battery.
- The design needs to have a *small size* so that it can be implanted in the skull of the patient. Although the device size is dominated by the volume of the battery it is important to keep other electronics as small as possible in order to achieve the goal of 2.2cm^3 of total volume. Ideally the design is integrated on a chip together with other electronics so that the total system composes of only a single chip and a battery.

In order to be able to design a battery charger, a literature study to the basic behavior of batteries was performed. In the next chapter of this thesis, the terminology used in battery technology is explained together with the basic behavior of a lithium ion cell. The third chapter focuses on different charging algorithms that are available for charging lithium batteries and specifies the scenario in which the device is going to be used.

Selection of the best suited algorithm for our application was done on the basis of a simulation run in Matlab/Simulink. In Chapter 4 an potentially new algorithm is introduced and compared with existing algorithms. The algorithm that is best suitable for our application is selected by comparing the charging time, power consumption and expected implementation costs.

An implementation of the best suited algorithm was designed and put to the test. The designed system is introduced in Chapter 5 where it is compared to an existing system and compared on the basis of Matlab/Simulink simulations. An implementation of the design in an Integrated Circuit (IC) technology is introduced in the sixth chapter and results of circuit simulations run in a Cadence Virtuoso Analog Design Environment are discussed.

In the seventh and final chapter an prototype of the design that was built, using discrete and off the shelf components, is described. Measurements were performed on this prototype and the results are compared with the results from the simulations from the previous chapters. Finally, the report is wrapped up with conclusions as well as recommendations for further research.

Batteries, types and terminology

2-1 Introduction

Before we can start the design of a charger circuit we first need to review our knowledge of batteries in general. This first chapter will give a general overview of batteries. Non-rechargeable cells, also called primary cells, are reviewed since the current Implantable Pulse Generator (IPG) is often equipped with a non-rechargeable battery. So called secondary or rechargeable cells are discussed to know what properties of these cells are important during charging and discharging. First, however, some terminology that is used throughout this thesis is explained.

2-2 Terminology

In the field of batteries and chargers quite some terminology is used that can result in some confusion. This section clarifies this confusion by explaining each term in a short section. The terms are used throughout this thesis. However, readers do not need to return to this section for each term or acronym. In the glossary there is a alphabetically ordered list of acronyms that is usually enough explanation to understand the term.

2-2-1 Ampere Hour (Ah)

The capacity of a battery is denoted in Ah. A battery that is said to have a capacity of one Ah can sustain a current of one ampere for a duration of one hour. This battery will thus be drained in half an hour if the current is increased to two ampere and, similar, will last for two hours at a current of 0.5A

2-2-2 C rate

The C rate is a way of scaling charge and discharge currents to the capacity of the battery. One C is one times the nominal capacity of the battery. Charging a one Ah battery at one C means that the charging current is 1A. Charging now takes exactly one hour if we neglect the losses in the system and battery. Similarly a 2C charge or discharge of the 1Ah battery corresponds to a charge or discharge current of two ampere.

2-2-3 State of Charge (SoC)

The State of Charge is a percentage to indicate the charge that is remaining in the battery. Commonly the voltage of the battery is used as an rough indication for this level. In this case the percentage is set to 100% if the voltage of the battery is at the maximum voltage (typically 4.2V) and set to 0% at the minimum voltage (typically 2.8V). The exact voltages depend on the chemistry of the battery. In Appendix B the reaction that determines the voltages are given. In between the minimal and maximal voltages a linear or more advanced polynomial interpolation is used to calculate the percentage. An typical shape of this curve is shown in Figure 2-1

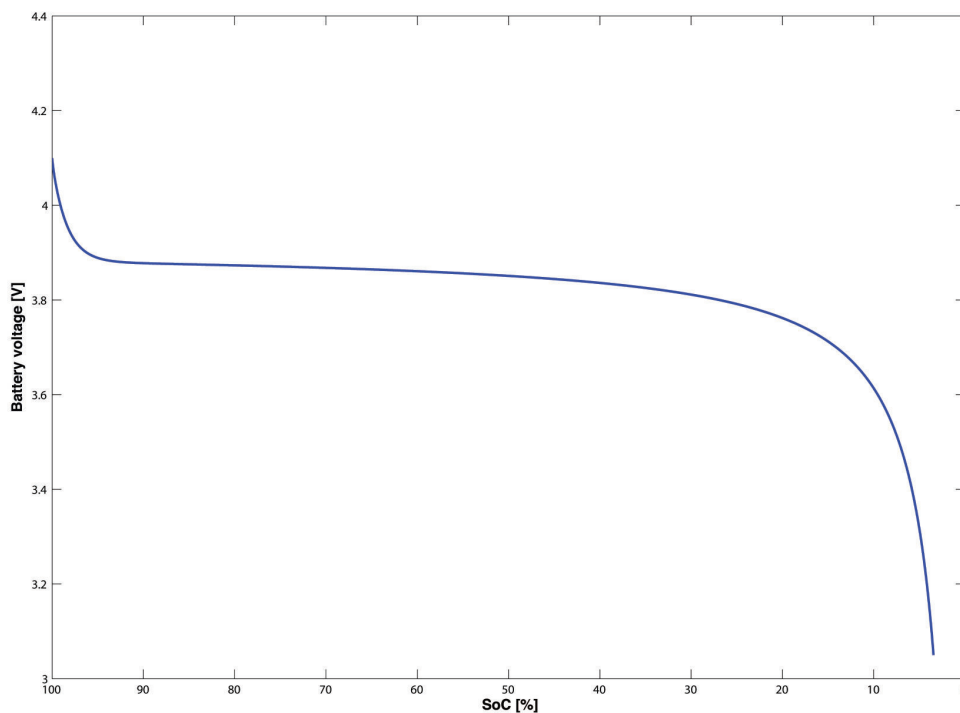


Figure 2-1: Typical discharge curve used for SoC calculation.

Instead of a voltage based SoC indication a ‘coulomb counting’ could be used to integrate the current drawn from the battery and dividing this with the nominal capacity of the battery.

This will in general result in a more accurate calculation of the state of charge since we now actually 'count' the charge that is stored or consumed.

2-2-4 State of Health (SoH)

The State of Health (SoH) is a percentage to indicate the fraction of the original capacity that is still usable. Over time every battery ages and less and less capacity remains. How healthy the battery is can be calculated dividing the current maximum capacity that can be drawn from the battery by the original capacity via Equation 2-1.

$$\frac{C_{start}[Ah]}{C_{current}[Ah]} * 100\% \quad (2-1)$$

Commonly a battery is considered to be at its end of life and ready for replacement and recycling if the SoH has dropped below 80%.

2-2-5 Depth of Discharge (DoD)

The Depth of Discharge (DoD) is an percentage to indicate how deep an battery is discharged. Commonly a battery is not discharged to 0%. For testing how many cycles a battery can sustain, an typical DoD of 80% is used. This means that only 80% of the available 100% SoC is used and that thus 20% remains in the battery after discharging.

Note that an 80% DoD cycle does not necessarily mean that the battery was fully charged before discharging. A cycle from 90% SoC to 10% also is an 80% difference and thus an 80% DoD. For testing DoD capabilities of a battery a state of charge of 100% usually is the starting point.

2-2-6 Cycle life

During use a battery suffers from aging processes that degrade the performance. The number of cycles that the battery can handle before the usable capacity has dropped to 80% of the original capacity is defined as the cycle life of the battery. 80% is considered the minimal capacity that is needed to provide sufficient runtime to the device it is supposed to power. However, a battery can be used for more cycles than its specified cycle life. This only means the runtime is below the 80% of the original runtime. A cycle life curve of the Eaglepicher Lithium-Ion family implantable battery is shown in Figure 2-2. As can be seen the loss of usable capacity is rather gradually. In general the degradation starts to speed up after the 80% point and more and more capacity is lost with each additional cycle.

2-2-7 Shelf life

Even if the battery is unused and is stored on a shelf some aging processes continue to degrade the capacity of the battery. After a couple of years these processes will degrade the battery so much that less than 80% of the original capacity remains. Once this battery is used the

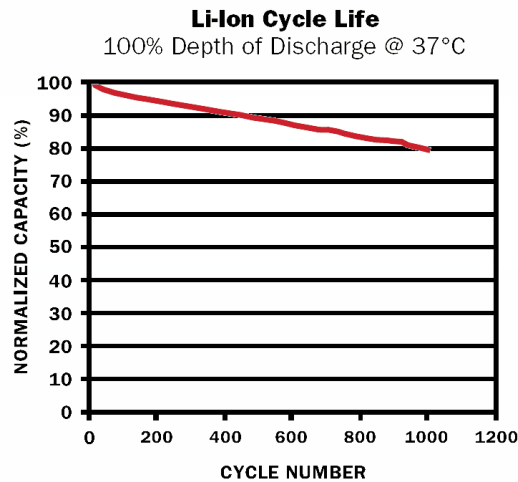


Figure 2-2: Cycle life of EaglePicher Lithium-Ion family. Picture courtesy of EaglePicher [14].

runtime of the device it is powering will be insufficient. The shelf life of a battery is thus the time needed to degrade the battery to 80% of the original capacity without cycling it.

In non-rechargeable batteries shelf life refers to the self-discharge that also results in a reduction of the capacity that is available for the first use.

2-2-8 Over- and under-potential

When charging or discharging a battery, especially at high currents, the voltage measured at the terminals does not reflect the actual Electro Magnetic Force (EMF) that the battery can supply at its current SoC. During discharge the measured voltage will be lower than the actual EMF. The difference is called the under potential of the battery. During charging the measured voltage will be higher than the actual EMF generating an over potential.

Part of the over or under potential is found across the internal resistance of the battery. More properties of this resistance will be discussed in Section 2-5 . Another effect that is playing an important role is the movement of ions that cannot keep up with the current that the battery should supply or absorb.

2-3 Primary cells

The first (practical) electrochemical battery, or cell, was (re)invented by Alessandro Volta in 1799 [15, 16]. Although Volta got the credits for the invention there is proof of a similar design dating back to the ancient Persians some 2000 years ago [17]. These cells were capable of storing energy and supplying a more or less constant voltage to a load, making portable applications possible.

A cell consists of three major components namely [18]:

1. The anode or negative electrode that donates electrons to the external circuit and is oxidized during the electrochemical reaction.

2. The cathode or positive electrode that accepts electrons from the external circuit and is reduced during the electrochemical reaction.
3. The electrolyte which provides the medium for transfer of charge, as ions, inside the cell between the anode and cathode. The electrolyte is typically a liquid, such as salted water, but can be a solid as well.

As said before primary batteries are not rechargeable. This means that the chemical oxidation and reduction reactions are not (easily) reversed. After being discharged once the cells are disposed and recycled if possible. In general, primary cells hardly discharge during storage resulting in a good shelf life. They usually require no maintenance and are easy to use. Furthermore they can provide a large amount of energy in a small volume and weight if they are discharged slowly.

In the 1970's the first lithium based batteries were developed and commercialized. Due to their high voltage and low weight, lithium based batteries started to replace the traditionally used Alkaline-MnO₂ primary batteries [16, 19]. The same is true for medical applications. The IPG of today also uses lithium based batteries. In Appendix A some non-rechargeable lithium based batteries that are available for medical applications, and thus allowed to be used in a IPG, are compared and details of the electrochemical reactions are given.

2-4 Secondary cells

Secondary, rechargeable, batteries can be recharged electrically after being discharged. This is done by passing an current through the battery in the opposite direction reversing the movement of ions and chemical reduction and oxidation processes. In Figure 2-3 the movement of ions between the anode and cathode in both directions is illustrated.

Traditionally Lead based batteries dominated the market in rechargeable cells but again due to the high cell voltage (4 volts versus 2 volt), high energy density (over 500Wh/L versus 180Wh/L) and long charge retention (years versus months) lithium based cells are the first choice for mobile devices today [20].

The domination of the market was slowed down by safety concerns. Lithium batteries have been known to self-destruct drastically in abuse situations, such as short circuit, overheating and overcharging, causing dangerous situations. Under these conditions the first generation of rechargeable lithium cells experienced thermal runaway resulting in explosion and fire. The solution was found in materials that can replace the lithium metal anode but still can absorb and release lithium in a high rate. In 1991 an anode based on carbon and a cathode of layered lithium cobalt oxide was introduced to the market by Sony [16]. Modern lithium batteries are quite safe but still need to be handled with care to prevent capacity fade. What processes deteriorate the battery performance in abuse situations is discussed in Section 2-6. To prevent damage extra protection circuitry is often provided to disconnect the battery in abuse situations. A battery combined with protection and monitoring electronics is often referred to as a 'smart' battery.

In general the energy density of rechargeable batteries is lower than of primary cells. For example an primary Li-MnO₂ cell has a volumetric energy density of 600Wh/L while a

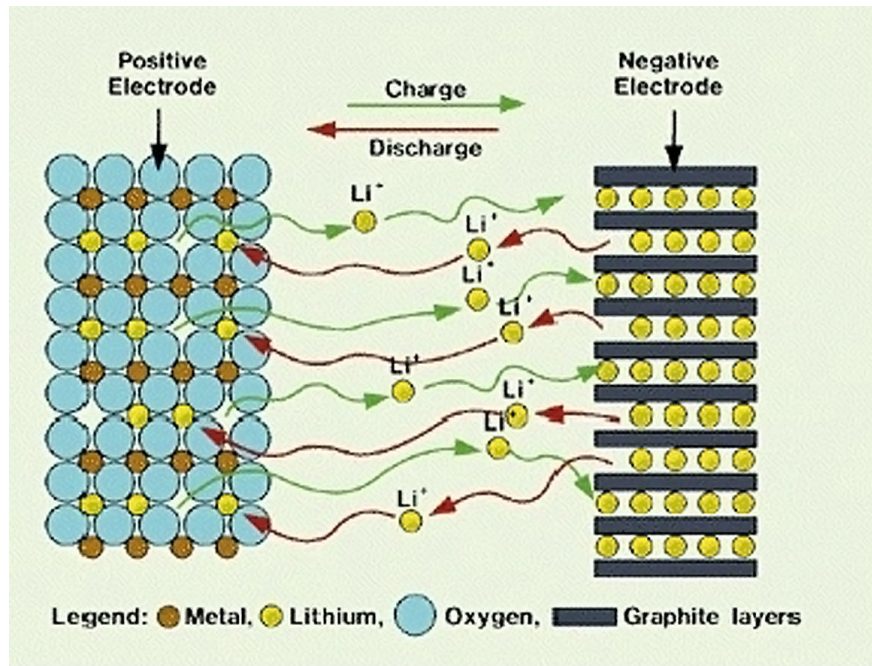


Figure 2-3: Transport of lithium ions in a rechargeable battery.

secondary Li-FePO₄ cell has only 130Wh/L. This means that if we replace a primary cell with an equivalent size secondary cell the runtime of the device will decrease almost fivefold. However, after depletion of the secondary cell they can be recharged hundreds of times before replacement is needed. If we assume an cycle life of 800 cycles the available energy between replacements will be 173 times the original available energy making rechargeable batteries the best choice for small and power hungry devices such as implantable stimulators. In Appendix B some rechargeable lithium based batteries that are available for medical applications, and thus allowed to be used in a IPG, are compared.

2-5 Modeling of batteries

There are several ways to model and understand the behavior of batteries. At system level a battery is often replaced by an ideal voltage source with a fixed value representing the EMF of the battery. This is the most simple way of modeling a battery and is already quite accurate as long as the battery is between the 90% and 20% SoC. As already depicted in Figure 2-1 the terminal voltage of a lithium battery is almost flat in this region and varies only a tenth of a volt.

At the extremes (above 90% SoC and below 20% SoC) the discharge curve starts to deviate substantially from the ideal voltage source. Exponential regions can be observed in Figure 2-1 that need to be taken into account. Also the temperature and discharge rate will have an influence on the chemical reactions and thus on the terminal voltages. Changing the fixed voltage source in a variable voltage depending on the SoC and temperature will cover this deviation. By doing cycle test a function for the terminal voltage can be found by curve fitting the results [21].

If load currents become high (over five times the nominal current) the terminal voltages start to deviate from the expected voltage. Practical implementations of the voltage source also show this behavior due to deviations from the ideal voltage source. Just as with a practical voltage source a battery also suffers from non-idealities such as a parasitic resistance. A more accurate model thus takes this resistance into account. Often a fixed value resistor in the order of milliohms will already cover most of the observed voltage drop and results in a more accurate model. The reality is of course different.

Besides an ohmic resistance batteries also have a certain frequency behavior pointing to a capacitive component in the current path. For example after applying a current pulse the terminal voltage does not jump directly to the value that can be expected from the non-ideal voltage source model. Instead it settles to this voltage with a certain time constant. By splitting the ohmic resistor in a resistor in series with an RC network we can include this dynamic behavior. The resulting model is shown in Figure 2-4. The exact values of the resistors and capacitors vary greatly over size and composition of the battery and should be deduced from datasheets and measurements.

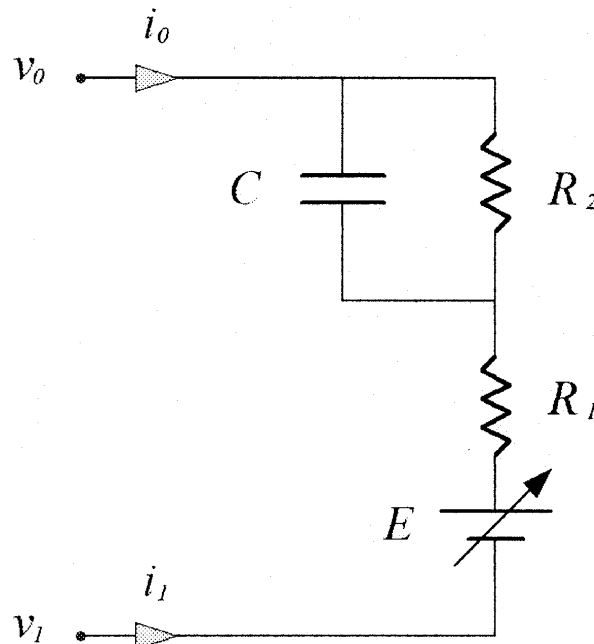


Figure 2-4: Equivalent circuit of a lithium battery. Picture courtesy of Lijun Gao[21]

For most applications the model shown in Figure 2-4 is accurate enough. However when high load currents are applied at nearly empty or nearly full batteries the accuracy of this model goes down. Just as with the EMF of the battery it turns out that the internal resistance of the battery is dependent on the SoC. By doing cycle test a U-shaped impedance curve can be measured. In Figure 2-5 it is shown that the impedance can rise up to a factor of two when the cell is operated at low SoC (voltage below 3.4V for the shown cell). This shows that when the battery is operated at low SoC and high currents we need to take this increasing impedance into account. We can do this by replacing one of the fixed value resistors by a non-linear and SoC dependent resistor. The resulting model is shown in Figure 2-6.

Whenever possible, we will use this model in the following chapters of this thesis for our

simulations. However battery datasheets often do not specify the dynamic behavior of batteries. Instead they only specify a worst case internal resistance. In these situation we need to resort back to the simple model of a SoC depended voltage source in series with an resistor. Measurements with an actual battery will need to show if the additional dynamic behavior causes the designed system to fail.

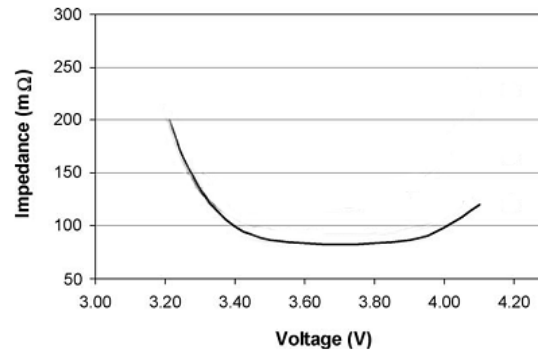


Figure 2-5: U-shaped impedance curve of Li-ion cell. Picture courtesy of J. Vetter [22].

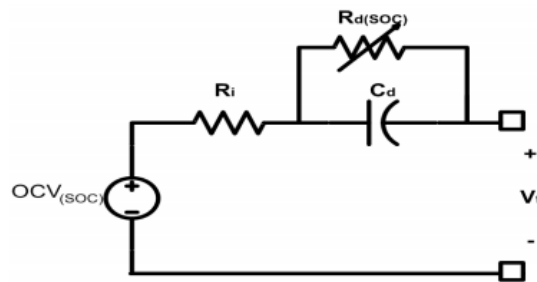


Figure 2-6: Equivalent circuit of a lithium battery with non-linear resistor. Picture courtesy of Low Wen Yao [23].

2-6 Aging of batteries

The performance of a battery deteriorates over time and cycles due to (1) loss of active material due to leakage or material transformations and (2) the buildup of resistive layers over the interfaces. The first effect leads to a reduction in battery capacity while the second effect results in an increase in the internal impedance of the battery. Both effects are often observed together but which effect determines the battery life depends on the application.

For high (pulse) power applications the resistance is often dominating due to the increased voltage drop (lower operating voltage) at high currents. For these applications the buildup of layers over the electrodes, also known as passivation, determines the useful life of the battery. when these layers grow over time the minimum operating voltages of the system will be reached sooner. Similar, for low current long runtime applications the loss of active material is most important [24].

The aging of batteries is inevitable but there are several factors that determine the rate at which a battery deteriorates. By proper operation we can control some of these factors and therefore extend the lifetime of the battery. In this section we will discuss how the operating voltage, temperature, C-rate and DoD affect the lifetime of a battery.

2-6-1 Operating voltage

Lithium Ion batteries have a very strict voltage window in which they are allowed to operate. charging a battery that is already full (overcharging) will result in severe damage of the cell. Since all available ions have been used, the supplied energy can no longer be stored and other reactions start to take place. These unwanted side reactions consume active material and cannot be reversed resulting in permanent capacity loss. Furthermore heat and gas is generated by these reactions resulting in possible dangerous situation. If overcharging conditions are sustained for longer periods pressure may rise to the point of explosion. It is clear that overcharging must therefore be avoided at all times [25].

Even when overcharging is avoided, long time operation and storage of batteries at a fully charged state will still damage the battery. Storing batteries at 100% SoC will result in oxidation of the positive electrode that will cause an increase in internal resistance. This effect is usually small but is easily noticed at alleviated temperatures. Figure 2-7 shows a comparison of two batteries stored at 60°C. One is maintained at 50% SoC and the other at 100% SoC. After just 404 days the impedance is already tripled if the battery is stored at 100% charge while, if stored at 50% charge, the resistance has not even doubled after 712 days. It is clear that long time operation near 100% SoC should thus be avoided.

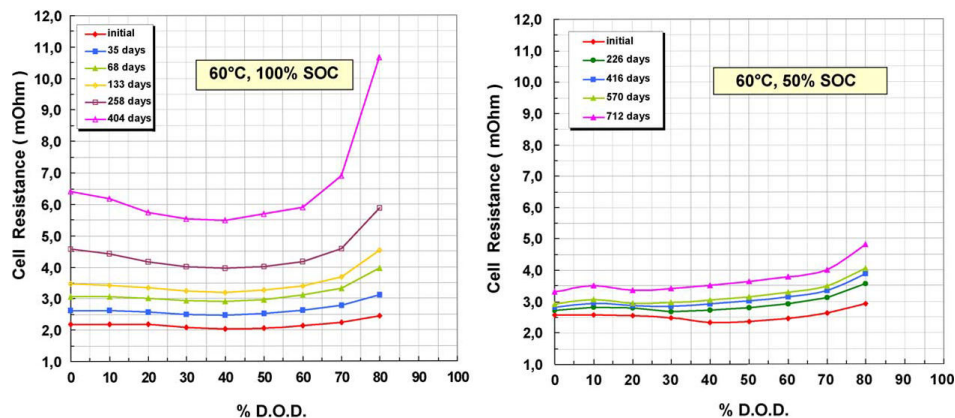


Figure 2-7: Left, battery stored at 100% SoC. Right, battery stored at 50% SoC. Picture courtesy of M. Broussely [26].

Besides a upper voltage limit that should be carefully monitored also a lower voltage limit exists. Draining batteries that are completely empty (over-discharge) will also result in permanent damage. This is caused due to corrosion of the current collector. Corroded current collectors can dilute into the electrolyte and eventually damage the separator. An conductive path will now be formed between the two poles of the battery [27].

The cell is now internally shorted and is no longer usable. By itself over-discharging is not dangerous, upon recharge however, high (local) currents can run through the internal

short causing a dangerous temperature rise. Deeply discharged batteries must therefore be recharged with great care.

2-6-2 Operating temperature

Lithium batteries are designed to operate within a specific temperature range. Both above and below this range the cycle life of the battery goes down. Since the system we are designing should be implanted inside the body we are not considering the low temperature effects. The environment of the system is well controlled by the patient's body so therefore the temperature should be around 37 °C. High temperatures, however, might be important for this system. Due to power dissipation inside the battery temperatures can (locally) rise and result in accelerated aging.

Damage from elevated temperature is caused by two different processes. Firstly, layers that form the interface between the electrodes and the electrolyte will dissolve. Active material is consumed in order to regenerate these layers resulting in a decrease in storage capacity. Secondly the lithium ions that are dissolved in the electrolyte gain in energy due to the elevated temperature. Ions now intercalate more violently into the graphite layers and might hit them with such force that they take the solvent molecules with them. These solvent molecules together with the lithium deform the graphite that will eventually crack. If these cracks spread across the electrodes, pieces might even lose their electrical connection and no longer participate in collecting current.

Depending on the currents and the thermal conduction from the battery to the environment, we might need to consider the thermal aging due to over temperature. In Chapters 3 and 4 we will discuss how the battery is used in our system and if this is a relevant factor to consider during the design of a charger.

2-6-3 Charge and discharge rates

When batteries are used with relative high charge and discharge currents compared to their capacity, large voltage drops will develop across the internal resistance. The cut-off voltages during both charge and discharge will be reached before the battery is actually completely full or empty. The connected charger or load has no notion of the actual voltage drop inside the battery and thus shuts down too soon. Besides the unused capacity due to early cut-off also more power is dissipated in the battery resulting in poor efficiency.

By continuing to charge or discharge at a lower current the voltage drop is again lowered and the total capacity can be used. It seems like that high C-rates will thus only cause temporary losses however some processes also cause permanent damage. First of all, the increased power dissipation might heat up the battery causing the temperature effects as described above. Secondly local over- or under-voltage might occur.

If high currents are sustained for longer periods the diffusion of ions might be too slow to keep up with the rate they are absorbed or released at the electrodes. Also concentration gradients may build up across the electrodes due to inhomogeneous distribution of currents. This causes the battery potential to be locally higher or lower than the average potential that can be monitored from the terminals. Some regions may thus already experience overcharging

or undercharging while the total battery voltage is still within limits. These regions will nevertheless experience the degradation described earlier in this section.

2-6-4 Depth of Discharge (DoD)

The cycle life of a battery heavily depends on the depth of each discharge. When the battery is discharged less deep more cycles can be made before the capacity of the battery drops below acceptable levels. However, this also means that less energy is delivered by the battery in each cycle. The relation between the number of cycles and the discharge depth is (almost) linear. Cutting the DoD in half will result in twice as many cycles before the end of life is reached.

Although twice as many cycles can be made at an 50% DoD, the energy delivered by the battery is also halved in each cycle making the net available energy over the lifetime equal. This indicates that the degradation is actually not determined by the DoD but instead by the energy processed. At high DoD the results of cycle are, however, in contrast with this conclusion.

In situations with deep discharges the battery will be frequently operated at low voltages increasing the risk of (local) under voltage. This will decrease the lifetime as described above. It is therefore best to avoid deep discharges and operate the battery in the nominal region. Cycle tests with batteries designed for satellites showed that making daily cycles with a low DoD can result in a very good lifetime. Figure 2-8 shows that, when only 30% is discharged at each cycle, there is hardly any degradation visible after 6000 cycles. Note that these cycles were made from an initial voltage of 3.8V and not from the maximum of 4V for this type of battery. Also the benefits of operating below the 100% SoC plays a role in this experiment.

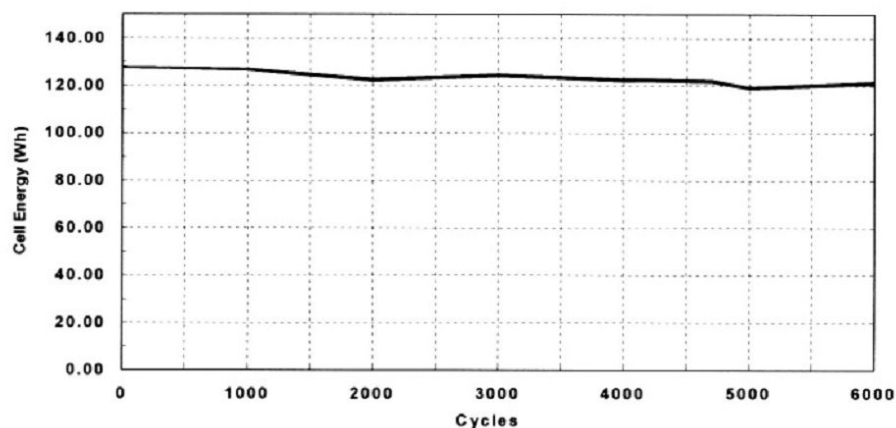


Figure 2-8: High Energy cells designed for satellites. Cell Energy measured every 1000 cycles of 30% DoD from 3.8V. Diagnostic cycle made from 4V down to 2.7V. Picture courtesy of Walter van Schalkwijk [28].

2-7 Conclusion

Now that we have seen what terminology is used in the world of batteries, how batteries are basically build up, how we can model them and determined how we should treat them to increase their life, we can draw some conclusions that are important for the rest of this thesis.

Looking at the models presented in this chapter we can conclude that a battery is not the ideal voltage source often depicted in circuit diagrams. Instead it can only sustain a load for a certain amount of time and behaves in a highly non-linear fashion and. How much of the battery's maximum capacity can still be consumed before recharging is needed is indicated by the State of Charge (SoC). Important battery parameters like the equilibrium terminal voltage EMF and internal resistance vary over SoC.

To guarantee the lifetime of the battery there are several rules we need to obey. First of all, the EMF of the battery may never fall below or rise above fixed thresholds. If this does happen over-discharging or respectively overcharging occurs and irreversible damage is done to the battery. Even if these limits are maintained, care must be taken not to charge or discharge too fast and the temperature must be well controlled.

Furthermore it is best to avoid long time operation (or storage) at SoC's near 100% or near 0%. Local overcharging or over-discharging may occur in these regions and interfaces between the electrolyte and electrodes may be damaged. Due to this risks it is better to cycle regularly in the nominal region instead of making complete 100% DoD cycles all the time. The system that houses this battery should be designed to obey these rules as much as possible.

Using batteries, Charging and Discharging

3-1 Introduction

Due to the sensitive nature of Lithium Ion (Li-Ion) batteries special care has to be taken during charging and discharging of these cells. Severe damage can be done to the cells if they are overcharged or over-discharged resulting in permanent capacity loss and dangerous situations. Especially in implanted medical equipment explosions and excessive heat generation due to overcharging are intolerable. Chargers must be capable of guaranteeing a safe charging of the battery and thus operate via a predetermined algorithm that specifies when charging can begin, what voltages and currents are allowed and when charging should be terminate.

Safe operation, however, does not necessary mean optimal operation. Some (fast) charge algorithms may for example reduce the cycle life of a battery while others may terminate charging to soon resulting in a battery that is not used to its full capacity. Another issue that should be considered is the cost and complexity of the implementation. In this chapter, different existing charge algorithms will be discussed. The different advantages and disadvantages will result in the development of a potentially new algorithm. In the next chapter, Chapter 4, this new algorithms will be simulated and compared with existing methods. First, however, a user profile is introduced which specifies the demands for the system. The charge and discharge scenarios are introduced and on the base of these scenarios the most suitable algorithm will be selected.

3-2 Battery use profile

3-2-1 Discharge scenario

The current lifetime of a (non-rechargeable) neurostimulator is about three to five years [1]. If there are no further complication the device is at its end of life because the battery has

been depleted over this time period. Using this information we can work out the average load the battery has to sustain. If we know the typical battery capacity in Ampere Hour (Ah) we can now calculate the average discharge current using Equation 3-1 where I is the current in Ampere, C is the nominal capacity in Ah and T the lifetime in hours.

$$I = \frac{C}{T} \quad (3-1)$$

Let us consider the situation where the nominal capacity is 1.5Ah and the lifetime is 25632 hours (three years). The discharge current now becomes $\frac{1.5}{25632} = 58.5\mu\text{A}$. This low current is beneficial for battery powered devices. Low currents means low I^2R losses, low self-heating and a low under-potential making almost all stored energy available for discharge. However the current is not constantly this low. If we take the pulses used to stimulate the brain into account, a totally different image arises. A typical pattern used to stimulate neural tissue is depicted in Figure 3-1.

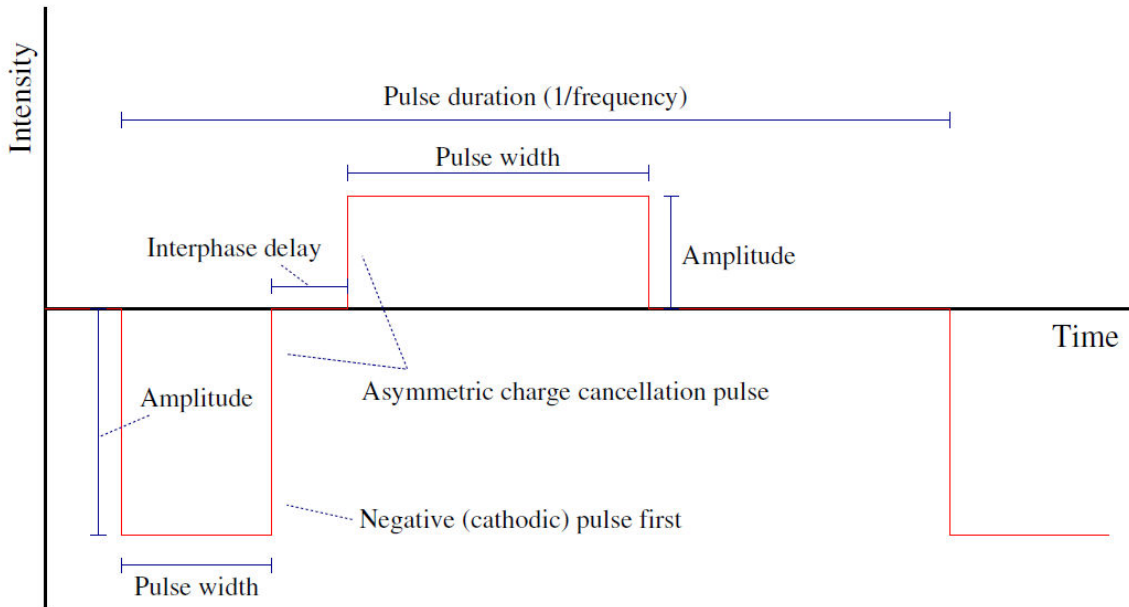


Figure 3-1: Example of an stimulation pattern. Picture courtesy of M.N. van Dongen [29].

Looking at the specification of the Eon Implantable Pulse Generator (IPG) we can see that it is possible to generate pulses of 25.5mA at 12V providing that the tissue impedance is low (below 400Ω)[4]. The 12V needs to be supplied from a 3V battery so obviously up-conversion is needed. The power at the input of the up-converter has to be equal to the power at the output plus the losses in the conversion system. In Equation 3-2 the power drawn from the battery is calculated by multiplying the battery current I_{bat} with the battery voltage V_{bat} . The output power and losses are calculated by multiplying the stimulation current I_{stim} with the stimulation voltage V_{stim} and multiply this with the conversion efficiency η .

It follows from Equation 3-2 that even if we can do the conversion with a 100% efficiency, $\eta = 1$, we draw over 100mA from the battery. Although these pulses can be smoothed with capacitors they will never disappear completely and thus we need a battery that can cope

with high pulse currents. The medical grade battery like the MST Litronik LiS3150M is an example of battery with such characteristics and can cope with pulse currents of up to 250mA [30].

$$I_{\text{bat}} * V_{\text{bat}} = I_{\text{stim}} * V_{\text{stim}} * \eta \quad (3-2)$$

3-2-2 Charge scenario

The discharging of a battery inside an IPG is done via a low average but highly pulsed profile since the pulses needed to stimulate the brain have this profile. However, when an IPG needs to be charged we can think of different scenarios that all put their own demands on the profile to be used. This section will discuss two different possible scenarios that can be considered to be complementary to each other. First we will start with the so called ‘hand held’ scenario where the battery is charged in a matter of minutes. Secondly a ‘pillow based’ scenario is discussed where charging can take several hours to complete.

Hand held charger

As depicted in Figure 3-2 the hand held charger consist of a coil that needs to be held onto the skin on top of the location of the IPG. A coil inside the charger is inductively coupled to a coil inside the stimulator to transfer the energy. Since today’s stimulators are too large to be implanted into the skull the pulse generator is located in the chest cavity as depicted in the figure. The hand held coil needs to be aligned with the coil inside the IPG with an error margin of 1.3cm [31]. If the alignment is off, the charging will be less efficient or not effective.



Figure 3-2: Hand held charge scenario. Picture courtesy of Medtronic, Inc.

For patient comfort the charging must be finished as soon as possible. Hand held charger systems that are supplied with a rechargeable pulse generators today are quite slow and perform a complete charge in about 5 hours [4]. The stimulator can be charged daily or weekly depending on the stimulation settings and patient preferences. These daily cycles will take about 15 to 30 minutes because the battery will not be depleted completely before charging begins.

Research with patient using an rechargeable IPG showed that recharging with an hand held device interferes with the daily routine of the patient and forms a constant reminder that they have an implant [13]. On the other hand, daily charging generates a routine in peoples life so that patients do not forget to recharge their stimulator. If the charger is not placed, the battery cannot be charged and might be depleted too deeply resulting in a device failure. A regular charge pattern is thus critical for the lifetime of the device. In order to increase patient comfort the charging time has to be as short as possible to minimize the interference with daily routines.

Due to the short time that is available and the frequent charging this scenario needs an charging algorithm that is fast and does not degrade the cycle-life of the battery. An example of these algorithms are the ion relaxation methods described in Section 3-3-6 and Section 3-3-7. In this scenario, care has to be taken not to transmit too much (RF) energy. The regulation on maximum field strengths might be violated or, for high frequency, the skin in-between the stimulator and charger might be heated to unacceptable levels.

Pillow based charger

An impression of the pillow based scenario is depicted in Figure 3-3. Here the stimulator is charged automatically on a daily bases. For illustrative purposes a miniaturized stimulator that can be fully implanted in the skull is used. The charger is now hidden in a pillow and hence the name pillow based charger. As mentioned before today's stimulators are too bulky to fit in the skull and need to be implanted in the chest. A coil that is mounted to the backrest of an chair could be used for this situation. The only restriction is that the patient needs to spend multiple hours per day at the location where the coil is to be mounted. A suitable algorithm is especially gentle to the battery so that daily charging does not affect the lifetime of the battery.

Charging can be slow since several hours are available and the battery is likely not depleted completely once the patient returns to the charging location again. This system however needs to be able to deal with a large coil misalignment and larger distances between the two coils since the patient is not as close to the stationary coil and constantly moving. This can be a challenging problem since already with today's hand held charger 78% of the patients have problems in getting a stable energy transfer [13].

Increasing the transmitting power can off course help but this is not a wise solution. The added power might be harmful to the patient in the long term and in the short term cause skin heating and irritation. Besides gentle the used algorithm should thus be low power so that a large portion of the received power is available to charge the battery and thus reduce the demands on the transmitted power.

The battery can be charged without any action of the patient as soon as they return to the charge base. The risk of early device failure due to over discharging of the battery is hereby

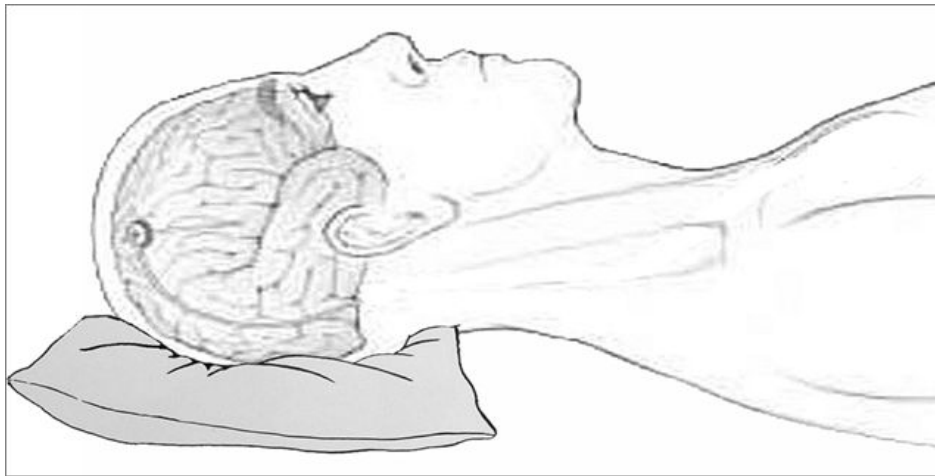


Figure 3-3: Pillow based charge scenario. Picture adapted from the Harvard Health Letter (September 2004)

eliminated making the pillow based scenario more user friendly and thus the best choice for our application.

3-3 Charge algorithms

Now that we now in what environment our battery charger should operate we can select an appropriate charge algorithm. In this section we will discuss some algorithms that are used today to safely charge lithium batteries. Each algorithm is explained in its own section and advantages and disadvantages of each protocol is mentioned.

3-3-1 Constant Current Constant Voltage (CCCV) charging

The most widely applied charge algorithm is the Constant Current Constant Voltage (CCCV) algorithm. Here, charging is initialized with a Constant Current (CC) phase where the battery is charged with a fixed current of typically up to 1C. As soon as the maximum allowed voltage of the battery is reached the algorithm is switched to the Constant Voltage (CV) phase. Here the voltage is kept constant at the maximum allowable voltage. Due to this the charge current automatically decreases and will reach zero in infinity. To terminate charging after a finite time, a minimum charge current is chosen. Typically this is 5 to 10% of the initial charge current, where the battery is considered completely full.

For deeply discharged batteries (voltages below 3V) a dedicated start of the algorithm is used. To test if the battery can still be safely charged and is not damaged by an too deep discharge the start current is limited to just 10% of the nominal capacity. During this trickle charging phase a healthy battery will charge slowly to 3 volt where the normal CC phase can begin. Damaged batteries will likely have an internal short circuit between the anode and cathode preventing the voltage to rise. Here the trickle charge will never finish and can be terminated by an additional timer.

Figure 3-4 depicted a complete CCCV charging cycle of a 1Ah battery. Charging starts with a completely drained battery at 0% SoC. The first 775 seconds the charge current is limited to 0.1A in the trickle charge phase and the voltage (blue solid curve) slowly rises to 3 volt. After the trickle charge the CC phase is started and the maximum current of 1A (depicted by the green dashed curve) is applied until the voltage hits the 4.1V. After this the voltage is kept constant and the current decreases. Finally the State of Charge (SoC) (point dashed red curve) approaches 100% and the current drops below 0.025A. At this point the charger is switched off and charging is completed.

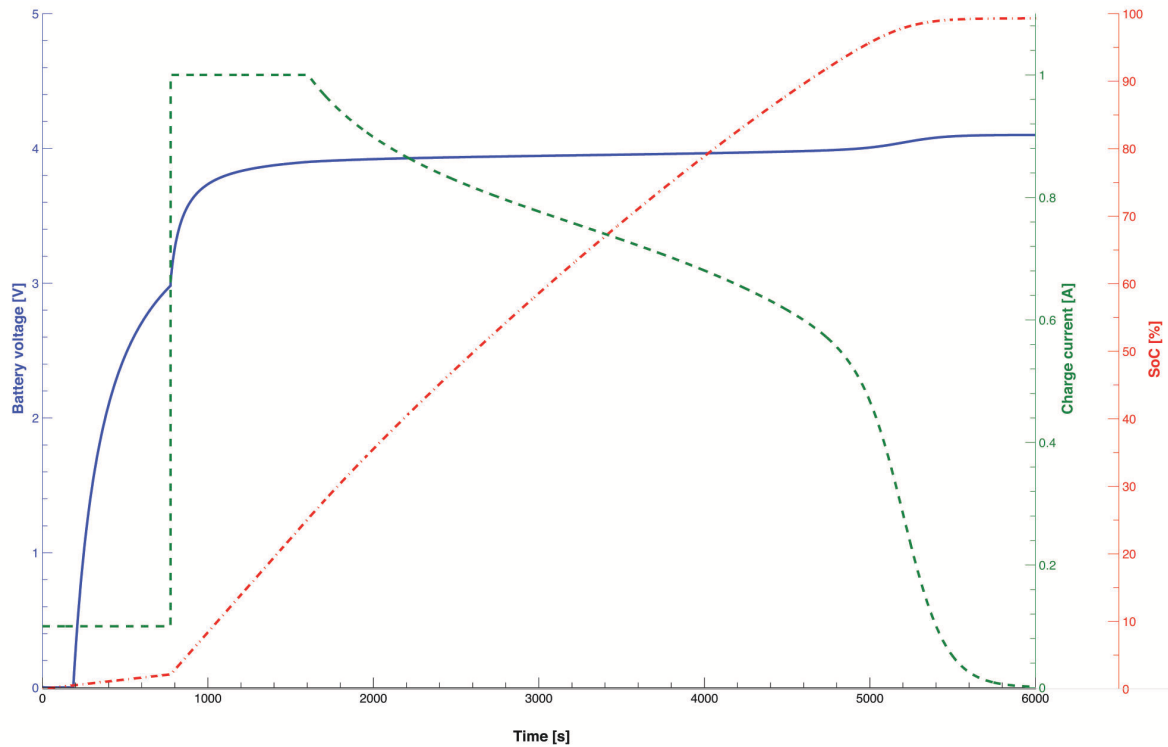


Figure 3-4: Simulation of Constant Current Constant Voltage Charging of a lithium battery with a trickle charge start for deeply discharged batteries. The solid blue line shows the battery voltage during charge versus the charge time. The green dashed line shows the charge current versus the charge time. The red dash-dotted line shows the State of Charge (SoC) of the battery versus the charge time.

For decades the CCCV charging method provided a safe and complete charging for Li-Ion batteries and both microprocessor controlled as well as power efficient fully analog implementations of this algorithm are available. Besides the years of development and evolution there are some restrictions to the use of this method. For example the total charge time is approximately fixed making this method unsuitable for fast charging. Even if the charge current is increased this will only result in a shorter CC phase. Due to the higher current the over potential in the battery is increased causing an early switchover to the CV phase. However the batteries SoC is still low meaning that the gained time in the CC phase is roughly added to the CV phase [32].

Furthermore, the abrupt switchover point might introduce some stability issues in the system. As soon as the charger switches from CC to CV the current might be reduced causing the

battery voltage to drop below the switching threshold. If this happens the charger switches back and forth between the CC and CV phase. This can be solved by adding a fourth combined CC and CV stage in between making the switchover more smoothly [33].

Despite these drawbacks a complete charge close to 100% SoC is guaranteed even if the over potential is high, due to for example aged batteries with high internal resistance, without the risk of overcharging. Due to this safe and well developed nature this algorithm will be the benchmark in Chapter 4 for the comparison of other algorithms.

3-3-2 Multi-stage Constant Current (CC) charging

A different approach in charging lithium ion is a multi-stage constant current charging. Here, the battery is only charged by current limited sources that step by step decrease in magnitude. Figure 3-5 shows a charging profile of a five step CC charger. This method is optimized for fast and safe charging. It is shown that this particular implementation can push the battery to 57% more cycles and, at the same time, reduce the charging time by 11.2%. [34]

Experimental results show that the temperature rise during charging is considerably decreased with the five step approach and is at its peak value for only a couple of minutes [34]. This indicates that charging is more efficient and gentle to the battery resulting in the increased lifetime and faster charging. In this experiment the charger is controlled by software running on a personal computer. Before this method can be implemented in any mobile device this control should be made small and low-power in order to successfully compete with the CCCV method.

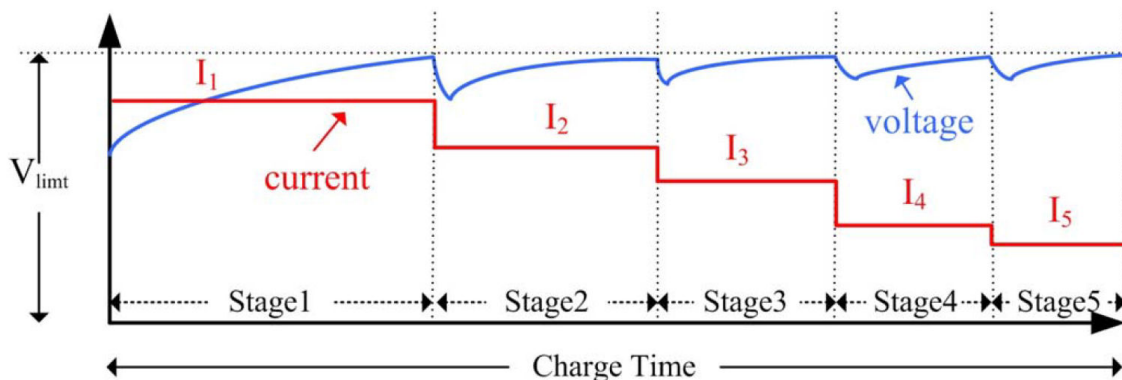


Figure 3-5: Five Constant Current steps Charging of a lithium battery. The blue curve show the battery voltage versus the charge time. The red curve shows the corresponding charge current versus the charge time. Picture courtesy of Yi-Hwa Liu [34].

3-3-3 Build-in Resistance Compensated (BRC) charging

As discussed in the section above the CCCV algorithm is not suitable for fast charging. Increasing the charge current during the CC phase will only result in an early switchover to

the CV phase due to the increased overpotential and voltage drop across the connecting leads. The BRC technique avoids this early switchover by dynamically estimating the resistance of the connections in and to the battery pack. Figure 3-6 shows the voltage waveform of a compensated and uncompensated charger.

Experiments show that the CC stage can be extended in time for 40% [32]. During this phase more energy is pushed into the battery resulting in a decreased overall charging time. However, the paper does not specify the resulting cycle life of the battery. Since the battery is being charged with a high current at high voltages the lifetime might be adversely affected by this method. More research needs to be done to give a fair conclusion on this.

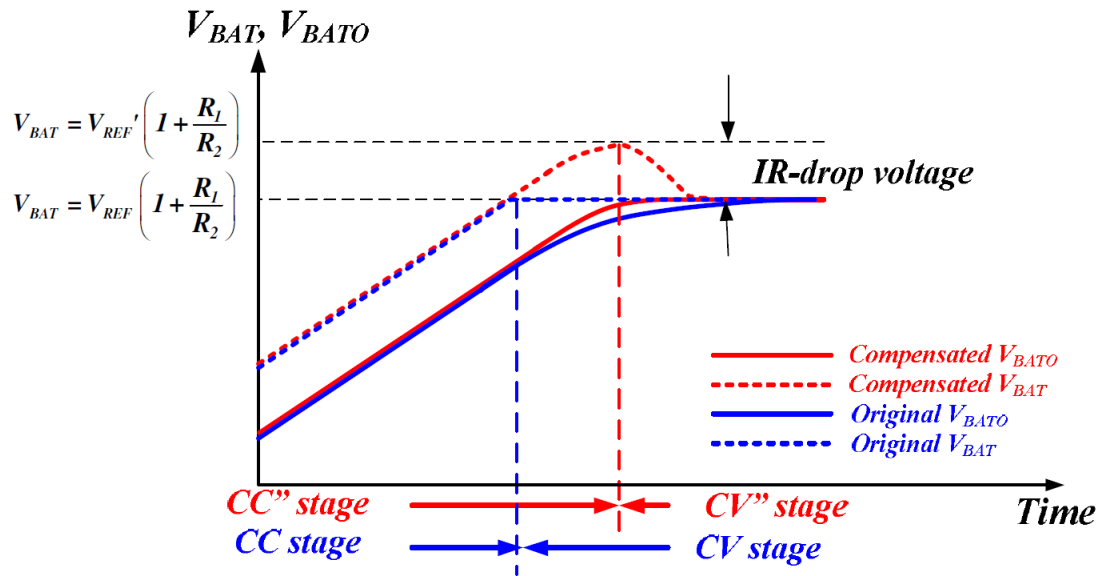


Figure 3-6: Build in Resistance Compensated Charging of a lithium battery. The solid curves show the open circuit voltage of the battery. The dashed curves show the voltage of the battery including overpotential. The blue lines are the waveforms of a traditional CCCV charger. The red lines show the charge profile of a BRC compensated charger. Picture courtesy of Chia-Hsiang Lin [32].

3-3-4 Pulse topping charging

Just as the name suggest the pulse topping charging uses an pulsed current to “top off” the battery after completion of the CC phase. Depending on the internal resistance and charge current the battery is charged in-between the 40% to 70% SoC during the CC phase. After this phase the battery voltage is at its maximum level just as is the case in the regular CCCV charging method. The charger now starts to give one-second pulses at the same magnitude as the initial charge current and waits with the next pulse until the voltage has dropped below the maximum voltage. This waiting time will gradually increase if the battery approaches 100% SoC and charging is finished if the duty cycle ($\frac{t_{\text{pulse}}}{t_{\text{pulse}} + t_{\text{off}}}$) has become smaller than typically 5% to 10% [35].

Because the magnitude of the current pulses remains constant the average charge current is higher than during CV charging resulting in a decreased charging time. Especially at lower

temperature this difference is significant due to the temperature dependence of the internal resistance. Experiments show an decrease in charge time of 37% at 0°C [35].

Figure 3-7 shows the voltage and current waveform of the pulse topping algorithm with an limited amount of pulses. The figure clearly shows that the measured battery voltage is pushed above the maximum 4.2V by the one second pulses. Despite this overvoltage the lifetime of the battery is not degraded but is, instead, increased. Experiments show that after 500 cycles the usable capacity was 4.6% more if the pulse topping algorithm was used instead of the conventional CCCV method [35]. This can be explained by the fact that the battery is only at this high voltages for an limited amount of time and that there is a voltage drop across the connection leads and safety circuit in the used setup resulting in an overestimation of the actual battery voltage.

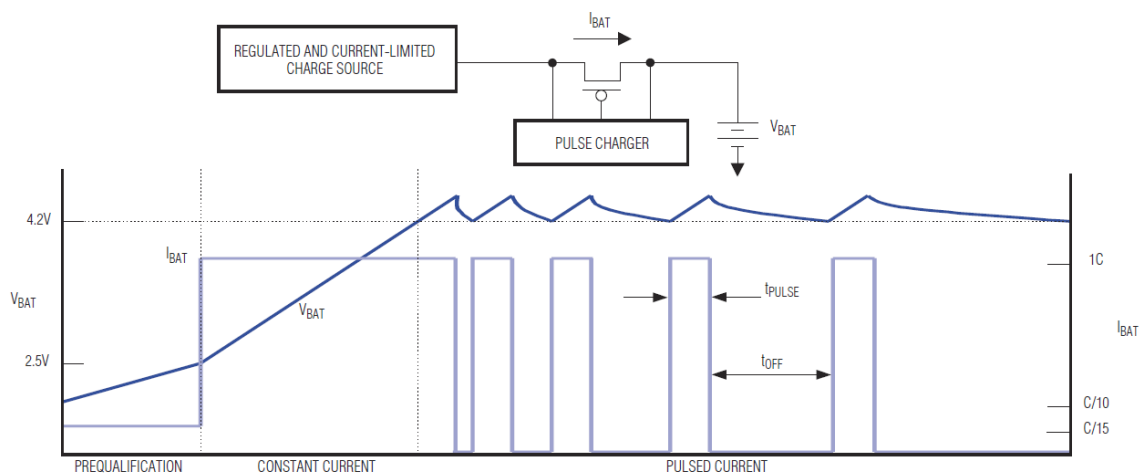


Figure 3-7: Topping of a battery with current pulses. Picture courtesy of Dallas semiconductor Maxim [35].

3-3-5 Float charging

Float charging is a technique to deal with the self-discharge of batteries. It is often used in uninterruptable power supplies or emergency power supplies in order to guarantee maximum available battery power if the regular main power supply fails. The essence of this technique is to maintain a fixed SoC and not to charge the battery completely. This is done by just applying a fixed voltage corresponding to the desired SoC (often close to 100%).

Basically float charging is just a continuation of the CV stage of the CCCV charging method without the shut-down if the charge current falls below a certain threshold. Obviously, if an complete discharged battery would be connected to a voltage source the charge current would become dangerously high. Without any additional control (current limitation) this method is thus not suitable for complete charging of batteries. However, in aging experiments where float charging is used to maintain a fixed SoC it performs extremely good. As long as the operating temperature is well controlled and the battery voltage is below its maximum, the expected lifetime does not depend on the float voltage [24]. Accelerated life tests show that

at ambient temperature it would take over 15 years before the capacity of the batteries drops below 80% of the original capacity [36].

3-3-6 Ion relaxation charging

If charge currents become very large (in general more than $5C$) the over potential in the battery becomes so large that the CCCV method or other methods described above are not suitable anymore. Movement of ions start to lag the charge rate and all sort of layers start to build up at the membranes causing material stresses and deterioration of the battery. There are four processes occurring simultaneously during charging of a battery all with their own speed. The processes are (described from cathode to anode) [37]:

1. Lithium ions diffuse out of the cathode and enter the electrolyte.
2. Driven by the electric current, the lithium ions in the electrolyte solution diffuse toward the anode where they form an electrochemical double-layer on top of the interface between the electrolyte and the electrode. The interface layer is referred to as the Solid Electrolyte Interphase (SEI), the double-layer on top of the SEI is referred to as the boundary layer.
3. Lithium ions shed their paired species (anions and solvent molecules) and enter the SEI where they continue to diffuse toward the anode that is usually carbon based.
4. Lithium ions move from the SEI into the carbon where they continue to diffuse and occupy available sites in the carbon.

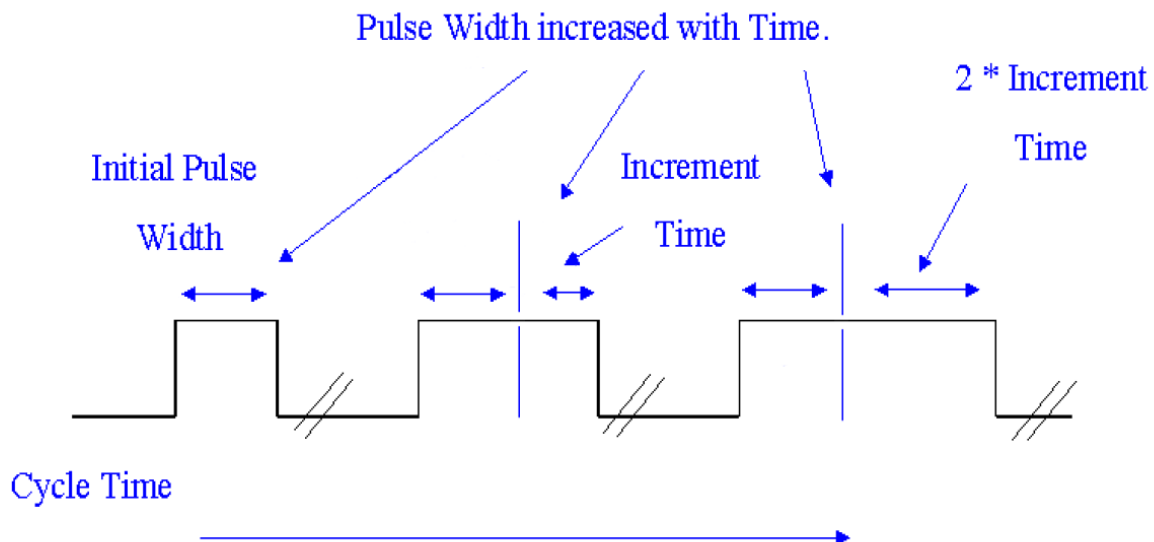


Figure 3-8: Pulse pattern of a microbattery charged with incrementing pulses. Picture courtesy of Vinesh Sukumar [38]

Diffusion through the solid carbon and SEI is relatively fast and poses no problems. The processes occurring at the boundary on the other hand are not that fast and limits the charging

rate. It is known from lead-acid and nickel batteries that applying the charge current in a pulsed fashion the rate limiting processes can be manipulated. However, the pulses need to be adapted to the specific time constants of lithium. For a lithium micro battery with a capacity of only $200nAh$ this can be done as illustrated in Figure 3-8 and described below. A 200ms pulse with a magnitude of 10C is applied. The duration of the applied pulse is slowly increased causing the voltage of the battery to raise slowly. As the microbattery potential nears its maximum value, the amplitude of the current pulses is slowly decreased. The OFF periods allow the ions to diffuse and distribute more evenly throughout the microbattery speeding up the diffusion through the boundary layer.

3-3-7 Ion relaxation charging with negative pulse

When high current pulses are applied to a battery voltage induced stress and gas bubbles can be introduced at the interfaces of the electrodes. A special pulse algorithm can remove these side-effects and result in an even shorter charging time. By introducing a short negative pulse the bubbles and charge carriers that are stagnated on the interface are loosened speeding up the relaxation processes [38]. This method is also referred to as “burp charging” or “reflex charging” and is the most complex charging method described here. The pulse shape used in this method is illustrated in Figure 3-9 .

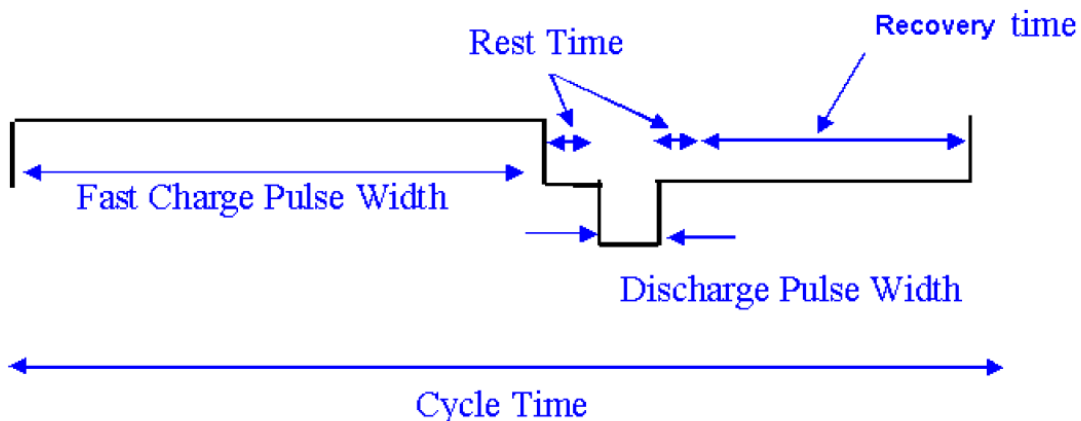


Figure 3-9: Pulse pattern of a microbattery charged with negative pulses. Picture courtesy of Vinesh Sukumar [38].

Although the algorithm is fast and does not adversely affect the lifetime of the battery it is slowly accepted in commercial products due to increased cost and size of the circuitry [37]. The power consumption of this algorithm is also larger since the losses over the parasitic resistances is high due to high charge currents. Usually the negative pulse power is dissipated in the charger resulting in an even higher power consumption.

3-3-8 Boostcharging

In some cases, for example in electric vehicles or life supporting devices, it happens that the battery is drained at an unexpected and inconvenient moment. Users then wish to be

able to very rapidly charge their battery to a usable SoC without degrading the lifetime. Boostcharging is a method that does exactly that. Nearly drained batteries have shown to be capable of handling very high charge currents for a limited amount of time without adversely affecting the lifetime. By this technique, up to one third of the total capacity can be recharged in not more than five minutes. The other two thirds is charged by standard CCCV charging. This ensures a complete charge if the time is available but also a system that is ready for use in just five minutes [39].

The total charge cycle is basically a CCCV cycle with higher current and voltage limits followed by a standard CCCV cycle. The total cycle could thus be denoted as CCCVCCCV or $(CCCV)^2$ and is depicted in Figure 3-10. In the first 100 seconds the current is set to $4.5A$ that equals $4.5C$ for the simulated battery. If the battery voltage hits the $4.25V$ the voltage is kept constant. After 5 minutes charging time the boost charge is completed and the battery is charged with the regular CCCV method.

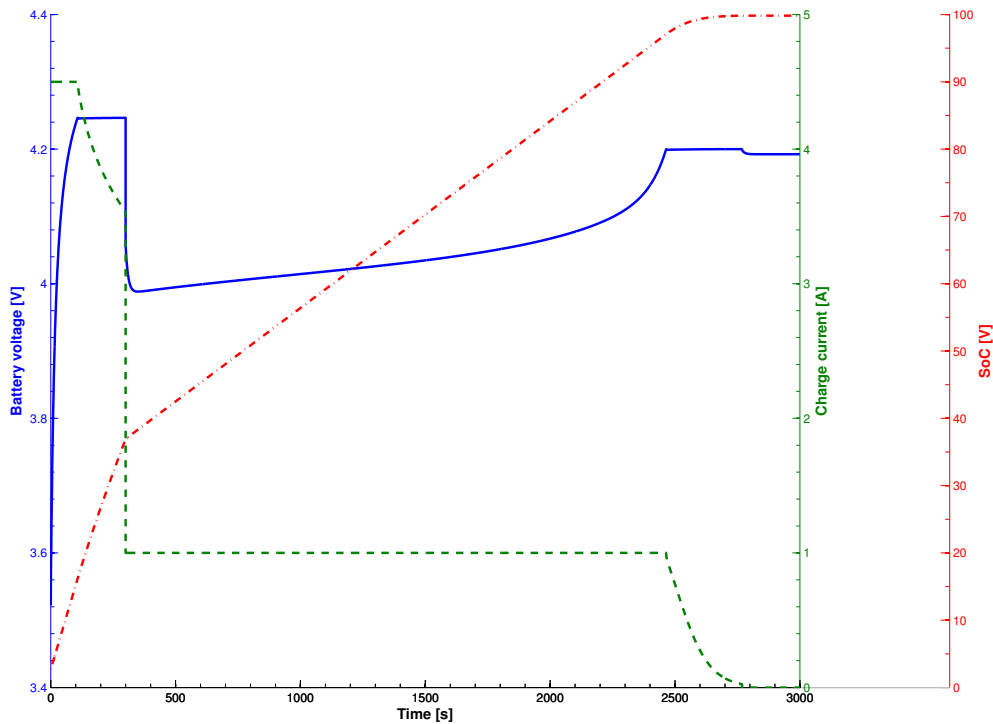


Figure 3-10: Simulation of the boost charge algorithm. The solid blue line shows the battery voltage during charge versus the charge time. The green dashed line shows the charge current versus the charge time. The red dash-dotted line shows the State of Charge (SoC) of the battery versus the charge time.

Since the current is only high at low SoC the aging effects that occur at high SoC are not altered compared to the traditional CCCV charging method. It should be noted that in [39] an empty battery is still above the 3V and thus is not completely drained. Whether medical grade batteries can handle the high currents at 3V or even lower voltages is not known since

this research is done with cylindrical (US18500, Sony) and prismatic LP423048 (Philips) Li-ion batteries only.

3-4 Conclusion

In Figure 3-11 all discussed charging methods are listed with their special features. A subdivision is made between the fast charging (about 5C) and slow charging (below 1C) algorithms. This division corresponds to the two possible charge scenarios that are discussed.

A hand held charger would preferably use fast charge algorithms while the pillow based charger could also use slow charge algorithms. Due to medical safety reasons and regulations the RF power that can be used is limited, possibly limiting the charge current as well. Also patients might forget to charge the stimulator with their hand held charger resulting in a device failure. The pillow based charger together with an slow charging algorithms is thus the better choice for our application.

Although there are quite some low power slow charge algorithms available that also provide good cycle life they all come with their own benefits and disadvantages. The classical CCCV algorithm for example can have stability problems but needs only a small chip area for its implementation. The other algorithms all improve the charge behavior but need complex control logic with more stages or additional components for their implementation.

In conclusion the ideal charge algorithm for our application still needs to be developed. For our application we need a charger that has a simple control, is low power, provides good cycle life and can be implemented on an integrated circuit. In the next chapter, Chapter 4, we will develop such an algorithm based on the features of the existing algorithms as described above. The result will be compared with existing algorithms on the base of simulation.

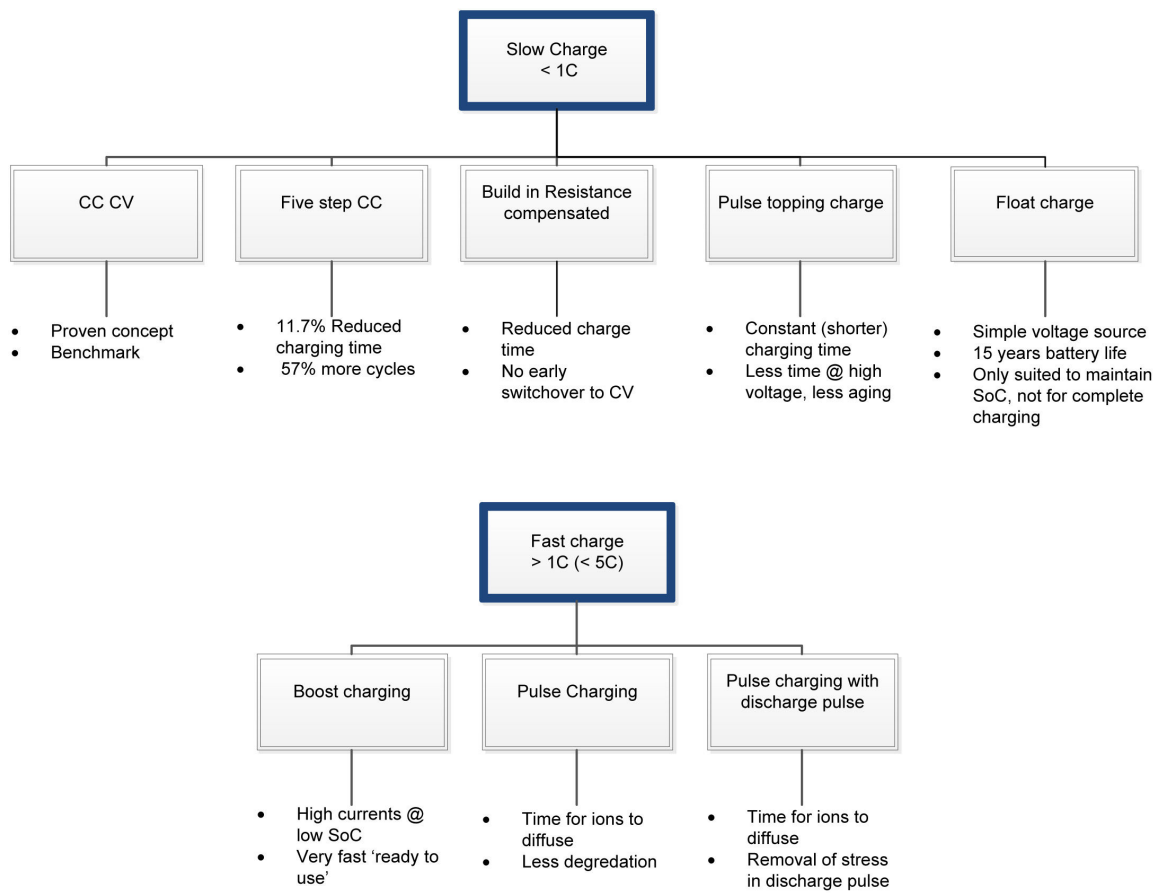


Figure 3-11: Overview of discussed charge algorithms.

Selection of charge algorithm

4-1 Introduction

The previous chapter we wrapped up with the conclusion that the perfect charge protocol still needs to be developed for an optimal charging of an Implantable Pulse Generator (IPG). We know that this algorithm should guarantee safe charging conditions at all times, should be simple to control and avoid excessive aging of the battery. In this chapter we will propose an new charge algorithm that can potentially provide this functions. We will compare the performance of this algorithm with the classic Constant Current Constant Voltage (CCCV) algorithm and rate them on three criteria.

The charging time is considered to be the first criterion. Although we have several hours available for a complete charge in the pillow based scenario, as described in Section 3-2-2, we need to recharge within a limited timescale. Especially if the battery is depleted completely and the system has shut down, the patient would like to have the system ready for use as soon as possible. Therefore we do not only consider the time it takes to do a full charge but also the time to recharge only one third of the total capacity. Performance of the classic CCCV algorithm and the proposed algorithm are compared on the basis of a full charge cycle simulated in Matlab/Simulink.

Next we compare the power consumption of the two algorithms. In this case we do not compare the power consumed by the charger circuits, but instead the losses inside the battery. Losses in a charger might be reduced by changing the implementation or selecting different components. The power lost in the battery, however, is a conceptual loss of the algorithm and is independent of the implementation. We therefore compare the two algorithms on the power lost due to the overpotential of the battery. The battery's overpotential is modeled over the full charge cycle using a Matlab/Simulink simulation.

The last comparison criterion is the expected implementation complexity and cost. For this the chip area of an existing implementation of the CCCV algorithm published in literature is compared with the expected chip area of the proposed algorithm. Also we will make some remarks on the expected stability and behavior over process variations. Afterwards we

will conclude if the proposed algorithm is suitable for our system. We start, however, by introducing the new algorithm

4-2 Proposed new algorithm, Smooth Charging

As shown in Section 2-5 the impedance of a battery varies over the charge cycle in a U shaped profile. The impedance of a battery is significantly higher at a State of Charge (SoC) below 20%SoC and above 90%SoC. Charging with high currents in these extreme regions will result in an increase in battery over-potential and higher I^2R losses. This will thus lead to an extensive waste of available energy and possible damage to the battery due to heat generation.

Note that during the classical CCCV charging method as described in Section 3-3-1, problems that might occur above the 90% SoC are already prevented. The charger will be in the Constant Voltage (CV) mode and the charge current is automatically decreased if the impedance of the battery starts to increase. In fact, due to the gradually decreasing charge current the over-potential will also decline to nearly zero before the charger is switched off.

For extremely deep discharged batteries a trickle charge phase is usually used at the beginning of the charge cycle. In this case the charge current and thus the over-potential and losses are limited until the battery has reached a threshold voltage of about 3V. As shown in Figure 2-5 the impedance is still significantly higher between 3.2V and 3.4V. One could argue that shifting the switchover from trickle charge to Constant Current (CC) charge to a higher voltage will prevent the buildup of an over-potential and reduce losses. Indeed this would be the case but if the switchover is set at for example 3.4V the duration of the trickle charge phase will increase dramatically.

An better approach would be to gradually increase the charge current in the low SoC region and gradually decrease the current in the high SoC region. In this way the charge current can be maximized over the whole charge cycle while keeping the overpotential and losses within a certain limit. Furthermore there is no longer a need for a separate trickle charge control loop, current control loop and voltage control loop. Instead, there will be just one loop controlling the charge current over the total charge cycle. This will eliminate possible instability of the charger near the switchover points.

Due to the smooth current curve over the charge cycle we call this method the smooth charging algorithm. An example of how this smooth charging algorithm would look like is shown in Figure 4-1. During the first 1500 seconds the battery voltage rises from a deeply discharged 2.5V to about 4V as indicated by the solid blue curve. In this phase the impedance will drop from its maximum value to the minimum value. The charge current is ramped up from the minimal value to the maximum value as shown by the green dash dotted curve. After reaching the maximum charge current the remaining charge profile is similar to the classical CCCV method. The current will smoothly drop to zero when the battery is fully charged.

4-3 Simulation setup

In order to compare the smooth charging algorithm with the classic CCCV method both algorithms are simulated in a Matlab/Simulink environment. To model the battery the Simulink

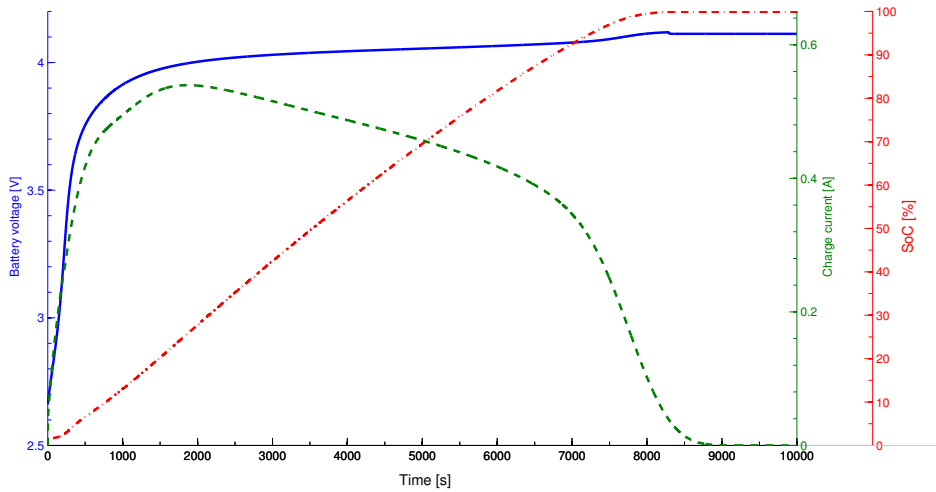


Figure 4-1: Charging of Li-ion cell according to the smooth charging algorithm. The solid blue line shows the battery voltage during charge versus the charge time. The green dashed line shows the charge current versus the charge time. The red dash-dotted line shows the State of Charge (SoC) of the battery versus the charge time.

battery block is used with the battery type set to lithium-ion. The rated capacity is set to be 1Ah so that maximum charge currents can be easily scaled to the battery capacity using the C-rate. For both charge algorithms a control loop was constructed with the appropriate sources. We will discuss these in more detail in the sections below.

4-3-1 CCCV simulation

In order to simulate the CCCV algorithm a current source and a voltage source are used. A diode guarantees that the charge current can only flow in the battery and not through the voltage source. The diode also prevents discharging of the battery through the voltage source once the charger is switched off. An additional resistor representing the resistance of the battery leads is added. The simplified schematic of this simulation setup is shown in Figure 4-2

The current source is active in the first part of the charge cycle. The value of the source is controlled by Matlab code and is dependent on the battery voltage. Below 3V the charge current is set to 0.1C that equates to 0.1A since we set the capacity of the battery to 1Ah. Between 3V and 4.1V the current is set to 0.5A based on the maximum advised charge rate of a EagelPicher medical grade rechargeable battery [14]. As soon as the battery has reached the 4.1V the current source is set to zero and charging is continued by the voltage source. The value of the voltage source is now set to 4.1V, the maximum charge voltage of the EagelPicher battery [14]. Once the charge current of the voltage source has dropped to 10% of the maximum charge current, 50mA in this situation, the charger is switched off and the battery is considered fully charged.

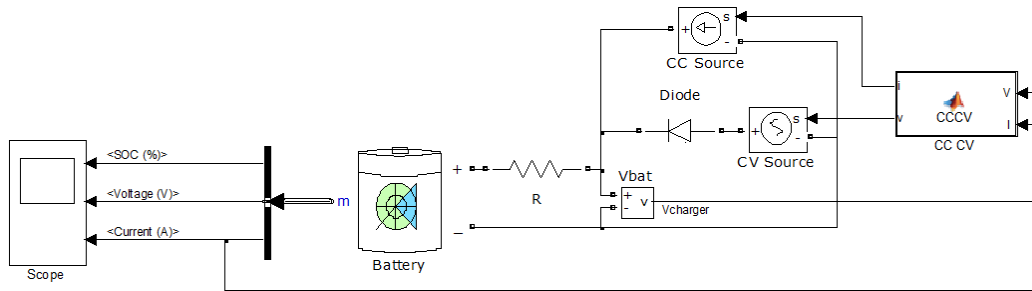


Figure 4-2: Simplified schematic of Simulink model of the CCCV charge algorithm.

4-3-2 Smooth charging simulation

For the smooth charge simulation only one controlled source is needed to charge the battery. In theory it does not matter if the controlled source is a voltage source or a current source. However, the nature of our charge algorithm is such that the charge current needs to be depended on the SoC which can be represented quite accurate by the battery voltage. Therefore we chose to sense the battery voltage and control a current source. The diode we needed in the previous simulation can be omitted since a current source has a (infinite) high internal impedance and does not allow current to flow from the battery back to the source. The only components needed are a battery, a resistor representing the battery leads, a controlled current source and a control loop. In Figure 4-3 a simplified schematic of the simulation setup is shown.

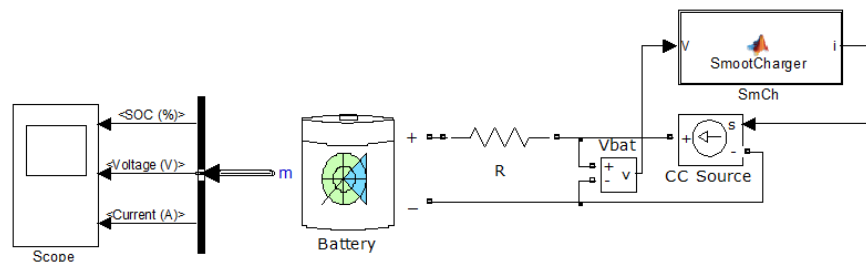


Figure 4-3: Simplified schematic of Simulink model of the smooth charge algorithm.

During simulation the value of the current source is controlled depending on the battery voltage by exponential and polynomial equations obtained by curve fitting a smoothed CCCV profile. Important to note is that the exact value of the charge current is more important at the low SoC and high SoC and is allowed to deviate in the nominal region of the battery. This means that we allowed the maximum charge current to surpass the advised maximum rating of $0.5C$ in the region where the impedance of the battery is low. We assumed here that the advised rating is based on worst case (high impedance) conditions and that higher currents in the low impedance area will not damage the battery.

4-4 Simulation results

In Figure 4-4 and 4-5 the results of, respectively, the CCCV simulation and smooth charge simulation are shown. As can be seen from the red dash-dotted curves, both algorithms are capable of recharging the battery close to 100% SoC. Also the maximum voltage limit of 4.1V is maintained indicating that both provide safe charging. Which of the two provides optimal charging is evaluated next.

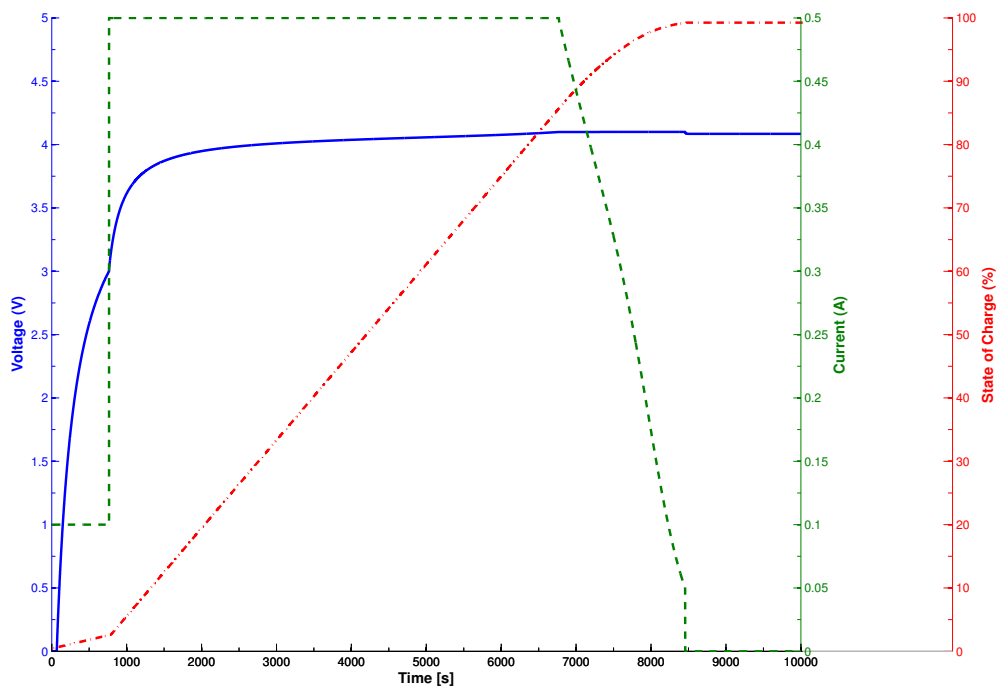


Figure 4-4: Results of Simulink simulation of the CCCV charge algorithm. The solid blue line shows the battery voltage during charge versus the charge time. The green dashed line shows the charge current versus the charge time. The red dash-dotted line shows the State of Charge (SoC) of the battery versus the charge time.

4-4-1 Charging time

In Table 4-1 the charge time in seconds of the CCCV algorithm and smooth charging algorithm are shown. Two different comparison points are chosen. First we compare the time it takes to get the system ready for use after a deep discharge situation. For this situation restoring only 33% of the charge is considered enough for a patient to use their stimulator with minimal interference of their regular activities. This is based on a system that is designed to be recharged daily. We assume that a system like this can run a full 24 hour day if the battery was completely charged. Charging one third will thus give the patient 8 hours of runtime before recharging is needed.

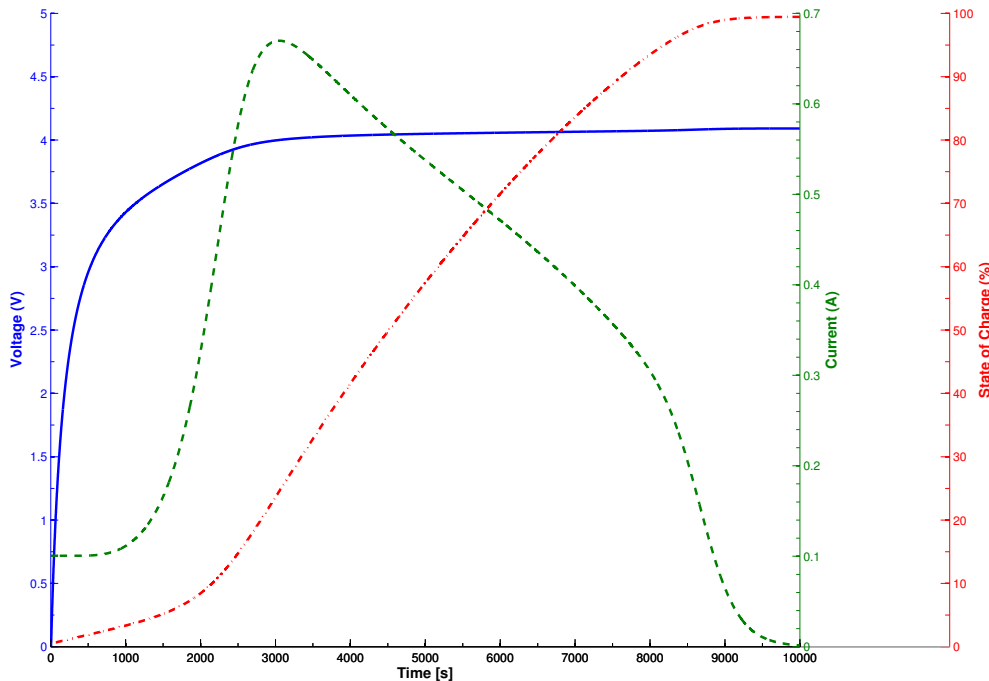


Figure 4-5: Results of Simulink simulation of the smooth charge algorithm. The solid blue line shows the battery voltage during charge versus the charge time. The green dashed line shows the charge current versus the charge time. The red dash-dotted line shows the State of Charge (SoC) of the battery versus the charge time.

We also compare the time it takes to do a full charge. Since the CCCV algorithm is usually cut off when the current has dropped to 10% of the initial current, the battery will never reach exactly 100% SoC. This is why we compared the two algorithms at 99% SoC. Both algorithms are capable of reaching the 99% SoC and it is still close enough to the 100% SoC to consider it a full charge.

Ready to use (33%SoC)

As can be seen in Table 4-1 the Smooth algorithm takes 557 seconds (about 9 minutes) longer than the CCCV algorithm to reach the 33% SoC level. The difference can be explained by comparing the current profiles of the two algorithms shown by the green dashed curve in Figure 4-4 and 4-5. For convenience the two current profiles are shown in one plot in Figure 4-6.

While the CCCV charger is in the trickle charge phase, the two charge currents are comparable and both charger charge at the same rate. After the trickle charge phase, the CCCV charger abruptly switches to the maximum charge current of 0.5A while the smooth charge is still slowly increasing the current. The smooth charge algorithm is therefore slower in reaching a usable 33% SoC.

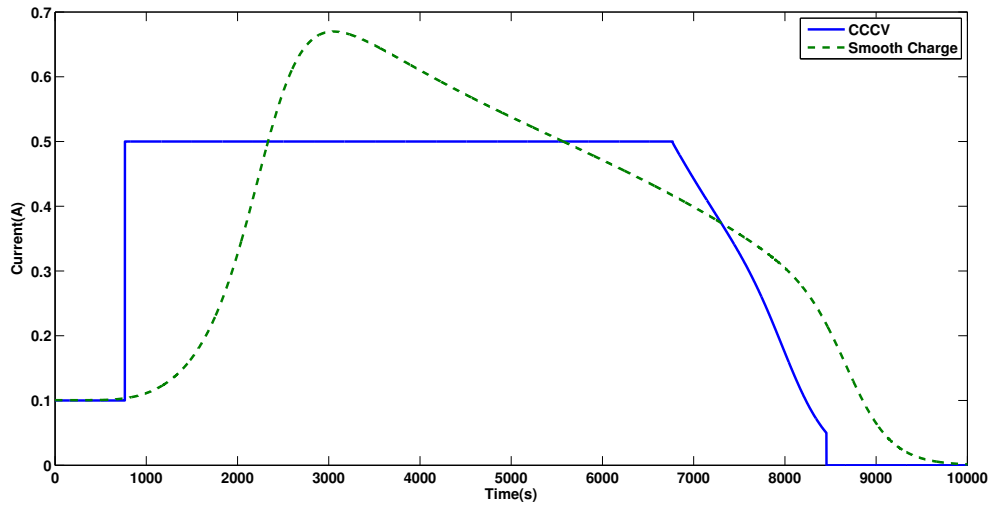


Figure 4-6: Current profiles of the CCCV and Smooth charge algorithms.

Full charge (99%SoC)

Also for a full charge, the smooth algorithm is slower than the classic CCCV algorithm. About 12 minutes after the CCCV algorithm has reached the 99% SoC level the smooth charge algorithm follows. Part of this delay is caused due to the slow charge rate of the smooth algorithm at low SoC. We already showed that the smooth charger is 9 minutes behind the CCCV algorithm after the first 33% SoC.

As shown in Figure 4-7 the smooth charger has a lower charge current in the first 12%SoC. Between the 12% and 65% the charge current of the smooth charger is actually higher than the current of the CCCV charger. In this region the smooth charger will thus charge faster than the CCCV charger and reduce the delay generated in the first 12%.

In the phase from 65% until 99% the smooth charger will actually again charge at a slower rate than the classical CCCV algorithm. The whole cycle of 0% until 99% will take longer if we use the smooth charge algorithm making it a less attractive algorithm to choose.

However, in Chapter 2 we concluded that due to aging effects it is best to avoid the extreme high and extreme low SoC's. A typical cycle therefore is limited between the 10% and 90%. As shown in Table 4-1 a 10% to 90% cycle is actually faster using the smooth charge algorithm.

\	0% - 33% SoC	0% - 99% SoC	10 - 90%SoC
CCCV	2953	8318	5785
Smooth	3510	9030	5462

Table 4-1: Comparison of charge time in seconds of CCCV and smooth charging algorithm until 30% and 99% SoC

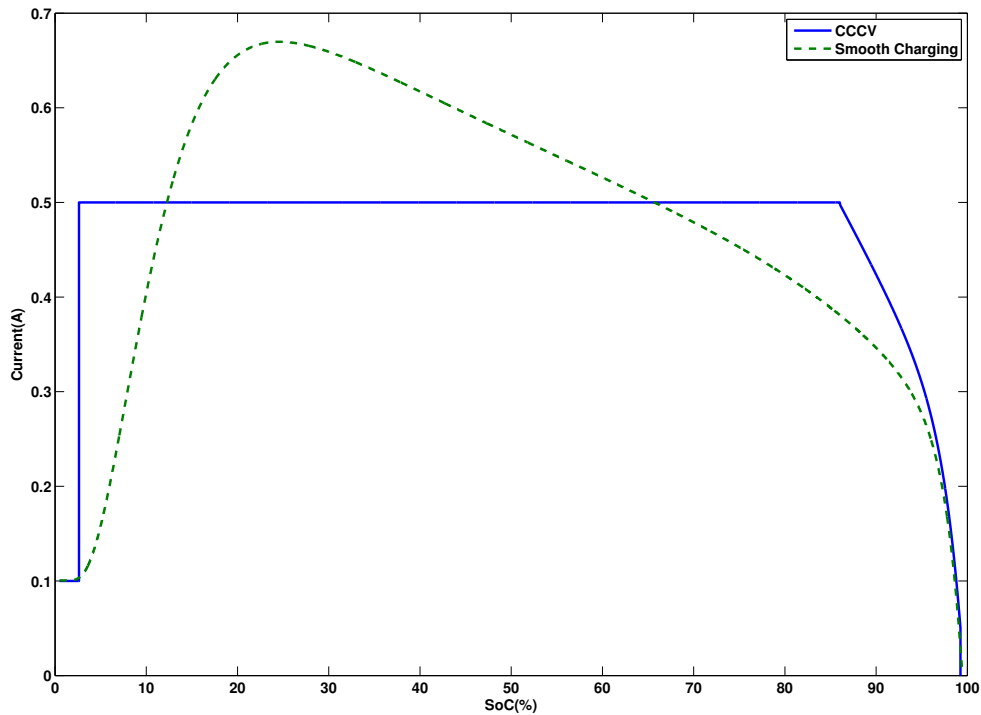


Figure 4-7: Current profiles of the CCCV and Smooth charge algorithms versus the State of Charge.

4-4-2 Power consumption and over-potential

During charging, the battery voltage measured at the terminals will be slightly higher than the actual Electro Magnetic Force (EMF) of the battery at the current state of charge. Due to the internal impedance and various other chemical effects not all the energy supplied to the battery, by either of the charge algorithms, can be absorbed. The energy that is lost due to the voltage drop results in heating of the battery that may even cause damage. All charge algorithms suffer from these losses. How much energy is lost is however different for each charging method.

As can be seen in Figure 2-5 the internal impedance is not constant over the whole charge cycle of a battery. By carefully controlling the charge current we can thus control the energy lost in this impedance and in turn the heating of the battery. This is exactly the goal of the smooth charge algorithm as we explained before.

To compare the overpotential of the battery during CCCV charge or smooth charge we used the mathematical model developed by Pop et al.[40]. The resulting equation is shown in Equation 4-1. This equation can be used for both charging and discharging. During discharge the battery current I is considered positive and for charging negative. The value, unit and physical meaning of the other variables in Equation 4-1 are listed in Table 4-2. Note that the model is based on curve fitting measurements of a Sony US18500G3 Li-Ion battery. Since we have no measurement data available of a medical grade battery we assume that at least the

shape of the overpotential curve is similar but that the actual value might be different. Since we use the same model for both algorithms we can still make a fair comparison and conclude which of the two performs better.

$$\eta[V] = I \left[R_{\Omega k} + R_{Ik} + (R_d^0 + R_d^I) \left(1 - e^{-\frac{c_2 \sqrt{t}}{\tau_d}} \right) + \frac{(E_q^0 + E_q^I) \left(1 - e^{-\frac{c_4 Q_{in}}{\tau_q}} \right)}{[Q_{in}]^{n_0 + n_1}} \right] \quad (4-1)$$

In our simulation we scaled the charge present in the battery, Q_{in} , to the capacity of the US18500G3 battery. In this way we can use all the parameters described in [40] and repeated in Table 4-2. As shown in the table the parameters vary over temperature and curve fits at three different temperatures were made by Pop et al.[40]. Although our system will be operated inside the human body and thus at a body temperature of 37°C we used the 25°C parameters for the comparison. We take into account that a medical grade battery would be designed to operate at body temperature while the US18500G3, used for the modeling, was designed to operate at room temperature. To make sure the model represents a battery under normal operation conditions we used the 25°C parameters.

Parameter	5°C	25°C	45°C	Unit	Physical meaning
$R_{\Omega k}$	3.6310^{-1}	1.1110^{-1}	1.0810^{-1}	Ω	Ohmic battery resistance
R_{Ik}	$c_0 * I$	$c_0 * I$	$c_0 * I$	Ω	Kinetic battery resistance
c_0	-2.4010^{-1}	-2.0210^{-2}	-1.1610^{-2}	ΩA^{-1}	Constant
R_d^0	1.9910^{-1}	9.2410^{-2}	4.7710^{-2}	Ω	Diffusion battery resistance
R_d^I	c_1/I	c_1/I	c_1/I	Ω	Diffusion battery resistance
c_1	-1.1310^{-2}	-4.7610^{-4}	-7.8610^{-3}	V	Constant
c_2	1.00	1.00	1.00	\sqrt{s}	Constant
τ_d	3.4110^{-1}	1.05	7.7710^{-1}	s	Diffusion time constant
E_q^0	1.1010^{-7}	2.2110^3	1.0010^6	JA^{-1}	Energy that cannot be used
E_q^I	c_3/I	c_3/I	c_3/I	JA^{-1}	Energy that cannot be used
Q_{in}	variable	variable	variable	C	Charge present in the battery
c_3	1.4310^3	5.57102	5.9010^4	J	Constant
c_4	1.00	1.00	1.00	A^{-1}	Constant
τ_q	0.00	5.4210^{-2}	3.4110^{-3}	s	Overpotential time constant
n_0	1.37	1.81	3.27	–	Temperature coefficient
n_1	c_5/I	c_5/I	c_5/I	–	Temperature coefficient
c_5	2.6010^{-2}	1.0610^{-2}	2.4010^{-2}	A	Constant

Table 4-2: Parameters of battery overpotential model for different temperatures

Figure 4-8-a shows the result of the overpotential simulation. Since we are investigating a charge situation the value of the battery EMF is lower than the potential measured at the terminals. The battery is thus in an underpotential situation which is represented here with a negative overpotential. The curve of the CCCV simulation shows a steep drop when the

charger switches from trickle charge to fast charge at 2.7% SoC. In this phase the smooth charger is still charging slowly resulting in a significant reduction of the difference between the battery EMF and terminal potential. We do have to note that at these low SoC the used models starts to deviates from the reality.

In Figure 4-8-b the energy that is lost due to the overpotential is plotted over the charge curve. Although the smooth charger has a reduced overpotential in the low SoC phase, the total energy that is dissipated in the battery over the whole cycle is slightly higher compared to the CCCV charger. Although the power lost might be reduced in the low and high SoC regions the charging is also slowed down by the reduced charge current. This means that when we integrate the power over time the net loss will actually be slightly higher if we use the smooth charger.

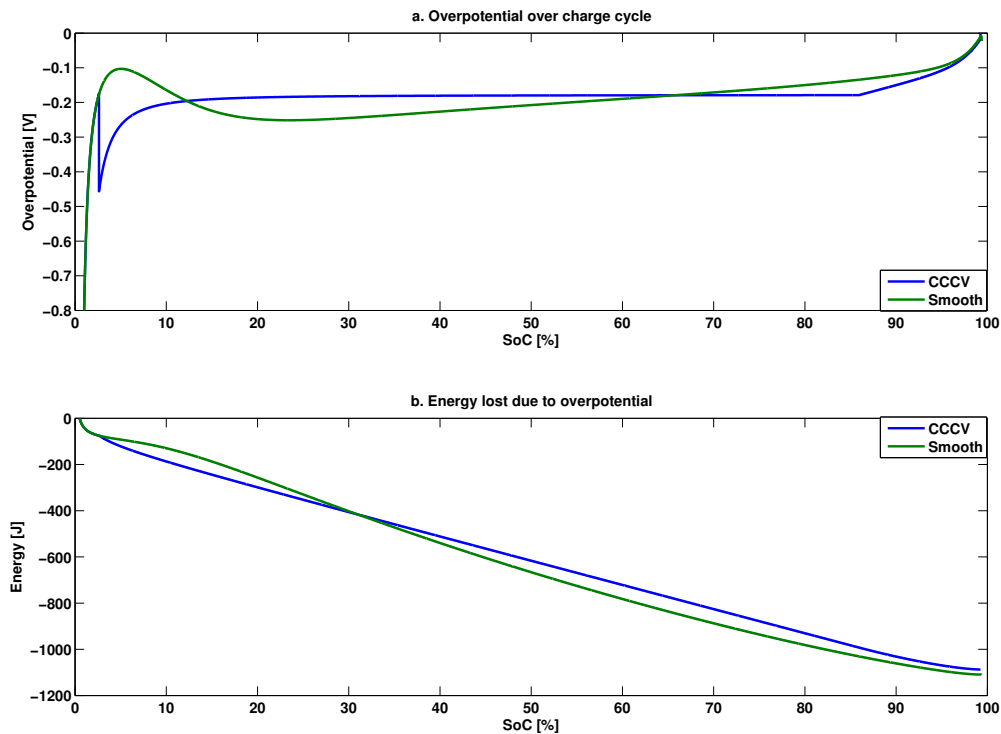


Figure 4-8: a. Overpotential over charge cycle. b. Energy lost due to overpotential.

4-4-3 Expected implementation complexity and cost

In order to compare the smooth charger algorithm with the CCCV algorithm on the bases of expected implementation cost and complexity we selected an published implementation of the CCCV algorithm as our benchmark. Bruno Do Valle et al. [41] developed an implementation of the CCCV algorithm specially for small size batteries that can be found in implantable devices. Since this circuit outperforms other available implementations we take the specifications described in [41] as our benchmark.

The specifications of the smooth charger will be estimated based on the system we simulated and depicted in Figure 4-3. The building block we will focus on is the polynomial control circuit. The controlled current source and references are left out of the comparison. These are considered to be equal for both algorithms and thus will not result in any advantage or disadvantage. The control circuit is however different for both algorithms.

Loop stability

As described before the CCCV charger sometimes shows unstable behavior around the switchover point from CC to CV. In [41] this switchover point is eliminated by clever design. Instead of abruptly switching over from a current source to a voltage source there is a smooth control of the charge current. By doing this there is only one control loop that mimics the behavior of a CCCV system without the stability problem. The switchover point from trickle charge to CC charge does not present any problems. Due to the increased charge current after the switch from trickle charge to CC the battery potential will be increased and force the system away from the switchover point.

Since the CC and CV phase are essentially controlled by a negative feedback amplifier we still need to check the loop stability in this phase. However, due to the low pass characteristic of the battery the loopgain is quickly reduced below unity for increasing frequency resulting in a stable operation. It is expected that the smooth charge controller will behave in a similar way.

Behavior over process variations

In [41] trimming of the voltage reference is incorporated in order to guarantee accurate operation over fabrication variation. Furthermore a process dependent parameter is used to determine the switchover point from CC to CV. This would mean that a redesign would be needed if the system is upgraded to another process technology.

Using a polynomial equation for the smooth charger would eliminate the need for redesign if other technologies are used. This loop can be either implemented in a digital manner by a micro controller or in the analog domain by means of a translinear loop. However both will suffer from fabrication variations. Since a high order polynomial is needed in order to guarantee low charge current at both the low and high SoC region, the polynomial is also sensitive to small deviations. If a microcontroller would be used the AD conversion would need to be accurate and probably trimming of the reference would be needed. If a translinear loop is used the transistors in this loop need to be well matched. It is thus expected that the smooth charger will be less dependent on technology but will suffer from fabrication variations.

Chip area

The chip area of a CCCV charger has been reduced to a minimum over many available designs. The whole control can be implemented by a few small size transistors and only the transistors carrying high current need to be of substantial size. For the implementation of the smooth

charger probably a bigger area is needed for the control logic. If the control is done digital a microcontroller will have to be implemented. For analog control by means of a translinear loop big size transistors will be needed to guarantee matching. The expected total chip size will, however, be dominated by the transistors carrying the full battery current. Since both the CCCV method and the smooth charging method need these high current transistors both designs will be approximately equal in size.

4-5 Conclusion

In the classical CCCV charger the U shaped internal impedance is not taken into account and the charge current is fixed over the whole CC phase. In the smooth charge algorithm the current is continually adapted to the state of the battery optimizing the charge current over the whole cycle.

Simulation however showed that due to the low charge current in the beginning and end of the charge cycle the smooth charger charges slower than the CCCV charger. The time needed to recharge 33% of the total capacity after a deep discharge is about 9 minutes longer for the smooth charger. Also fully charging the battery from a deeply discharged state takes 12 minutes longer if we use the smooth charge profile instead of the CCCV method.

We can see a significant reduction of the overpotential around the 2.7% SoC if we use the smooth charge algorithm. The time spent in this region is however extended due to the reduced charge current. The total energy that is lost due to the overpotential is therefore not reduced but instead slightly increased. Also the energy consumption of the smooth charger is thus worse compared to the classical CCCV method.

Due to the high order polynomial we used to implement the control large sensitivity over fabrication variations can be expected. Additional trimming circuitry or large transistors would be needed in order to cope with these variations. The overall circuit size will however be dominated by transistors that need carry the full battery current that are present in both designs. In terms of circuit size the two designs are equal but in terms of circuit complexity the smooth charger is outperformed by its predecessor.

We can conclude that the smooth charge algorithm as proposed in this chapter does not present any advantages over the classical CCCV charging method. It might be useful for applications where the charge current is substantially higher. Here the loss in the low SoC region might warm up the battery to dangerous levels. For our application the current is relatively low so that heating is not an issue. Also the temperature is well controlled by the human body. The classical CCCV method, especially with the stable switchover as described in [41], is still the best algorithm for our application. It provides safe charging with minimal energy loss in the battery and low implementation complexity.

System overview of charger

5-1 Introduction

In the previous chapter we concluded that the proposed smooth charge algorithm is not suitable for our application. Drawbacks like increased charge time, slightly higher energy consumption and larger expected chip area do not outweigh the benefits of a reduced battery overpotential. Although the instantaneous power loss is reduced by the smooth charge algorithm it is not expected that this translates into a lowered battery temperature and, with this, prolonged battery life. In our situation the battery is used inside the human body where the temperature is strictly controlled and thermal conductivity is good. If the battery is properly packed it will have no problem transferring the generated heat to the body before the temperature rises to a level that is dangerous for the battery or for the surrounding tissue.

Instead of the smooth charge algorithm the classical Constant Current Constant Voltage (CCCV) charging method was, and still is, a very suitable method for medical applications. However we also concluded that this method has some drawbacks that should be overcome. For example stability near the switchover point from the Constant Current (CC) phase to the Constant Voltage (CV) phase might be an issue. Since the CCCV method is the most widely used charging method for lithium batteries several techniques to overcome the stability issues have been developed over the years.

One technique to overcome the stability issues is to introduce a smooth transition in between the CC phase and the CV phases. Examples of this method can be found in [33] and [42]. Another option is the technique described in [41] where the two charge phases are completely deleted and only one control loop to control the charge current is used. The control loop has a hyperbolic tangent transfer so that the resulting charge curve is almost identical to the traditional CCCV charge profile. Since the method described in [41] provides safe battery charging and a simple, stable control with only one loop it is a good method for our system.

In this chapter we will present a charge system that implements the hyperbolic tangent charge curve. In Figure 5-1 a schematic overview of the designed system is shown. If we compare this system to an existing system as depicted in Figure 5-2 a couple of differences

should be noted. Firstly the inductive link that transfers the energy to the circuit inside the body is changed to a different topology. Secondly the charge current is regulated in a switched mode topology. Thirdly the need for an additional regulator is eliminated. In this chapter three key features of the system will be highlighted. First the increase in link efficiency will be discussed. Next the effects of the switched mode regulation are explained and finally the control loop is discussed. At the end of this chapter results of an Matlab/Simulink simulation will be presented that show correct operation of the proposed system.

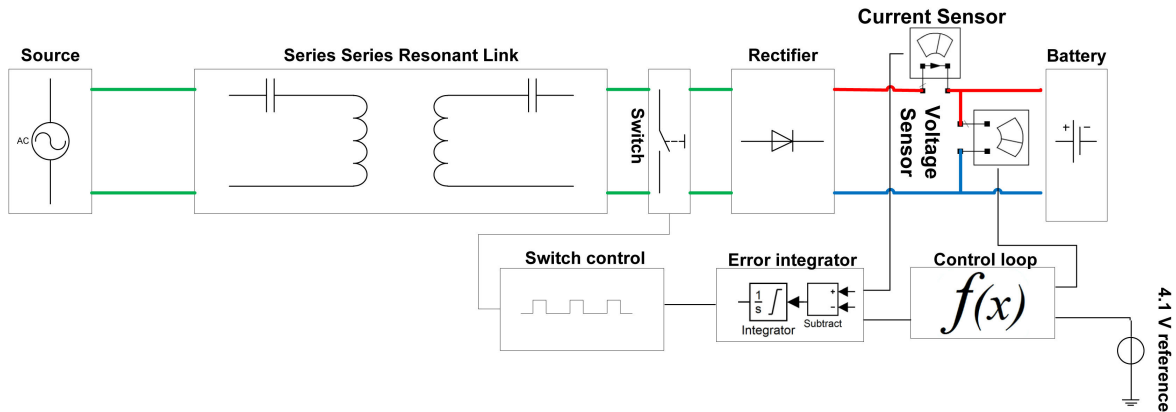


Figure 5-1: Schematic system overview of proposed charger. Current is regulated in a switched mode topology by periodically shorting an inductive link.

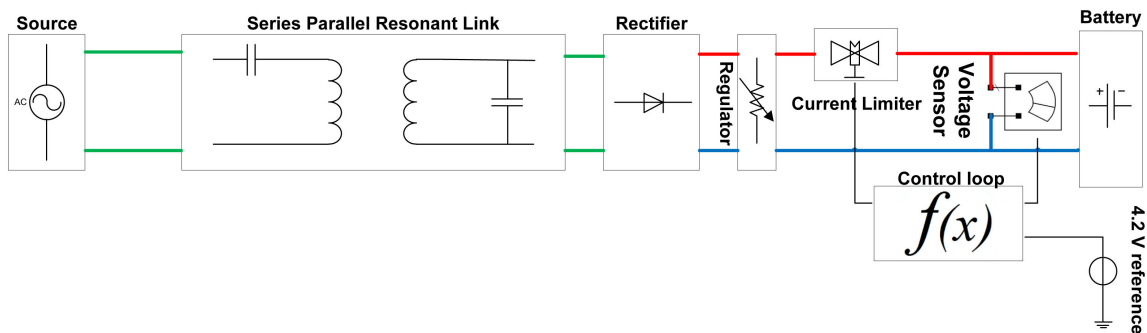


Figure 5-2: Schematic system overview of existing implementation as described in [41]. Input voltage is first rectified and regulated. The charge current is controlled by a current limiter.

5-2 Inductive link

Since our system is to be implanted inside the human body energy has to be transferred through the skin. A common method for doing this is by use of an inductive link. A basic inductive link consists of two inductors that are in close proximity. Due to this the two inductors will interact with each other. Current flowing in the primary winding will induce a voltage in the secondary and vice versa. The behavior is more or less similar to a transformer only in this situation the coupling between the primary and secondary windings is much

weaker than what you would normally see in transformers. The leakage inductance, the inductance that appears to be in series with the windings, is therefore relatively high. A circuit model of a basic link and the resulting equivalent model is represented in Figure 5-3

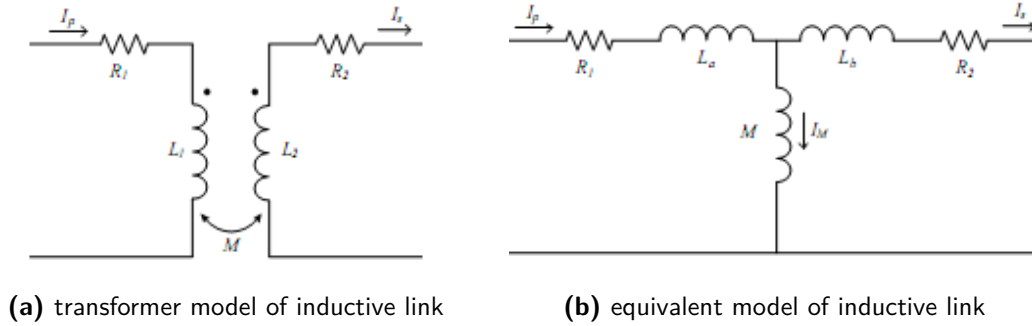


Figure 5-3: Transformer model and equivalent circuit of inductive link. The coupled inductors L_1 and L_2 are split up in a mutual inductance M and leakage inductances L_a and L_b . Pictures courtesy of Swagat Chopra [43].

If the operating frequency becomes high the leakage inductance becomes problematic. Large quantities of energy oscillate in the inductance while only a small portion is actually transferred to the load. This means that the used source needs to have a high VA rating in order to get a reasonable output to the load. Fortunately the leakage inductance can be compensated with a capacitor with a value such that the resonance frequency is equal to the operation frequency.

On the primary and the secondary side the compensation capacitor can be placed in series or in parallel with the link windings. There are thus four possible combinations for the compensated inductive link. The parallel-parallel link, the series-series link, the parallel-series link and the series-parallel link. Detailed analysis of the link is beyond the scope of this thesis, the interested reader is referred to [44] and [43]. Here, however, we will use the results of the analysis done by [44] and [43].

Links with parallel resonance on their secondary side have a voltage output where links with an series resonance on the secondary side have a current output [44]. Since most chargers, for example the system described in [41], use a voltage source input the parallel-parallel or series-parallel link is a suitable choice. The link efficiency of these types of links is given by Equation 5-1. Here R_L represents the impedance of the battery in series with additional circuitry like the rectifier. R_1 represents the resistance of the primary coil, R_2 the resistance of the secondary coil, L_b the leakage inductance of the secondary coil, M the mutual inductance of the windings that form the link and ω_0 the resonance frequency. If we design the resonance frequency ω_0 such that Equation 5-2 is satisfied we can maximize the link efficiency and simplify Equation 5-1 to 5-3.

$$\eta = \frac{R_L}{R_L + R_2 + \frac{R_1(L_b+M)^2}{M^2} \left(1 + \frac{R_2 R_L^2 M^2 + R_1 R_2^2 (L_b+M)^2}{\omega_0^2 (L_b+M)^2 M^2} \right)} \quad (5-1)$$

$$\omega \gg \frac{\sqrt{R_2 R_L^2 M^2 + R_1 R_2^2 (L_b + M)^2}}{(L_b + M)M} \quad (5-2)$$

$$\eta_{\max} = \frac{R_L}{R_L + R_2 + \frac{R_1(L_b + M)^2}{M^2}} \quad (5-3)$$

We can see from Equation 5-3 that the maximum link efficiency is, among others, dependent on the mutual inductance M . The mutual inductance of a coupled coil pair is given by Equation 5-4 where k is a coefficient between one and zero representing the amount of coupling between the coils, L_1 is the inductance of the primary winding and L_2 is the inductance of the secondary winding. Furthermore the leakage inductances can be calculated using Equations 5-5 and 5-6

$$M = k\sqrt{(L_1 L_2)} \quad (5-4)$$

$$L_a = L_1 - M \quad (5-5)$$

$$L_b = L_2 - M \quad (5-6)$$

Assuming for simplicity that the primary and secondary coil are equal we can simplify Equation 5-3 to 5-7 where $R_1 = R_2 = R$ and $L_1 = L_2 = L$. If we now consider that the coupling between the coils is usually weak ($k < 0.1$) we can show that the voltage type link needed for the existing chargers can only reach high efficiency if the load impedance is high ($R_L \gg \frac{1}{k^2}$). Unfortunately this is not the case for the large charge currents during the bulk of the charge cycle.

As an example we calculate the link efficiency for a battery at 4.0V that is being charged with an current of 25mA. We can represent the battery under these conditions as a load resistor of 160Ω. The difference is that instead of dissipating the supplied energy like an actual resistor, the battery is storing the energy making it available for later usage. Assuming the coil impedance to be 1Ω and the coupling factor to be 0.1 then, according to Equation 5-7, the maximum link efficiency is limited to just 1%.

$$\eta_{\max} = \frac{R_L}{R_L + R + \frac{R}{k^2}} \quad (5-7)$$

In order to improve the poor link efficiency the proposed system is designed for a current source input. Now a series-series or parallel-series link, that has an current output, can be selected. The maximum link efficiency of these types of links is given by Equation 5-8. If we again design the operating frequency to be reasonably high so that Equation 5-9 is satisfied the resulting maximum link efficiency is given by Equation 5-10. The efficiency of links with a series output are not dependent on the coupling between the primary and secondary coil but instead only on the load impedance and the parasitic resistance of the secondary coil. As long as we can keep the secondary parasitic resistance small the load impedance is allowed to drop without effecting the link efficiency too much.

$$\eta = \frac{R_L}{(R_L + R_2) \left(1 + \frac{R_1(R_2 + R_L)}{\omega_0^2 M^2}\right)} \quad (5-8)$$

$$\omega \gg \frac{\sqrt{R_1(R_2 + R_L)}}{M} \quad (5-9)$$

$$\eta_{\max} = \frac{R_L}{R_L + R_2} \quad (5-10)$$

Also on the primary side of the inductive link a series resonance compensation capacitor is selected. By doing this a source with a relative low voltage can be used. Furthermore, in the series-series topology the value of the primary compensation capacitor is only determined by the selected operation frequency and the self-inductance of the primary winding while for other topologies the value is also dependent on component values on the secondary side and the amount coupling between the two windings [43]. Since the amount of coupling can vary substantially this would mean that we have to tune the value of the capacitor over a wide range if we select an other topology while for a series-series link the value is fixed.

5-3 Switched mode current regulation

Many existing charger implementations use an inductive link with a voltage source output (for example [45] and [41]). Due to variations in the alignment and distance between the primary and secondary coil the output voltage will not be stable but instead will show substantial variations. Voltage regulators are used to stabilize the output to ensure proper operation of the battery charger. If we would connect the voltage output of the regulator directly to the battery the charge current would become unacceptable high during the bulk of the charge process. An additional block is therefore placed in series with the regulator and the battery that limits the current. Usually an MOS transistor is used and by controlling the gate of this transistor the current flowing into the battery can be controlled.

Although this current control is needed in order to guarantee safe charging it introduces large energy losses. During a large phase of the charge cycle the battery voltage will be at the nominal value of about 3.6V [14] while the voltage regulator supplies a constant 4.3V. This means that the difference of 0.7V is across the current limiter that, at the same time, is conducting the full charge current. The charger efficiency in this region will be limited to 83.7% and slowly increase when the battery voltage starts to increase. Over the full charge cycle this results in a limited average power efficiency of 89.7% that is reported in [41]. However losses in the regulator are not included in the efficiency. In situations where the output of the inductive link is high there will also be a substantial power loss in the regulator resulting in decreased system efficiency.

From switched mode power supply technology we know that changing from a linear regulation as described above to a switched mode topology can improve the system efficiency. The use of pulse charge techniques showed us that Lithium Ion (Li-Ion) batteries can handle large currents as long as the duration is short. Therefore the system proposed in this thesis allows the full current output of the inductive link to flow into the battery for a short pulse with duration D and short circuit the link output for duration $1 - D$. Since we used an series-series link with an current source like output we are allowed to short circuit the link without any negative consequences.

If we now keep track of the average current flowing into the battery and adjust the duty cycle D of our system accordingly we can regulate the current flowing into the battery. We are now able to adapt the charge current to the actual State of Charge (SoC) of the battery as well as compensate for variations in the output capabilities of the link. We have thus eliminated the need for a regulator and an additional current limiter. Excessive energy is no longer absorbed by the charge circuitry but instead reflected back to the source by the short circuited link.

5-4 Control

When the classical CCCV charge method is implemented, careful design is needed to ensure proper switchover from CC to CV. Some designs use two separate loops to control the charge voltage and the charge current and switch from one loop to the other. To ensure stable operation and prevent the charger from unnecessary switching between the two loops this switchover can be done gradually as presented in [33] and [42].

5-4-1 Hyperbolic tangent function

It is also possible to combine the voltage and current control in one loop. The result is a current control loop that is dependent on the battery voltage via a hyperbolic tangent function. This function is given in Equation 5-11 where A is a scaling factor to scale the current to the battery capacity, V_{ref} the end of charge voltage reference, V_{bat} the battery voltage and S a variable to determine the voltage where the charge current starts to decrease. Figure 5-4 shows a plot of this function with A set to one, the end of charge voltage set to 4.1 and S set to 0.05. The output of this function provides a reference for the charge current. For low battery voltages the current is high (1C) and remains flat until the transition point has been reached. This resembles the CC phase. After the transition point the charge current drops to zero while the battery voltage is hardly changing. This resembles the CV phase of the charge curve. The hyperbolic tangent function thus implements both the CC and the CV phase as well as the transition between the two phases.

$$I_{\text{bat}} = A \cdot \tanh\left(\frac{(V_{\text{ref}} - V_{\text{bat}})}{S}\right) \quad (5-11)$$

5-4-2 End of charge voltage reference

To prevent the battery from overcharging it is important that the used reference voltage is stable and well defined. If the reference is only a few millivolts higher, the battery will already be damaged due to overcharging. In some systems, like the one described in [41], the reference is therefore trimmed after production to the correct voltage to compensate for production variations. This prevents overcharging and ensures the battery is fully charged.

In this system, however, we choose to lower the reference voltage so that it will never reach dangerously high voltages and cause overcharging. Not even at the process corners of the used technology. The drawback of this is that the battery will not be fully charged and that a substantial amount of battery capacity remains unused. Due to the exponential rise in

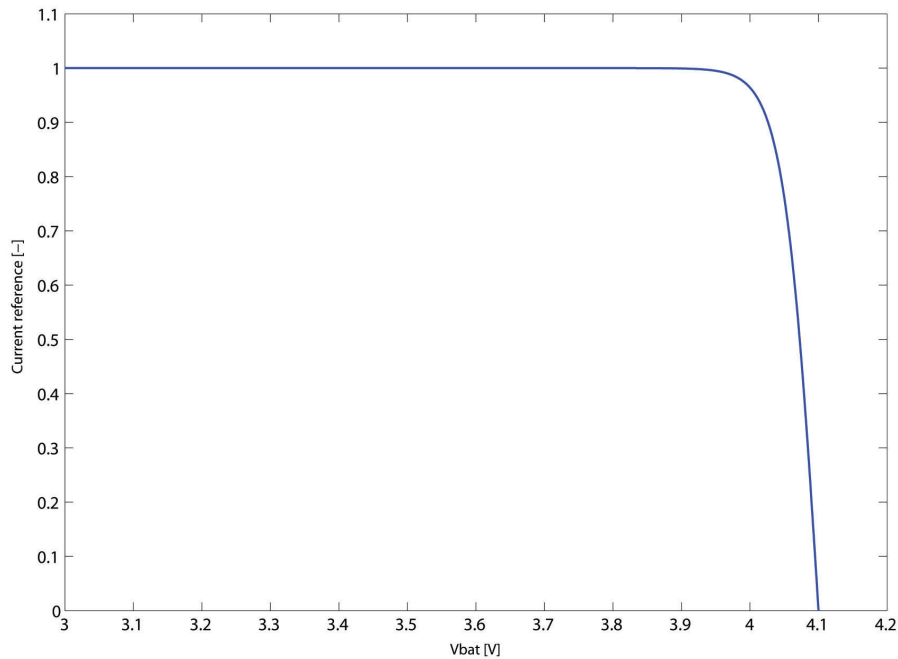


Figure 5-4: Hyperbolic tangent function for charge current control. Plot of Equation 5-11 with $A = 1$, $V_{\text{ref}} = 4.1$ and $S = 0.05$

battery voltage near the end of charge, a reduction of only 1% in end of charge voltage will already cause a 7% drop in usable capacity [46].

Besides the drawback of reduced usable battery capacity, lowering the end of charge voltage can be beneficial over multiple cycles. In Section 2-6-1 we showed that continuous use at high SoC results in faster aging of the battery. Lowering the end of charge voltage will prevent the battery from reaching high SoC and hereby eliminating the aging processes that are related with high operating voltages. Although the battery must be recharged more frequently if the end of charge voltage is lowered, the performance of the battery is more stable over time. Since we are designing a system that has to be implanted inside the human body it is extremely difficult to replace the battery. Performance over many years is thus considered more important than the runtime of one single charge.

5-5 Simulation result

In order to verify the correct operation of the system, a simulation in a Matlab/Simulink environment has been performed. The goal of this simulation was to, first of all, check if the system is able to safely and completely charge a battery. Furthermore we need to verify if the power consumption of the system is indeed lowered once the output of the inductive link is short-circuited. After this we also make some predictions about the overall system efficiency.

In order to be able to compare the results of the simulation to the performance of the prototype we are about to build we used realistic component values for our simulation. The battery to

be charged was set to a capacity of 150mAh, the maximum charge current was set to 25mA and the end of charge voltage to 4.1V. The parameters for the inductive link were chosen on the bases of existing implementations and are listed in Table 6-1. We start now with presenting the complete charge curve that resulted from the simulation.

5-5-1 Charge curve

In Figure 5-5 the battery voltage and current have been plotted versus the SoC of the battery. As can be seen the battery charge current is approximately the maximum allowed 25mA over a large range. It should be noted that, at this design stage, no trickle charge phase for deeply discharged batteries was implemented. This is why the charge current is already at the maximum level while the battery voltage is still well below the 3V threshold for safe fast charging.

When the battery is nearing the end of charge reference the control loop starts to decrease the charge current. the shape of the charge current curve closely resembles the hyperbolic tangent function as plotted in Figure 5-4. At 100% SoC the battery has reached the end of charge voltage and the current has dropped to zero. This indicates that the system is able to safely and completely charge the battery.

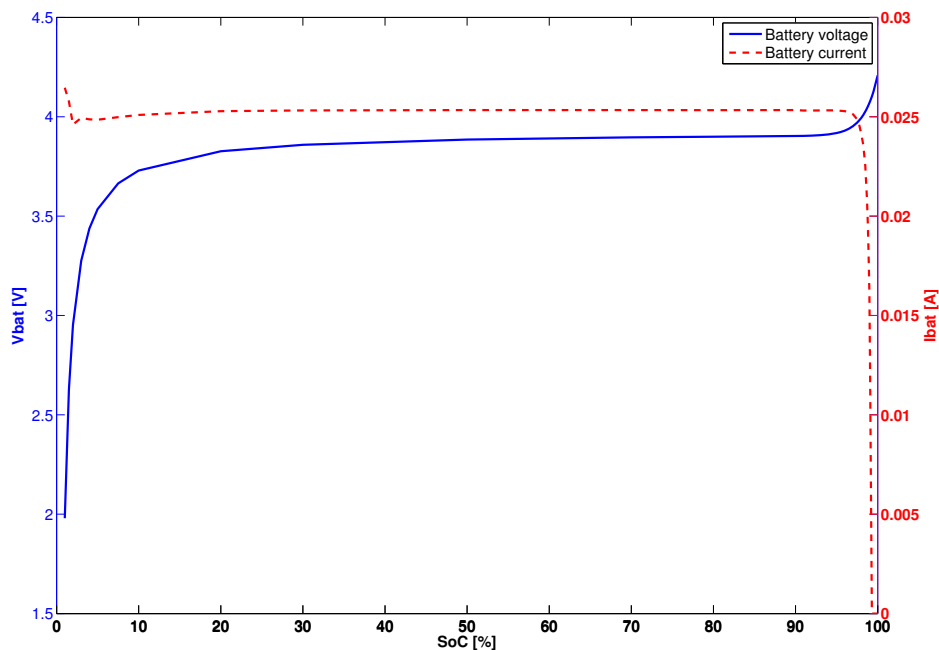


Figure 5-5: Charge curve of proposed charge system simulated in Matlab/Simulink. The solid blue line shows the battery voltage versus the SoC of the battery. The dashed red curve shows the charge current versus the SoC

5-5-2 Power consumption

In Figure 5-6 the power at three different positions in the system is plotted when the battery is at about 50% SoC. In this region the charger is short-circuiting the link periodically to maintain the average charge current at the maximum 25mA. When the switch control signal is low the short-circuit switch is open and current is allowed to flow into the battery. We can see from the plot that in this state power is being absorbed by the battery. Due to losses in the rectifier between the inductive link and the battery, the power delivered by the link during this period is slightly higher than the power absorbed by the battery. Due to losses in the inductive link the power delivered by the external source is even higher.

Once the switch control signal goes high the short-circuit switch is closed and the output of the link is shorted. We can see that the power delivered by the link is close to zero. Since the rectifier is now no longer conducting, no power is absorbed by the battery. Also the power delivered by the external source is lowered, however does not drop completely to zero. There is still power being dissipated by parasitic resistances of the link windings and switch.

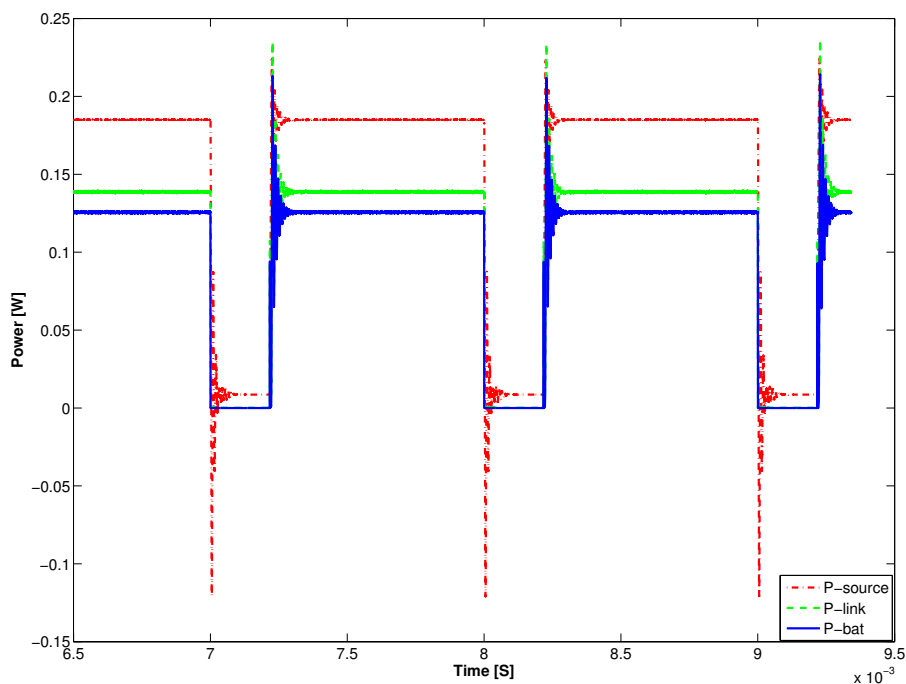


Figure 5-6: Decrease in power delivered by the source once link is short-circuited at secondary side. The red dash-dotted line shows the power delivered by the external source. The green dashed line shows the power at the secondary side of the inductive link. The solid blue line shows the power absorbed by the battery.

5-5-3 System efficiency

By averaging the delivered and absorbed power over a large number of pulses we can calculate the average power consumption and charger efficiency. In Figure 5-7 the average power, at

three different points in the system, is plotted versus the battery SoC. By dividing the output power of the inductive link by the power delivered by the external source we obtain the efficiency of the inductive link. Dividing the output power of the link by the power absorbed by the battery the efficiency of the charger system is obtained.

The two efficiency curves are plotted in Figure 5-8 versus the state of charge of the battery. The inductive link reaches an efficiency of approximately 64% over a large part of the charge curve. Nearing the end of charge the efficiency drops due to the decrease in charge current. Now the output of the link is short-circuited most of the time and hardly any power is transferred. The efficiency is thus dominated by the losses in the parasitic resistances of the coil windings.

The expected efficiency of the selected link can be calculated using Equation 5-10. Using the component values from existing implementations (listed in Table 6-1) we can determine that the link should have an efficiency of 99.7%. The difference between the maximum efficiency and the obtained efficiency can be explained using Figure 5-6. We can see that already at a SoC of 50% the link is periodically shorted to maintain the charge current below the maximum allowable value. For short periods of time the link is thus shorted and no power is transferred to the charger circuit. There is however power dissipated in parasitic resistances of the coils that has to be supplied by the source. There are thus periods where there is no (useful) output power where there is still some input power. The average power transfer efficiency is therefore significantly lowered.

Furthermore the operating frequency is only six times the minimal frequency. Equation 5-9 is thus not fully satisfied and the simplified equation, Equation 5-10 is not completely valid. Instead we should use Equation 5-8 to calculate the link efficiency. The Simulation showed that the average transfer efficiency over the full charge cycle is lowered to 64.7% due to the relative low operating frequency and periodically shorting of the link.

The efficiency of the charger circuit peaks at a value of 90.7%. Although existing implementations like [41] report a value of 89.7% the two systems cannot be compared. In the proposed system the efficiency is limited by the voltage drop over the rectifier block. In [41] the rectification function is not included in the charger circuit and thus should be implemented separately. Taking this into account the specified efficiency of 89.7% should be multiplied with the rectifier efficiency before the systems can be compared.

Furthermore, in [41] the average efficiency over the full charge cycle is specified. This number is not simply an average of the curve plotted in Figure 5-8. Instead we also need to take the duration of each charge phase into account. Also the exact properties of the inductive link influences the average charge efficiency since they influences the duty cycle of our system.

By calculating the charge time for each data point we can estimate the average charger efficiency over the full charge cycle. Due to the low efficiency near the 100% SoC the average charger efficiency is 90.2%. Over the full charge cycle the proposed charger performs approximately equal to the charger reported in [41] but does include more functionality.

5-6 Conclusion

For optimal battery cycle life and implementation simplicity a charger system that implements the classical CCCV charge algorithm in a special manner is proposed. When the charge

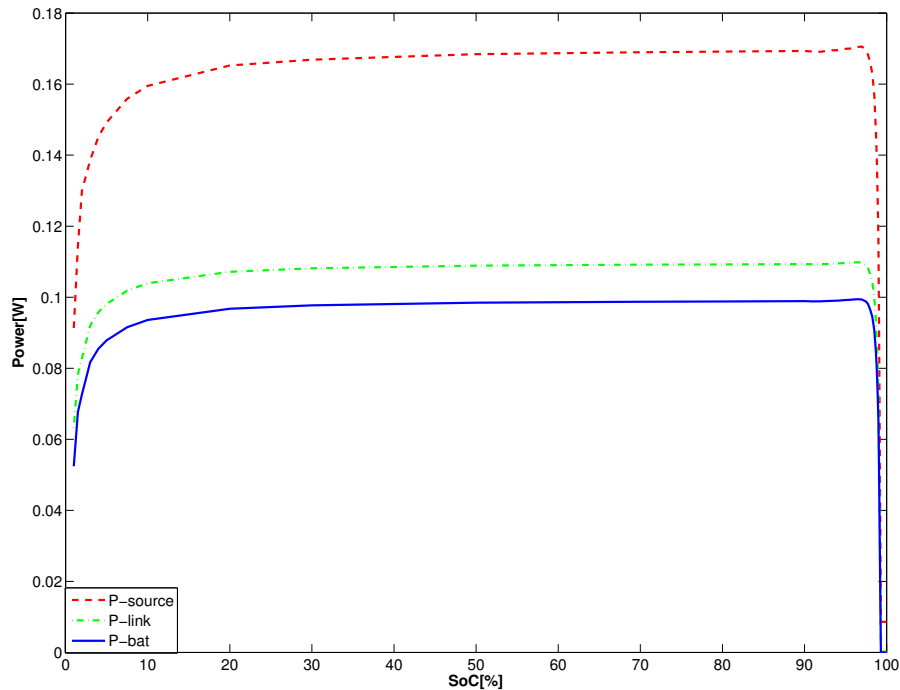


Figure 5-7: Power consumption of proposed charge system over a full charge cycle simulated in Matlab/Simulink. The red dash-dotted line shows the power delivered by the external source. The green dashed line shows the power at secondary side of the inductive link. The solid blue line shows the power absorbed by the battery.

current is controlled by only one control loop, possible stability problems that might occur when switching from the CC phase to the CV phase are eliminated. The different control loops are combined in one hyperbolic tangent function that determines the desired charge current dependent on the voltage of the battery.

A key feature of the system is the inductive link with a series-series topology. The current source like output better fits the need for a battery charger resulting in a higher maximum efficiency. Furthermore the current control is done in a switched mode topology. By tracking the average charge current the need for an additional regulator, to regulate link variations, has been eliminated.

Reduction of the end of charge voltage reference eliminated the need for additional trimming to prevent overcharging of the battery. Operation at high SoC has been prevented resulting in an increase in battery cycle life. Although the runtime on one single charge is reduced the performance of the battery is more stable over many cycles. Since the battery can only be replaced by surgery to the patient, performance over many cycles is considered more important.

Simulation of the system in a Matlab/Simulink environment has been performed. Results of this simulation showed that the charge current profile follows the desired hyperbolic tangent function. At low battery voltages the charge current is at the maximum allowable level and

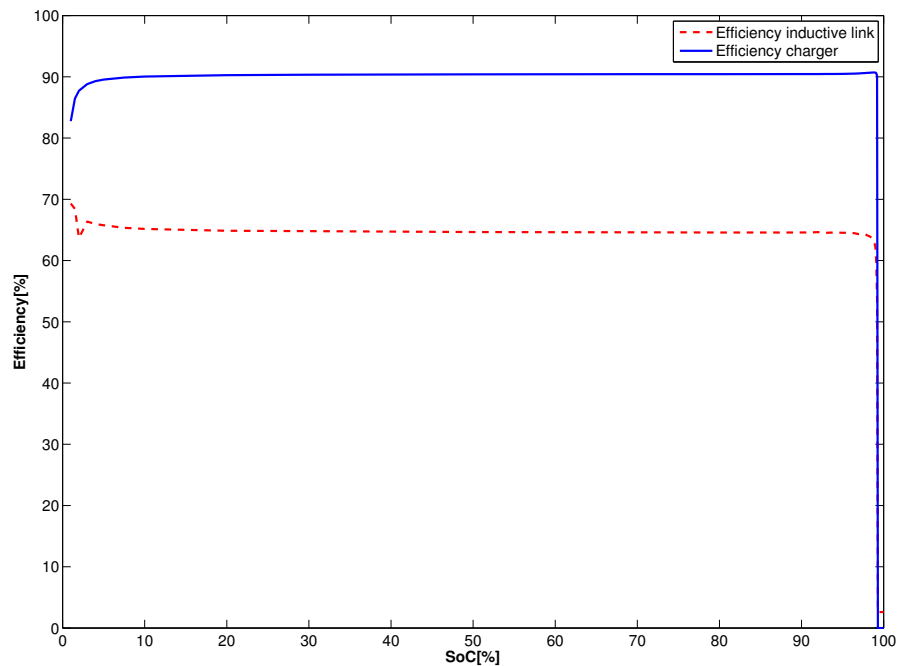


Figure 5-8: Link efficiency and charger efficiency of proposed charge system over a full charge cycle simulated in Matlab/Simulink. The red dash-dotted line shows the efficiency of the inductive link. The solid blue line shows the efficiency of the power transfer from the link output to the battery.

as soon as the battery is nearing the end of charge voltage the charge current is reduced.

Although in theory the efficiency of the selected inductive link should reach 99.7% the results of the simulation shows an efficiency of 64% over a large range. The difference is explained by taking the short periods where the link is short-circuited, and the limited operating frequency, into account. The circuit between the link and battery reaches a peak efficiency of 90.7%. The efficiency is limited by the voltage drop over the rectifier.

An Existing implementation report efficiency of 89.7%. These systems however do not include all functionality that is included in the proposed system. It is therefore not possible to compare these numbers directly. If the efficiency of other essential parts is taken into account the systems still cannot be compared. The exact properties of the inductive link as well as the time spent at each charge phase have to be known. Averaging the simulated data over a full charge cycle results in a charger efficiency of 90.2% which is approximately equal to the previously reported value. Since the existing system does not include rectifier functionality, it is to be expected that the overall system performance of the proposed system exceeds the performance of the existing implementations.

Hardware implementation

6-1 Introduction

In the previous chapter we introduced a new battery charger at system level and divided the system in different blocks (see Figure 5-1). Details about the exact implementations of the different building blocks were not discussed yet. In this chapter we will review the sub-parts of the system and select the proper components for their implementation. In order to be able to select the proper dimension for the various components, we assumed the same battery characteristics as used for the Simulink simulation of the previous chapter.

Since the charge circuit is designed to be a sub-part of an Implantable Pulse Generator (IPG), and needs to be as small as possible, we will implement as much as possible in an Integrated Circuit (IC). During the selection of the IC technology, compatibility with other subparts of the total IPG need to be considered as well. As a consequence the selected technology need to be capable of handling high voltage (over 15V) to implement the stimulation output stage [29]. Furthermore the digital control logic as well as analog sensing circuits has to be fabricated in the same technology.

Considering that not all the specifications of other sub-parts are known at this point, we did not select the optimal technology for the total IPG in this thesis. Due to previous experience from numerous designers within the group the AMS H18A4 18 μ M technology was selected for our implementation. This technology offers high voltage devices (over 50V) as well as low voltage (1.8V). Both MOS and bipolar devices are supported making the technology very versatile.

Due to this versatility it can be expected that all the sub-parts of the total IPG can be implemented in this technology and that the design, as presented in this thesis, can be used for a first prototype of the complete system. After the first total design is tested the choice of IC technology can be evaluated and changed if desired. First, however, we concentrate on the design of the charger circuit.

In the following sections we will go over the charger system block by block and select the proper components that are available in the selected technology. In the end we will present

results of an circuit simulation run in the Cadence Virtuoso Analog Design Environment that shows correct operation and gives some predictions on charger efficiency. We start our discussion with the implementation of the inductive link that forms the contact-less supply of the circuit.

6-2 Inductive link

As discussed in the previous chapter the inductive link should be implemented using a series-series topology in order to achieve maximum efficiency. This maximum efficiency, however, can only be reached if the selected operating frequency is high enough as stated by Equation 5-9. We can see from this equation that the minimal operation frequency depends on the resistance of the load (R_L) and the coil windings (R_1, R_2) but also on the mutual inductance of the primary and secondary winding (M).

The mutual inductance of the coil windings is in turn dependent on the coupling coefficient (k) and the self-inductances of the primary and secondary coil (L_1, L_2) as stated by Equation 5-4. If we combine Equations 5-9 and 5-4 we end up with Equation 6-1. When we fill in realistic component values we can calculate the minimal operation frequency ω_{\min} .

$$\omega_{\min} \gg \frac{\sqrt{R_1(R_2 + R_L)}}{k\sqrt{(L_1 L_2)}} \quad (6-1)$$

To get an indication of the component values that can be achieved in the actual design, an existing implementation together with battery datasheets were used. The component values used for our calculation can be found in Table 6-1. Here we assumed that the load resistance is dominated by the battery and that the resistance of the rectifier block, that is in series with the battery, can be neglected. If we fill in the component values from Table 6-1 we can show that the operation frequency ω should be higher than 2.17Mrad or 345kHz.

\	Value	Unit	Source
R_1	5	Ω	implementation [47]
L_1	51.3	μH	implementation [47]
R_2	3.7	Ω	implementation [47]
L_2	24.24	μH	implementation [47]
R_L	160	Ω	*
k	0.1	-	implementation [48]

Table 6-1: Component values for calculation of the link operating frequency. * R_L is based on a battery at 4.0V absorbing a charge current of 25mA. The equivalent load impedance would be $R_L = \frac{V}{I} = \frac{4[\text{V}]}{0.025[\text{A}]} = 160[\Omega]$.

Besides this minimal frequency we should also consider the maximum frequency of the coils itself. Above a certain frequency the parasitic capacitance between the coil windings will start to dominate. The coil will then no longer behave as an inductor but instead shows a more capacitive behavior and may resonate on its own. To avoid this operation, the frequency of the inductive link is selected to be approximately six times the minimal frequency at 2MHz.

6-2-1 Primary side

Since the primary coil is not to be implanted in the patient, the size requirements of the primary side inductor are not very strict. No IC technology is required here and the implementation can be done using regular of the shelf components. The optimal coil diameter is however dependent on the diameter of the secondary coil and the required operating distance [44]. The exact details on how to optimize the geometry of the coil is beyond the scope of this thesis.

The value of the primary resonance capacitor is, as mentioned in the previous chapter, only dependent on the operating frequency and the primary inductance. By using Equation 6-2 and the component values from Table 6-1 we can calculate that the primary capacitor should be 223pF.

$$C_1 = \frac{1}{\omega^2 L_1} \quad (6-2)$$

6-2-2 Secondary side

On the secondary side, inside the human body, the available volume is limited. Integrating all components into one single IC is therefore desirable. However, fabricating coil windings with a good quality factor in IC technology is challenging. Also important properties of the inductive link depend greatly on the coil geometry and placement.

In order to have more flexibility in the placement and geometry of the coil it is best to keep the secondary coil off chip. Now a small wire wound coil can be integrated in the casing of the device in such a way that the coupling between the primary and secondary winding is maximized.

Also the secondary resonant capacitor may be placed off chip due to the large size and voltage rating that are needed. Since the secondary coil is small the self-inductance will be limited. As can be seen from Equation 6-3 the capacitor value is proportional to $1/L_2$. This means that a small inductor value implies that the secondary capacitor need to have a high value.

Using the values from Table 6-1 and Equation 6-3 we can determine that, for the selected operating frequency, the secondary capacitor should have a value of 261pF. Implementing this capacitor on chip would consume an area of thousands of square micrometers. Compared to the rest of the circuitry this is an extremely large area. In for example [41] only 0.16mm² is used for the total charger circuit.

Because the inductive link is driven by an AC source and the capacitor and inductor are in resonance, large voltages, both positive and negative, appear across the capacitor. Especially when the quality factor of the inductor is high the voltage may resonate well above the breakdown voltages of standard on chip capacitors. Taking this into account it is best to use an off chip capacitor as well.

$$C_2 = \frac{1}{\omega^2 L_2} \quad (6-3)$$

6-3 Current regulation switch

The average charge current is determined by shorting the inductive link periodically as we explained before. In order to minimize energy loss during the shorted period and in order to prevent shorting of the battery, the switch is placed before the rectifier block.

The current that the switch needs to handle is in the same order of magnitude as the maximum charge current. For batteries of substantial size this can be from a few milliamperes up to one ampere. For our battery the maximum average current is 25mA. The transistors not only need to be capable of handling this current without device breakdown. They also need to provide an low impedance current path so that all the current flows through the switch, and not through the battery, when the switch is closed.

The voltage rating of the switch needs to be at least the maximum battery voltage plus any voltage drop that might appear over the rectifier during charge. The medium voltage transistors available in the selected $18\mu\text{M}$ technology are capable of handling up to 5.5V. Since a typical Lithium Ion (Li-Ion) is not allowed to be charged over 4.2V, and the EaglePicher medical grade rechargeable Li-Ion battery not over 4.1V [14], there is still over 1V headroom available if we use this medium voltage transistor. The cmhv7sf 5.5V NFET with a width of $100\mu\text{M}$ was used in this design. A separate DC simulation showed that the voltage drop over this transistor is no more than 100mV when the gate-source voltage is over 1.5V and a current of 100mA flows through the transistor.

6-4 Rectifier topology

Since the rectifier is the only block that is in series with the inductive link and the battery it will have to conduct the full charge current. Small voltage drops over the rectifier will therefore have a large influence on the total system efficiency. Careful selection of the rectifier topology is thus a must. Two different topologies were considered: a full bridge rectifier composed of Schottky diodes or an full bridge rectifier composed of MOS transistors. Both options will be discussed below.

6-4-1 Diode rectifier

An simple and effective rectifier topology is the full bridge rectifier composed of four diodes as shown in Figure 6-1. Efficiency of this topology is limited by the forward voltage drop of the used diodes. In the selected IC technology Schottky diodes with only 400mV forward drop are available. However, since during all phases two diodes are in series the combined voltage drop over the whole rectifier is 800mV.

An 800mV drop will limit the charger efficiency to just 78% when the battery is at an nominal voltage of 3.6V. The rectifier is always in series with the battery meaning that 22% ($0.8/3.6 = 0.22$) of the input power is lost. Replacing the diode with devices that have a lower forward voltage drop is therefore desired.

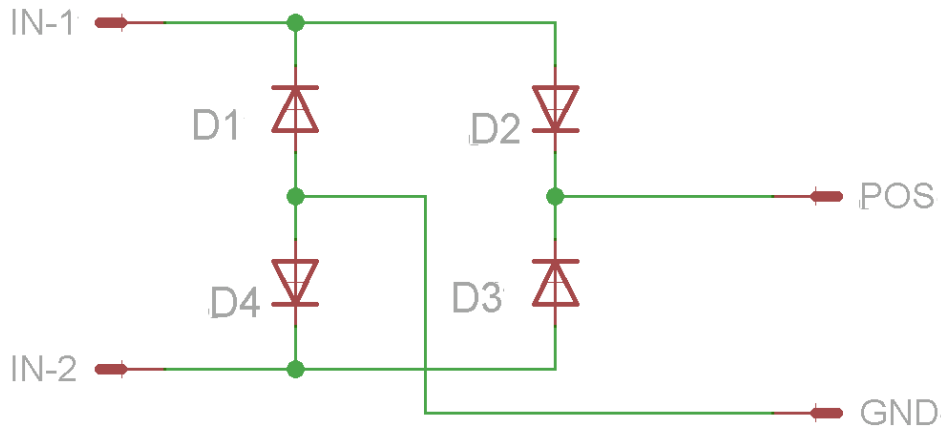


Figure 6-1: Full bridge rectifier composed of Schottky diodes.

6-4-2 MOS rectifier

MOS transistors that are switched at the proper instant can provide a rectifier function with a lower voltage drop. The resulting schematic is shown in Figure 6-2. Control of the transistor switching is done by observing the input signal. When the input is positive NMOS M2 and PMOS M4 are switched on while the other transistors are switched off. Similarly, when the input is negative, NMOS M1 and PMOS M3 are switched on and M2 and M4 are switched off.

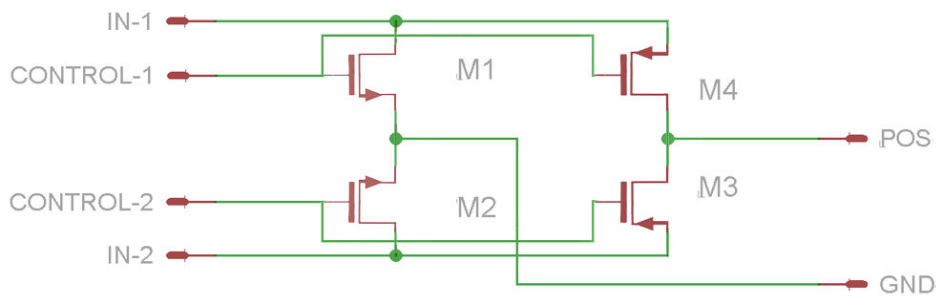


Figure 6-2: Full bridge rectifier composed of MOS transistors. Control logic not shown.

When the current is allowed to flow into the battery this type of rectifier provides a simple and effective rectification. However when the input is shorted by the current regulation switch, or when there is no input at all, problems may arise. In these situations there is no longer a usable input signal to control the switching of the MOS transistors. The consequence is that the transistors are switched at the incorrect moment. For example, both PMOS M3 and PMOS M4 may be switched on at the same time. This will short circuit the battery which

should, obviously, be avoided at all times. To solve this problem additional control logic that switches off all the transistors during this situation can be used. Also an additional diode to prevent discharging can be placed. The latter option led to the idea to combine the MOS rectifier concept with the diode rectifier concept.

6-4-3 MOS diode hybrid rectifier

By replacing only half of the diodes with MOS transistor switches, discharging of the battery can be prevented at all times. The resulting schematic is shown in Figure 6-3 where the two PMOS transistors are replaced by Schottky diodes. Still the total voltage drop is reduced compared to the full diode rectifier while protection of the battery against discharging via the rectifier is guaranteed.

For the two NMOS transistors the same type and size transistors as used for the current regulation switch were selected. Since the used transistors are symmetrical they can also be used to short circuit the inductive link by switching on M1 and M2 at the same time. When this is implemented, the large size transistor of the current regulation switch may be omitted at the cost of only a few small components for additional control logic.

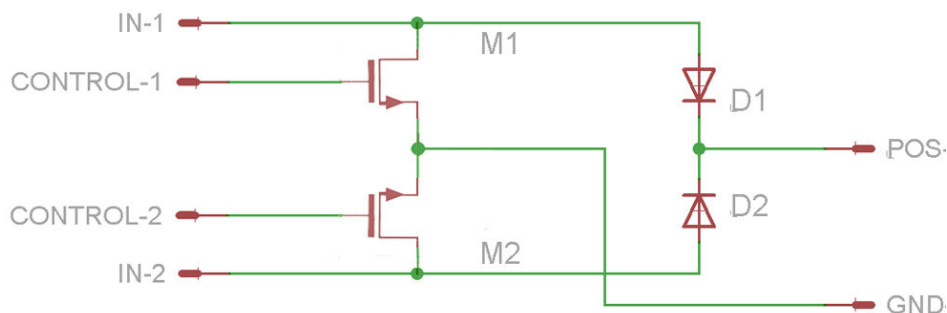


Figure 6-3: Full bridge rectifier composed of MOS transistors and diodes. Control logic for rectification and combination with current regulation switch not shown.

6-5 Control loop

The control loop provides a reference signal for the Pulse-width Modulation (PWM) block. This signal represents the desired charge current for the present battery voltage. As presented in the previous chapter the charge current should depend on the battery voltage via a hyperbolic tangent function. For the implementation of this transfer function an analog circuit was designed.

A digital implementation of the hyperbolic tangent might also be possible. Especially when in the total IPG a micro-processor is already present for other functions. A simple lookup

table might be programmed into the available memory. In this case, however, the charger is designed as an stand-alone block and implementing a micro-processor just for the charger would consume more chip area than an analog implementation.

For the analog implementation clever use of the exponential behavior of transistors can be used. Either a circuit composed out of bipolar transistors or out of MOS transistor that are operated in weak inversion can be used. Both options are available in the selected IC technology and will be discussed below.

6-5-1 Bipolar Junction Transistor (BJT)

Ever since the nineteen seventies, differential pairs composed of bipolar transistors have been used for generating extraordinary circuits. For example, B. Gilbert developed a method of linearizing the transfer of a transconductance cell over a larger dynamic range by combining multiple differential pairs [49]. A single transconductance cell will have a limited dynamic range and will gradually saturate at large differential input voltages. In this situation, the resulting hyperbolic tangent transfer function of a single transconductance cell is actually a useful feature.

By using the difference between a end of charge voltage reference and the battery voltage as input and the output current as a control signal for the charge current we automatically achieve the desired charge curve. At low battery voltages the difference between the battery voltage and reference voltage is high. The circuit is saturated so that it provides the maximum charge current to the battery. Near the end of charge voltage the differential input of the transconductance cell is small and the gain of the cell is high. A small change in battery voltage will thus have a large effect on the the output current in this region. This will cause a steep drop in output current near the end of charge so that overcharging is prevented.

The transfer function of a single hyperbolic tangent cell is given by Equation 6-4. Here I_{ref} is the output current that provides a reference for the charge current. I_{bias} is the tail current of the differential pair and serves as a scaling factor. V_{ref} and V_{bat} are respectively the end of charge reference voltage and the battery voltage. V_t is the thermal voltage that can be calculated by the well-known equation $V_t = \frac{kT}{q}$ and equals about 26mV at 25°C.

$$I_{\text{ref}} = I_{\text{bias}} \cdot \tanh\left(\frac{V_{\text{ref}} - V_{\text{bat}}}{2V_t}\right) \quad (6-4)$$

Since the exact transfer is dependent on the thermal voltage and thus on the absolute temperature one may expect that stability over temperature may be an issue for this circuit. The truth is however that, first of all, the expected operating temperature range is small since we deal with an implant for the human body. Secondly, as shown in Figure 6-4, the start and end point of the curves are stable over temperature. Temperature may, however, have an negative influence on the charging time since the current starts to decrease at a lower battery voltages when the temperature is above the nominal range. However, even at extreme temperatures, the battery will be fully charged and charging will be terminated at the proper battery voltage.

Although not directly visible from the transfer function, component mismatch due to fabrication errors may become problematic. Random emitter area mismatch may result in different

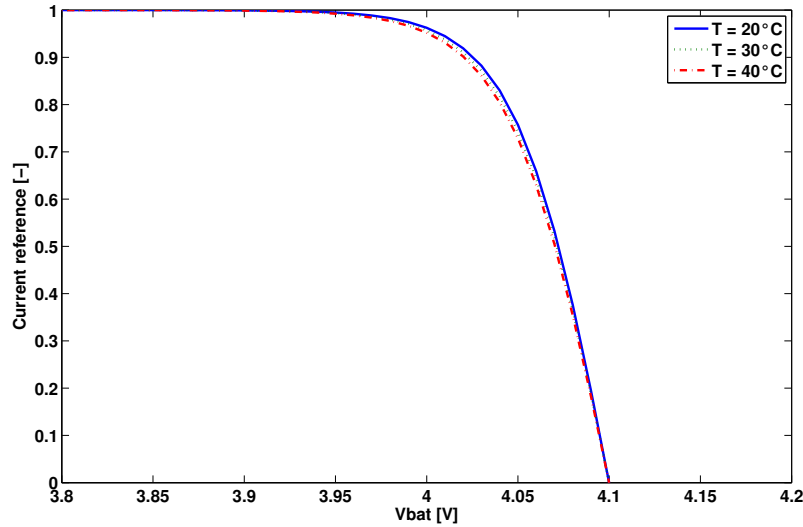


Figure 6-4: Temperature dependency the of hyperbolic tangent function. Plot of Equation 6-4 at 20°, 30° and 40°

bias currents in each branch of the differential pair. In this situation the output will be non zero if the battery voltage is equal to the end of charge voltage since the two branches do not cancel out anymore. This may result in a battery that is either not completely charged or damaged due to overcharge.

When both branches experience the same fabrication error, resulting in a increase or decrease of all transistors sizes, the circuit still functions properly. By careful placement of the transistors, for example by placing them in close proximity and in the same orientation, matching can be maintained. Also if the size of the transistors is increased the fabrication errors are less relevant compared to the total size.

6-5-2 MOS transistor

Because not all technologies offer the use of bipolar transistors in combination with MOS transistors that are needed for other parts of the system, it is beneficial if the control loop can be implemented using MOS transistors as well. Since the hyperbolic tangent transfer of the circuit is the result of the exponential behavior of bipolar transistors this is not as trivial as it might seem.

If exponential behavior is required MOS transistors can be used in their subthreshold region. In this region the drain current also changes exponentially with the gate voltage. Due to the way MOS transistors are constructed, changing of the gate voltage has less effect on the drain current as expected. Instead, only a certain fraction of the gate voltage has an effect on the drain current. To take this fraction into account the term κ is introduced.

κ is between zero and one and equals the ratio of the capacitive divider of two capacitors. One is the capacitor formed by the gate terminal and the conductive channel that are isolated

by the gate oxide (C_{ox}), the other is the capacitor between formed by the channel and the bulk isolated by the depletion layer (C_{dep}). The value of κ is given by Equation 6-5 and is typically in the range from 0.5 to 0.8 [50].

$$\kappa = \frac{C_{ox}}{C_{ox} + C_{dep}} \quad (6-5)$$

We can see from Equation 6-6 that an additional term κ is introduced in the transfer if we use MOS transistors. This term causes the switchover point where the charge current starts to decrease to move to a lower voltage. This results in a charge current that is lower than required near the end of charge and extends the charge time.

The parameter κ is different for each IC technology. As a result the total system becomes technology dependent. Implementing the design in a different technology is thus impossible without reconsidering the transfer of the control loop. Simulations showed that for the 0.18 μ m technology that was selected for our design the switchover point was unacceptable. This problem was tackled by introducing a voltage scaling at the input. By scaling down the battery voltage and reference voltage by $\frac{1}{\kappa}$ the switchover was moved to about 100mV before the end of charge voltage.

$$I_{ref} = I_{bias} \cdot \tanh\left(\frac{\kappa \cdot (V_{ref} - V_{bat})}{2V_t}\right) \quad (6-6)$$

Since the current reference depends on the difference between the end of charge voltage and the battery voltage rather than their absolute value, the transfer function remains unaffected if we would introduce an equal offset to both voltages. At battery voltages below 3.9V the hyperbolic tangent function is saturated at the maximum level. The desired battery current would thus remain the same if we would shift the battery voltage and reference voltage down by, for example, 3.5V and clip the input to 0V Below the battery voltages of 3.5V.

By introducing the scaling and the offset the total voltage swing was reduced. This meant we could use lower supply voltages and smaller transistors for the design. The control circuit is now designed for a 1.8V supply while, without voltage scaling, 5V transistors should be used. As second benefit is that transferring to a different technology is now just a matter of tuning the voltage scaling. No complex changes to the design have to be made.

Besides the additional circuits needed to scale the voltage, MOS transistors are selected over bipolar transistors in this design. Most of all since not all technologies offer the luxury of having a choice between bipolar and MOS but also for the sake of power consumption. For MOS designs the bias current can be lower than for the bipolar design. With bipolar devices the base contact conducts some current and the bias needs to be large enough so that the amount flowing through the base can be neglected. MOS devices have isolated gates that do not conduct (DC) currents, so that bias currents can be reduced. Combined with the lowered supply voltage the total power consumption is reduced provided that the voltage scaling can be done without consuming too much power.

6-6 Voltage sensing

In order to provide an accurate reference of the desired charge current the voltage of the battery is sensed and fed to the control loop. Due to the hyperbolic transfer of the control loop the desired charge current varies substantially with only a small variation in battery voltage when the battery is approaching the end of charge voltage. Although this is the desired transfer for battery charging, this also means that any ripple present on the sensed voltage would translate in a large ripple in current reference.

When the charge current is switched, ripples appear at the battery terminals. If these ripples are not removed properly they will propagate through the control loop into the pulse-width modulator. If this happens the modulator will not be able to set the proper duty cycle and starts to oscillate. To prevent oscillations a simple RC low pass filter, with a corner frequency below the switching frequency, was added.

6-7 Current sensing

To compensate for any variations in link strength the battery current need to be sensed and fed to the PWM generator. Four physical principals are available for sensing a current: Ohm's law, Faraday's law of induction, magnetic field and the Faraday effect [51]. Of all of them Ohm's law is the most suited for our system due to the simplicity, small size and low cost.

A device with a small, known and fixed, resistance is placed in the current path and the voltage across the device is sensed. For this design a separate shunt resistance was introduced in the current path. Although this results in a small voltage drop and additional loss it is a simple and reliable method. The resistance of the shunt was set to 0.1Ω making the loss due to the shunt negligible compared to the loss of for example the rectifier diodes.

Potentially, the voltage drop over a MOS transistor due to its on resistance ($R_{DS(on)}$) can also be used [52]. We can thus sense the battery current by sensing the voltage across transistors M1 and M2 that are already present in the rectifier block as shown in Figure 6-3. The sensing circuit, however, would become more complex since the current is flowing through transistor M1 for half of the time and through transistor M2 for the other half.

When the transistor that is used for sensing the charge current is not conducting, the full output voltage of the link is found across the transistor. In order not to saturate the sensing circuit, that would normally sense voltages in the millivolt range, additional protection is needed. These additional components might influence the accuracy of the current sensing. Furthermore, the $R_{DS(on)}$ of a transistor is dependent on the temperature as well as the current it is conducting [52]. Considering all the additional circuit and design effort that is needed it is best to implement the current sensing with a separate shunt resistance.

In contrast with the voltage sensing block, the ripple that will be present in the sensed charge current does not need to be filtered. Since the system is fed by an AC source and the charge current is switched on and off large ripples will be present in the charge current. Although we are interested in the average charge current we do not need to filter the current in the sensing block. This filtering is already taken care of by the PWM block that will be discussed next.

6-8 Pulse-width Modulation (PWM) generator

In order to periodically short the inductive link and lower the average current that is flowing into the battery a control signal has to be generated. The PWM block is responsible for this task. Voltages representing the reference current and battery current are fed to this block. The difference between the two voltages is integrated over time so that the average error is obtained. The time constant of this integrator is much longer than the period of the external supply. Therefore the current sensor does not have to filter the output as we mentioned above.

When the battery current is below the desired charge current the output of the integrator will go up and eventually clip at the maximum output voltage. Similar, when the current is too high the output will be lowered and eventually go down to zero. The output of the integrator is compared to a sawtooth waveform. When the sawtooth rises above the integrator value the MOS transistors will be switched on and the link will be shorted. In the other period, when the sawtooth falls below the integrator value, the link will not be shorted and current is allowed to flow into the battery.

6-9 Simulation results

To check if the implemented circuit is capable of fully charging a battery, a circuit simulation was performed in the Cadence Virtuoso Analog Design Environment. The system was designed to charge a 150mAh battery with a maximum current of 25mA to the end of charge voltage of 4.1V. These parameters were also used for the Matlab/Simulink simulation presented in the previous chapter.

For this situation, switches and diodes are modeled using realistic devices models instead of ideal components. The results can thus be used to predict the efficiency that can be expected in real life. We will compare the power consumption of the system with the results from the previous chapter and pinpoint the difference. We start, however, by showing that correct operation can be achieved using realistic components.

6-9-1 Charge curve

To reduce simulation time, the circuit was not simulated over the total charge cycle of the battery. Instead, a period of 300 μ s at different State of Charge (SoC) levels were simulated. The data was taken from a transient simulation from 300 μ s until 600 μ s. The data of from 0 μ s to 300 μ s was discarded so that the startup behavior of the system had no influence on the results. For each simulation the battery voltage and charge current were averaged and saved. Figure 6-5 shows the results of these simulations for 20 different SoCs. As can be seen the curve is less smooth due to the limited amount of data points but the results are in good correspondence with the results from the Matlab/Simulink simulations (Figure 5-5). The charge current is almost flat for low SoC and starts to decrease near the end of charge. Although it is not clearly visible due the limited amount of data points, the roll-off of the charge current follows the hyperbolic tangent function as described in Section 5-4-1. The circuit is thus able to safely and completely charge the battery when we simulate using realistic component models.

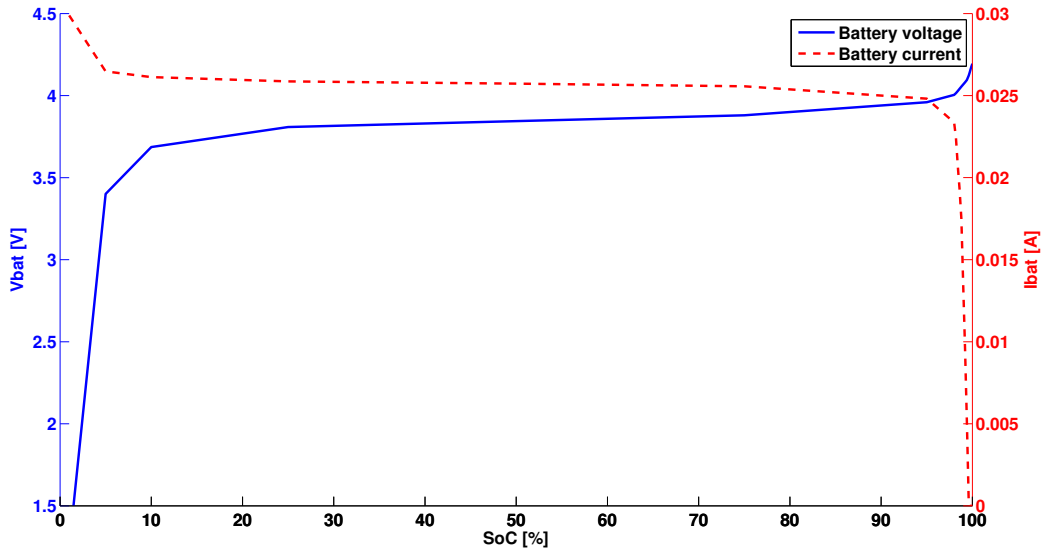


Figure 6-5: Charge curve of proposed charge system simulated in Cadence Virtuoso Analog Design Environment. The solid blue line shows the battery voltage versus the SoC of the battery. The dashed red curve shows the charge current versus the SoC

6-9-2 System efficiency

Figure 6-6 shows the power consumption of the system, simulated at three different nodes. The power absorbed by the battery decreases near the end of charge due to the reducing charge current. Also the power delivered by the inductive link and the external source reduces due to the increased time the link is short circuited. The shape of the curve is similar to the result of the Matlab/Simulink simulations of the previous chapter. The absolute value is however slightly different.

link efficiency

In the Matlab/Simulink simulation a little over 168mW was delivered by the external source when the charge current was at the maximum 25mA and the battery is at 50% SoC. In the Cadence Virtuoso simulation the source delivers 163mW while the charge current and battery SoC are equal. A lowered input power for the same output indicates that the inductive link performs better in during the Cadence simulations than during the Matlab/Simulink simulations.

The difference was caused by tuning of the source amplitude during the Cadence circuit simulations. The source amplitude was selected such that it was just high enough to power the charger at maximum output power. During the Matlab/Simulink simulations a margin was kept to ensure the charge current was not limited by the maximum output of the inductive link. When we calculate the efficiencies we see that the inductive link reached an average efficiency of 72.2% during the Cadence simulation while the Matlab simulation reached an average link efficiency of 64.7%.

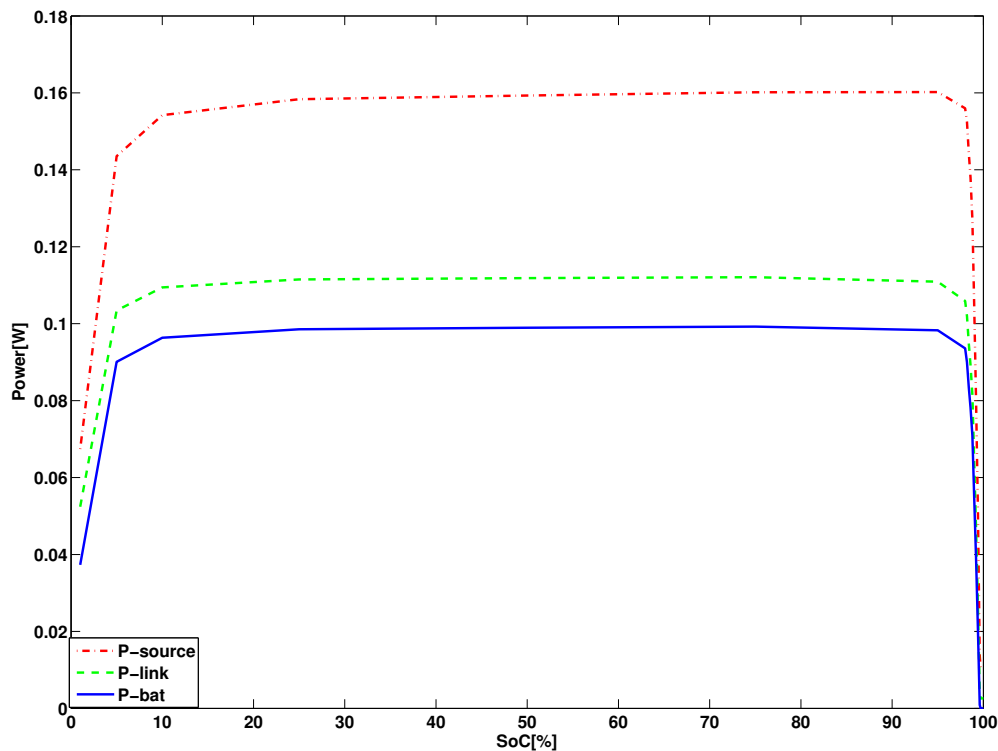


Figure 6-6: Power consumption of proposed charge system over a full charge cycle simulated in Cadence Virtuoso Analog Design Environment. The red dash-dotted line shows the power delivered by the external source. The green dashed line shows the power at the secondary side of the inductive link. The solid blue line shows the power absorbed by the battery.

When we recalculate the theoretical link efficiency using equation 5-8 instead of 5-10 and model the load impedance by dividing the battery voltage with the charge current we see that the maximum average efficiency is 69.6%. It seems that the inductive link performs better than theoretically possible but of course this is not the case.

The output power of the inductive link was calculated by multiplying the output current and voltage before the rectifier and thus also before the charge current regulation switch. Since the ideal switch has now been replaced by MOS transistors the link is no longer perfectly shorted when the switch control signal is high. Instead there will be a voltage drop over the switch in the order of 100mV. This means that the inductive link still delivers power even when the current regulation switch is shorting the link.

The link is thus alternately loaded with the battery and with the current regulation switch. The current regulation switch is loading the link with a far lower impedance than the battery for short periods of time. The average load impedance seen by the inductive link is thus lower than simply dividing the battery voltage with the charge current. If we fill in this average impedance into Equation 5-8 we get the same efficiency as resulted from the simulations.

If the link efficiency needs to be improved we can reconsider the operation frequency to get

the actual efficiency closer to the theoretical maximum. Another option would be to improve the quality of the secondary coil by reducing the winding impedance. Other material or wires composed out of multiple insulated strands ¹ could drastically boost the limiting efficiency as well as the actual achieved efficiency. Increasing the output power by increasing the power dissipated by the switch is however not an valid option.

Although the power dissipated by the current regulation switch may result in higher efficiency numbers for the inductive link it is power that is only used for generating heat and not for charging the battery. Still it is a loss of energy that degrades the system performance. This loss is taken into account when calculating the power transfer efficiency from the output of the inductive link to the battery. We can see the effect when plotting the two efficiency graphs in one figure. Figure 6-7 shows the efficiency from the external source to the output of the inductive link as the link efficiency, and the efficiency from the link output to the battery as the charge efficiency.

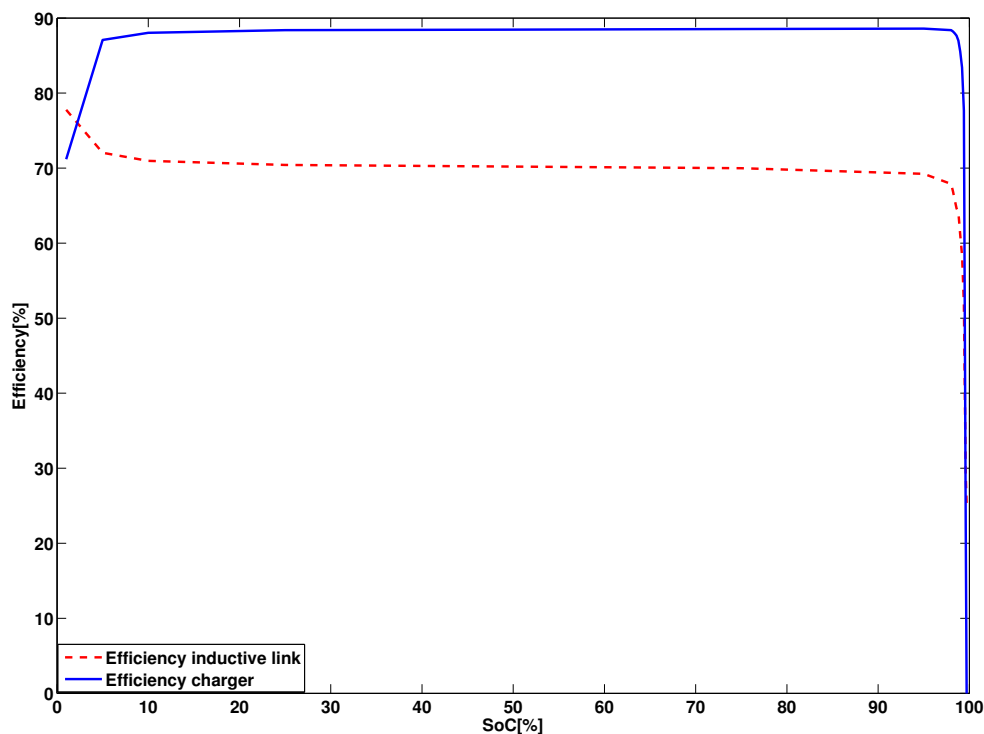


Figure 6-7: Link efficiency and charger efficiency of proposed charge system over a full charge cycle simulated in Cadence Virtuoso Analog Design Environment. The red dashed line shows the efficiency of the inductive link. The solid blue line shows the efficiency of the power transfer from the link output to the battery.

¹Using multiple strands reduces the skin effect so that the cross-sectional area is used more effective.

charger efficiency

The solid blue curve in Figure 6-7 shows the power transfer efficiency from the output of the inductive link to the battery as the charger efficiency. The efficiency peaks at an value of 88.59% while in the Matlab/Simulink simulation the peak charger efficiency was 90.7%. The average efficiency over the full charge cycle is 87.36% for the circuit simulation while the Matlab/Simulink simulation reached an average of 90.2%.

Already in the Matlab/Simulink simulation the rectifier block was simulated using diodes with a forward voltage drop of 400mV resulting in a limited charge efficiency. Also in the Cadence Virtuoso simulation, low drop diodes with only 400mV voltage drop were selected. Since the rectifier is the only block in series with the inductive link and the battery, it was expected that the results of the Cadence circuit simulation would be more or less comparable to the result of the Matlab simulation.

Three reasons can be used to explain the difference between the two simulations. First of all, The switches used in the Matlab/Simulink simulation had no on resistance as we already mentioned in the previous section. During the circuit simulation devices with a finite size were used so that their on resistance can no longer be neglected. An additional voltage drop over the switches of about 200mV will have to be taken into account.

Secondly, during the Matlab/Simulink the rectifier diodes and switches switched instantaneously from their conduction state to their blocking state. In reality, switches and diodes need some time to remove the conducting channel before they can turn off. If we zoom in on the profile of the current through one of the rectifier diodes we can see the effect of this turn off time. We can see the diode remains in conduction for a short period while the output of the inductive link has already reversed direction. The charge current is thus negative for a short period before the diode enters the blocking state.

The time needed to turn off the diode is only about 10ns. A half cycle of the input voltage takes 250ns meaning that most of the time current is allowed to flow into the battery with the proper direction. Furthermore the amplitude of the current flowing in opposite direction is much smaller than the amplitude of the charge current flowing in the correct direction.

The third cause for limited efficiency is found in the substrate the switches and diodes are fabricated on. If for example an N doped layer is fabricated in a P doped substrate an PN junction is automatically fabricated. It is thus inevitable that every device in an IC technology has parasitic diodes to the substrate. These diodes will form an conduction path as soon as any node voltage is below the substrate voltage.

Since we drive our circuit with an AC source the node that has the lowest potential is alternating. Half of the time one AC input is the lowest potential while during the other phase th other AC input has the lowest potential. An conduction path between the lowest AC inputs and substrate is formed until the potential of the two nodes are equal. In order to keep track of the current that is needed to equalize the two nodes we added the parasitic diodes to our circuit simulation.

In Figure 6-9 a plot of the current running through a substrate diode is shown. At the moment when the input changes polarity there is a spike in the current. Although the pulses are short they have a substantial magnitude and introduce some losses. Furthermore the substrate voltage is no longer constant due to the injection of charge.

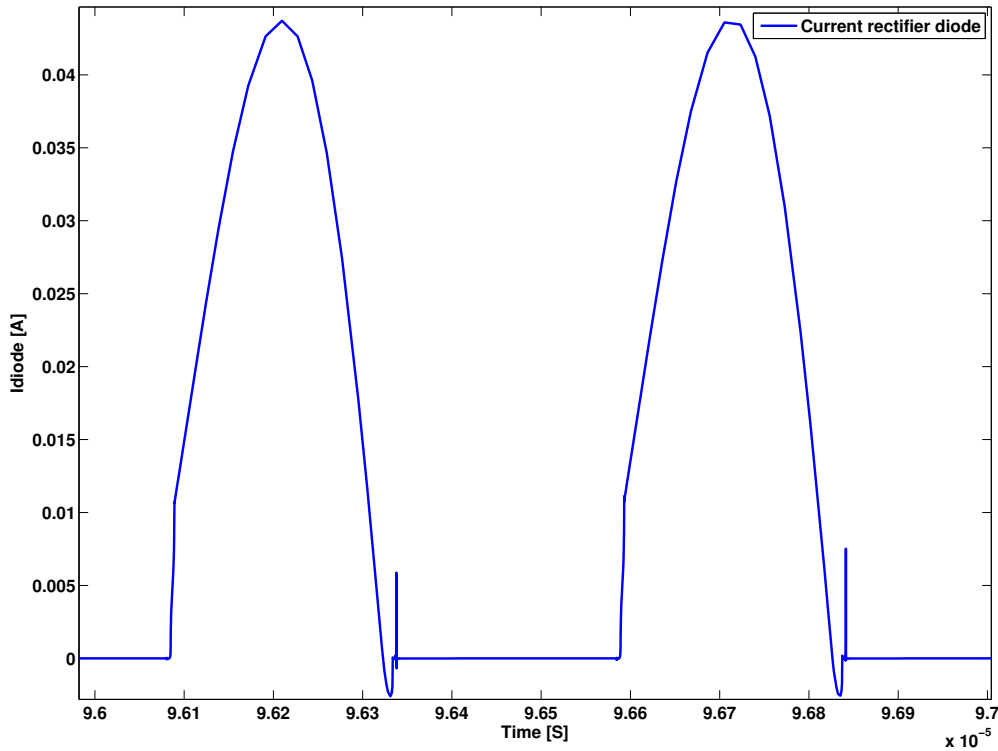


Figure 6-8: Current through one of the rectifier diodes. The current is negative for a short period due to the finite turn off time.

Fluctuating substrate voltages might also cause problems further down the circuit since the operating point of transistors can be affected. For now these problems are neglected since the prototype will not be implemented using an integrated circuit. Instead, discrete components will be used that all have a floating substrate so that any influence to other devices is eliminated. Before the circuit can be implemented in an IC proper biasing of the substrate node or additional circuitry to prevent substrate injections will have to be considered.

6-10 Conclusion

For implementation of the inductive link a series-series topology was selected in order to achieve maximum possible link efficiency. The antenna coils that are needed for the inductive link are not integrated on chip. This is done to have more flexibility in the placement and geometry of the coil for link optimization. Also the quality of off chip coils is in general superior over on chip coils. Besides the antenna coil also the resonant capacitor is kept off chip due to the large value and high voltage rating. Implementing the resonant capacitor on chip is possible but would require high voltage technology and extreme large chip areas.

The charge current is regulated by two large size, medium voltage, NMOS transistors connected back to back. This is done so that, by clever control of these switches, they can also

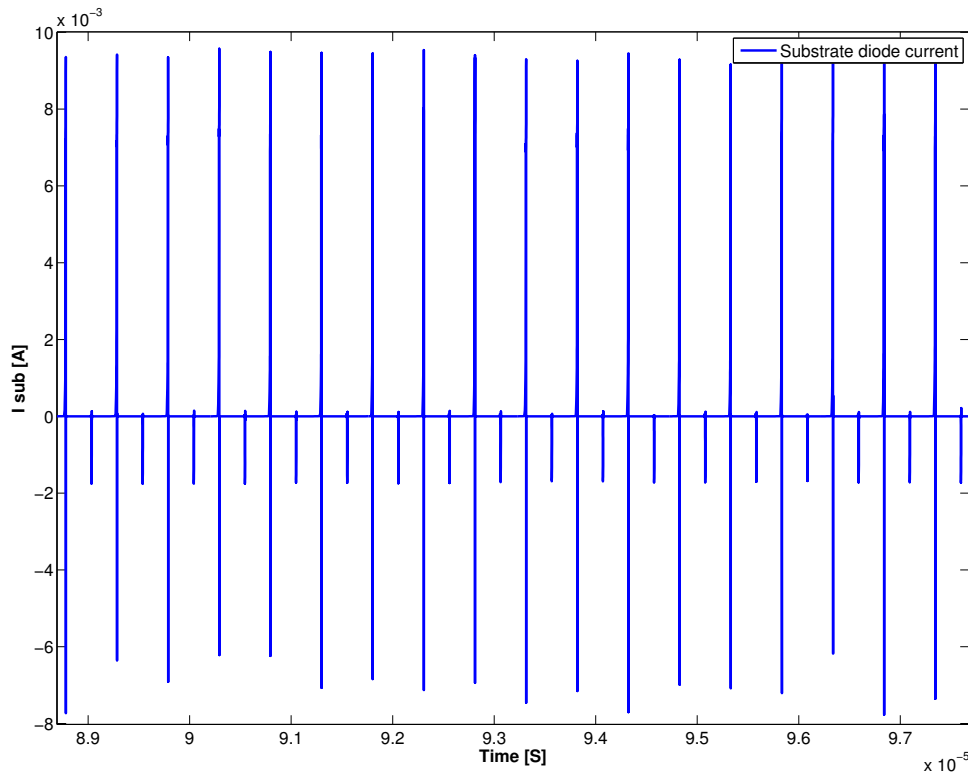


Figure 6-9: Current flow through substrate of rectifier diodes and switches.

be used as a part of a full bridge rectifier. Hereby two large size transistors or diodes can be omitted that would otherwise be needed for rectification of the input wave. Furthermore, the voltage drop over the rectifier is reduced compared to a full diode bridge.

Control of the charge current is done via a hyperbolic tangent function. This function is implemented using a differential pair of MOS transistors biased in weak inversion. Although the transfer of MOS transistors in weak inversion is dependent on the selected technology the desired transfer can be obtained by scaling the input voltage. As an added benefit low voltage transistors can be used for the control loop.

The on and off switching of the charge current causes ripples in the battery voltage. In order to provide an stable reference signal to the PWM block, the sensed battery voltage needs to be filtered before it can be supplied to the control loop. If these ripples are not filtered the system will start to oscillate and no stable duty cycle can be reached.

To accommodate fluctuations in the link properties, the charge current is sensed using a shunt resistor. Potentially the resistance of MOS transistors already present in the current path can be used but for simplicity an additional shunt is placed. The PWM block compares the actual charge current to the desired value with an integrator. A sawtooth voltage and a comparator is then used to generate the appropriate PWM signal. Additional filtering of the sensed charge current is not necessary, as this is automatically achieved by the integrator inside the PWM block.

Simulation results showed correct regulation of the charge current and the power transfer efficiency of both the inductive link and the charger circuit could be calculated. The inductive link an efficiency of 72% while earlier simulations got up to 64%. The difference is explained by the finite on resistance of the charge regulation switch. If we recalculate the maximum efficiency using realistic component values we see that the system is operating as the theory predicts. Improvements in link efficiency can be achieved by increasing the operating frequency or by reducing the secondary coil resistance.

Differences in the charger efficiency between the two simulations are not so trivial to explain. Besides the finite on resistance of the used components there are more complicated effects that limit the efficiency. We need to zoom in on the charge current to notice short periods where the charge current is flowing in the opposite direction. During this phase the rectifier is removing charge present on the gates of MOS transistors and setting up a new conduction path for the next half cycle. The period where conduction is in the wrong direction is short compared to the input signal. Other effects must thus play a role as well.

Also unwanted conduction to the substrate introduces losses to the system. For each polarity change at the input there is a short current pulse running through the substrate node. Besides loss of energy, these pulses may introduce problems in other parts of the circuit due to substrate voltages variations. These problems are not solved in this design since the prototype, presented in the next chapter, is implemented using discrete components that all have their own floating substrate node. For the current design that was made in the AMS H18A4 IC technology, simulations show that the charger efficiency reaches a maximum of 88.59%.

Practical tests setup using discrete components

7-1 Introduction

Although both the Matlab/Simulink system simulation as well as the Cadence circuit simulation showed correct operation of the charger with promising results, they offer no guarantee an actual implementation will function. For example the dynamic behavior of the battery, as mentioned in section 2-5, is not always included in the battery model. This may cause the actual battery voltage and State of Charge (SoC) to deviate from the simulations. Charging may be, for example, terminated too early because the battery voltage increases faster than expected from the model.

The best way to verify correct operation is therefore to fabricate the designed system and charge an actual battery. This chapter will describe the designed prototype, the test battery and the results of the measurements that were performed. To have a benchmark to compare the designed system with the test battery was also charged according to the classical Constant Current Constant Voltage (CCCV) method using computer controlled sources.

The goal of the measurements is to verify if the switching current regulation of the designed system has a noticeable effect on the battery. We therefore measure the energy that is pushed into the battery and the energy that can be taken out of the battery after charging. At the same time we will also measure the efficiency of the designed system and compare this to the results of the simulations presented in the previous chapters. We will evaluate the performance of the prototype on the charge time, the power transfer efficiency and the amount of energy that can be discharged after charging. Before the results of the measurements are discussed and evaluated an overview of the prototype is given.

7-2 The prototype

The designed prototype consists of three subparts: the inductive link, the control PCB and the test battery. Each of these parts is discussed in a separate section. We will start by introducing the inductive link that is needed to power the system.

7-2-1 Inductive link

In order to be able to charge a battery transcutaneously we need wireless energy transfer. The inductive link, that provides this functionality, is composed of a primary coil and resonance capacitor connected to a function generator and a secondary coil and resonance capacitor connected to the Printed Circuit Board (PCB). The design of the inductive link is based on an existing design presented in [31].

Primary side

The primary coil is composed of four enameled wires in parallel, each with a diameter of 0.2mm. The resulting wire was wound around a tube having a diameter of 32mm and a length of 40mm. Approximately 50 turns were made around the tube. To guarantee the magnetic field is not influenced by any ferromagnetic material, for example screws to mount the test setup, the coil was suspended in a acrylate sheet. Figure 7-1 shows the coil in the acrylate support structure.

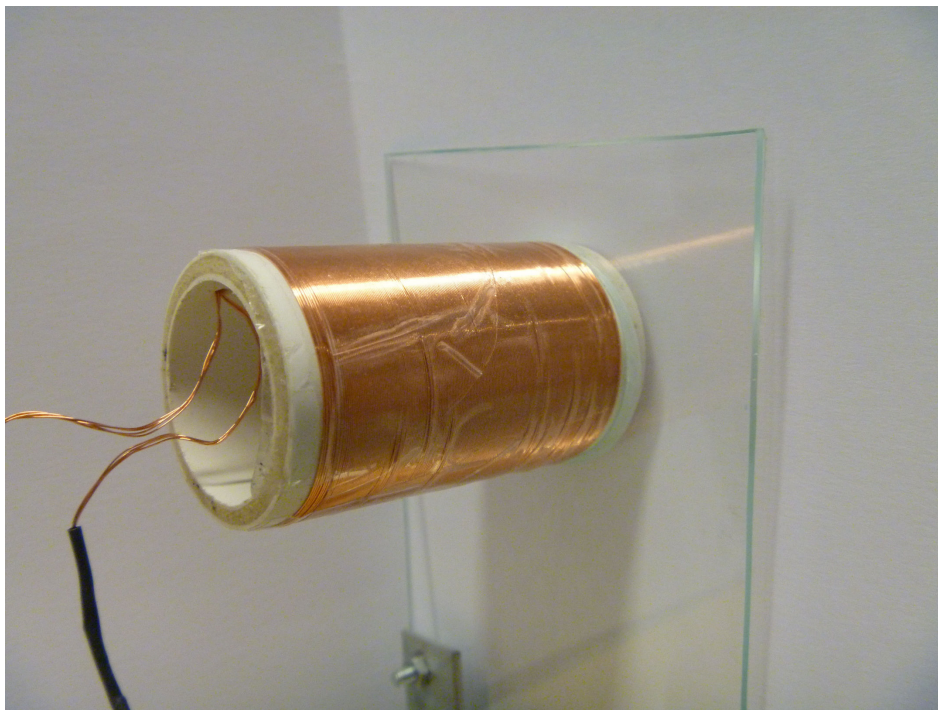


Figure 7-1: Primary coil mounted on a acrylate support structure

The inductance of the coil was measured to be $44.7\mu\text{H}$ at a frequency of 2MHz . The resistance at this frequency was measured to be 3.2Ω . The primary side was complemented with a resonant capacitor composed of two 100pF capacitors in parallel. The resonance frequency is hereby set to 1.71MHz

Secondary side

Since the secondary part should be implantable inside the skull we could not use the same cylindrical coil design that was designed for the primary side. Instead a flat spiral coil was constructed with a single 0.2mm enameled wire. The spiral was wound with a inner diameter of 2mm , an outer diameter of 32mm . Just as for the primary coil approximately 50 turns were used.

Again the coil was placed on a acrylate sheet so that it could be mounted without being influenced by surrounding ferromagnetic material. Figure 7-2 shows the coil mounted on the acrylate support structure. The inductance was measured to be $35.7\mu\text{H}$ and the resistance 6.3Ω . A 250pF capacitor was used as secondary resonance capacitor to get the resonance frequency as close as possible to the primary resonance frequency.

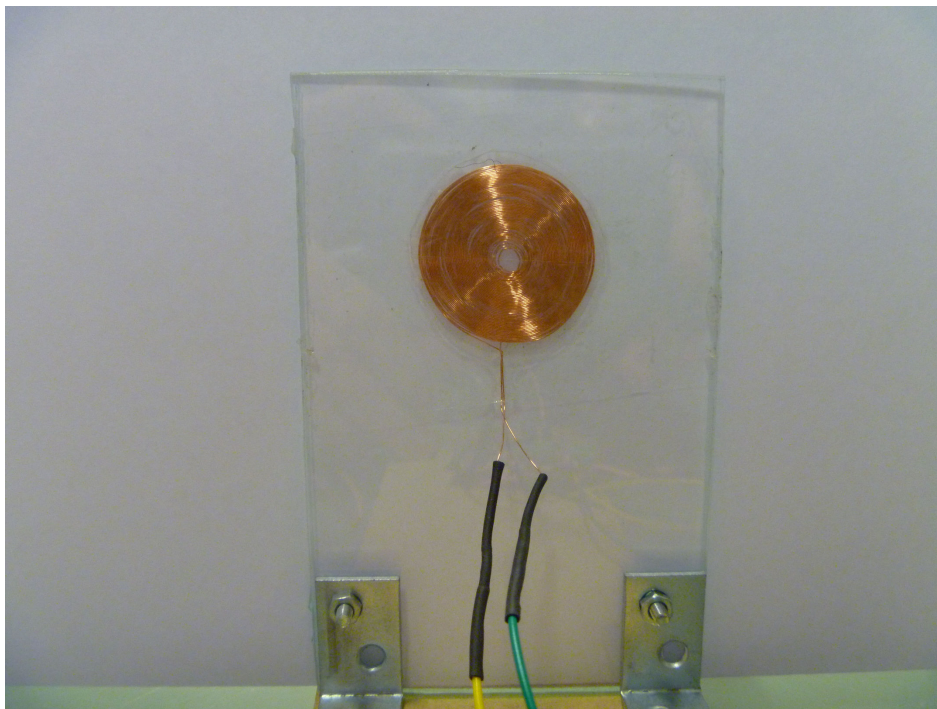


Figure 7-2: Secondary coil mounted on a acrylate support structure

Total inductive link

To keep both primary and secondary coil aligned during measurements they were mounted face to face on a wooden board. Figure 7-3 shows a side view of the two coils. Initially, the distance

\	inductance	resistance	resonance capacitor
Primary	44.7 μ H	3.2 Ω	200pF
Secondary	35.7 μ H	6.3 Ω	250pF
\	mutual inductance	coupling factor	operating frequency
Link	2.9 μ H	0.07	1.7MHz

Table 7-1: Component values of the inductive link.

between the coils was set to 20mm. After testing of the link the coupling between primary and secondary was lower than expected. The distance between the two coils is therefore reduced to 10mm. At this setting the mutual inductance was measured to be 2.9 μ H, which corresponds to a coupling factor of 0.07. The component values of the inductive link are listed in Table 7-1.

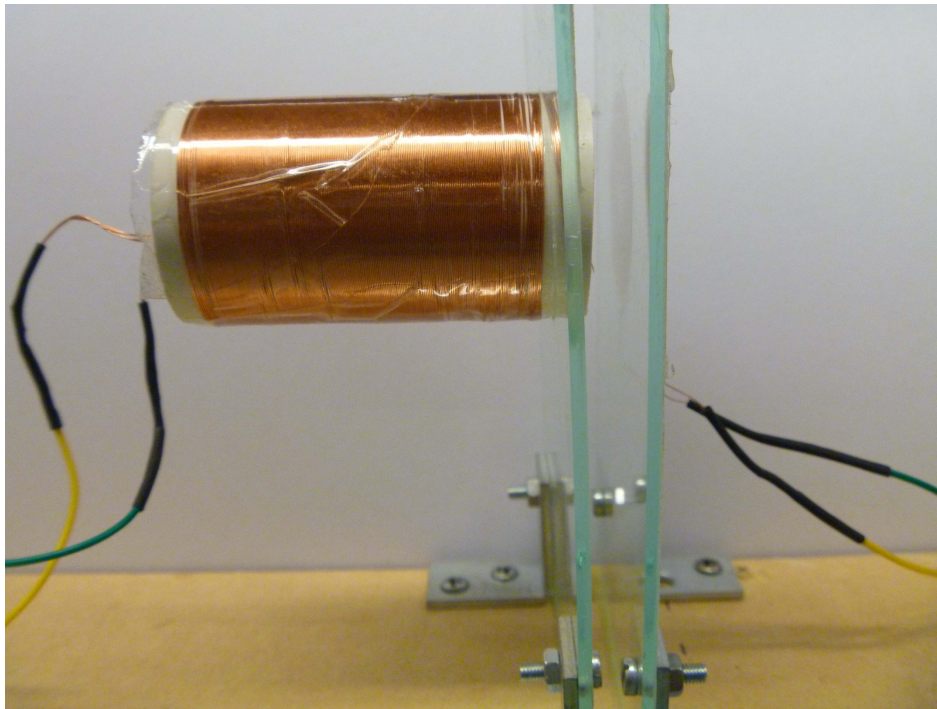


Figure 7-3: Primary and secondary coil mounted on a acrylate support structure, which form the inductive link

7-2-2 Control PCB

The Printed Circuit Board (PCB) accommodates various functions that are needed for the battery charger. Figure 7-4 shows the PCB with the different functions indicated by red ellipses. We will discuss the different functionalities one by one.

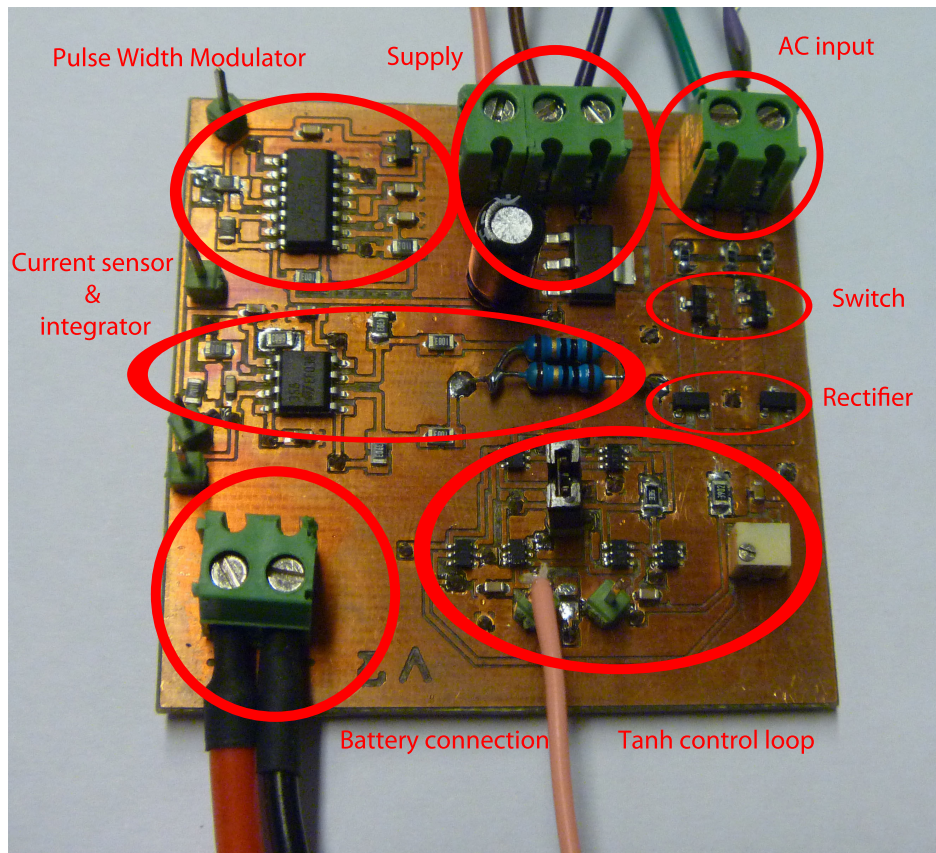


Figure 7-4: Printed Circuit Board of prototype. The red ellipses indicate the location of the different functions on the PCB

Current regulation switch

Below the AC input terminal, in the upper right corner, the current regulation switch is located. This switch, that short circuits the inductive link when the battery current is above the desired value, is composed of two 2N7002F MOS transistors connected back to back. Only one transistor is not suitable in this situation since the 2N7002F is not a symmetrical device. A diode connects the source and drain terminal that can become conductive, even when the transistor is turned off. Half of the AC input can thus not be used for charging the battery if one transistor is used. By connecting two transistors back to back (source to source) there is at least one transistor turned off when the switch control signal is low. This means the full input waveform can be available for charging.

Rectifier

The rectifier is located below the current regulation switch. It is a regular full bridge rectifier composed out of four Schottky diodes (two combined in one package). For simplicity a regular full bridge diode rectifier was selected over active MOS implementations or the hybrid MOS diode bridge introduced in Section 6-4. Although this will result in a high power loss in the

rectifier due to increased voltage drop, it simplifies the PCB design and reduces the number of components on the board.

Hyperbolic tangent control loop

The lower right corner of the PCB is consumed by the hyperbolic tangent control function. In contrast with Section 6-5, bipolar transistors are selected over MOS transistors for the prototype. This gives us more flexibility in the biasing of the control loop since bipolar transistors show the required exponential behavior over the full active region whereas MOS transistors would need to be kept in weak inversion.

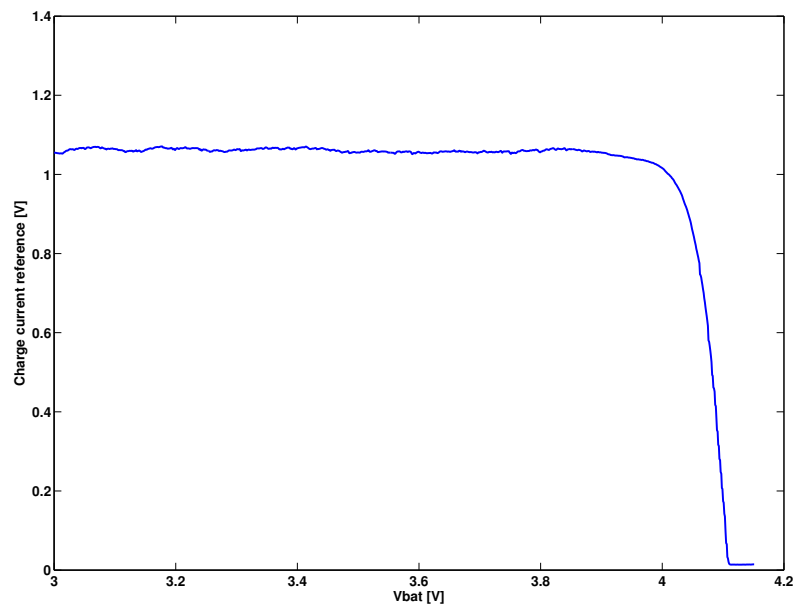


Figure 7-5: Measurement result of the hyperbolic tangent control loop. The charge current reference voltage is plotted against the battery voltage. One volt equals the full 25mA charge current, zero volts equals zero charge current.

The output current of the control loop is transformed into a voltage by a simple resistor in order to compare it one to one with the output of the current measurement. Figure 7-5 shows a plot of the measured charge current reference voltage versus the battery voltage. The shape of the curve is very similar to the desired curve we introduced in section 5-4-1. Only above the end of charge voltage a significant difference can be spotted. The charge current above the end of charge voltage should be zero to prevent overcharging of the battery. However, the measurements show that the control loop does not reach zero even when the battery voltage is above the end of charge voltage. This offset voltage needs to be taken into account to guarantee proper charge termination.

Current sensor and error integrator

The current measurement unit is located in the center of the circuit board. As a current sensor a shunt resistor is introduced composed of two parallel resistors in order to achieve the correct resistor value, accuracy and power capabilities. The differential voltage across the resistor is sensed and amplified by an operational amplifier. A second operational amplifier was used to compare the sensed current with the reference from the hyperbolic tangent control loop and integrate the error signal. To save space and simplify the layout of the PCB, a single package with two amplifiers was used.

Pulse-width modulator

The error signal provided by the integrator needs to be converted into a switch control signal. This is done by the Pulse-width Modulation (PWM) block located in the upper left corner of the circuit board. The block is constructed from a single NE556 timer IC which is basically two NE555 timers combined in one package. One timer was used to generate short pulses at a frequency of about 1KHz. This signal is used to trigger the second timer that in turn determines the pulse width of the switch control signal depending on the input voltage. The result is a switch control signal with a frequency of 1KHz and a pulse-width that changes according to the desired charge current.

Supply

Finally the circuit board requires a DC supply in order to function. For the final product this supply should be generated from the inductive link. Since the current sensor and PWM block has been implemented using off the shelf components the required power is relatively high. For this prototype the power is therefore supplied by an additional source. Note that the power supplied by this source is not taken into account when we evaluate the power transfer efficiency.

Most of the board is designed to operate from a 5V supply. The only part that requires a different voltage is the operational amplifier. Due to poor performance near the supply voltage an symmetrical -9V +9V supply was required. Without a symmetrical supply the amplifier is unable to reach a 0V output and thus cannot sense a 0A current. Instead the output will be larger than zero so that it seems there is a current flowing into the battery while the actual current is zero.

To make sure the control loop is functioning properly also zero current should be sensed accurately. An external symmetrical supply was connected to the board to provide power for the amplifier. Furthermore the positive side of the supply was fed into a low dropout voltage regulator to generate the 5V supply for the other parts of the circuit.

7-2-3 Test battery

The system was tested by charging and discharging a lithium battery. Although the selected battery was not designed for medical implants, the selection was made such that the characteristics do not deviate too much from medical grade implants. The test battery was selected

based on nominal battery voltage, maximum voltage and capacity. The nominal voltage should be between 3.6V and 3.7V, the maximum voltage at least 4.1V and the capacity between 13mAh and 325mAh. These values are based on the parameters of batteries available for medical implants [14, 53].

The selected battery was the LP-402025-1S-3 Lithium-ion Polymer Battery. This battery has a typical capacity of 165mAh, nominal voltage of 3.7V and an maximum charging voltage of 4.2V. The battery is supplied with a small protection circuit pre-installed to protect the battery from abuse situation.

Figure 7-6 shows a picture of the battery connected to the measurement setup. The battery leads were trimmed so that the voltage measurement could be connected as close to the battery terminals. This is done to minimize the effect of any voltage drop that can be found across the leads.

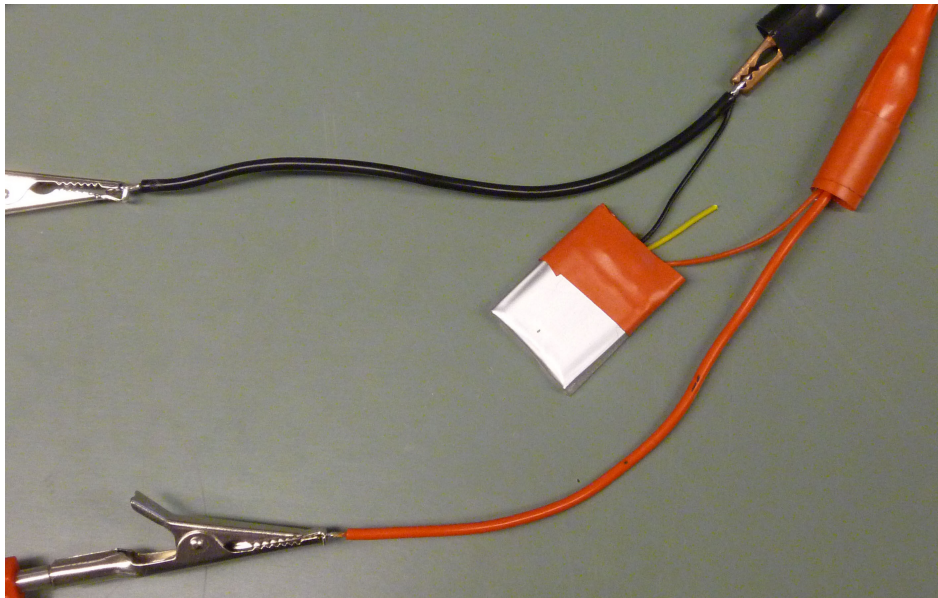


Figure 7-6: Lithium Ion battery under test. The voltmeter is connected as close as possible to the battery terminals to minimize the influence of the resistance of the connecting leads.

7-3 Measurement setup

To compare the performance of the charger the test battery was charged by both the prototype PCB as well as by a computer controlled current and voltage source that was programmed as a CCCV charger. The battery current and voltage were measured continuously and logged on a PC for processing. The HP 414202A and HP 41421B source/monitor units were used as sources for the setup, the Keithley 182 volt meter was used to measure the battery voltage and an HP 34401A multimeter was used to measure the battery current.

All instruments were connected to a HPIP communication bus so that they could be controlled using the HP Vee visual programming environment. Different HP Vee programs were written

to charge and discharge the battery according to the different methods as mentioned above. Details about the setup for the specific phase in the measurement are discussed in the sections below

7-3-1 CCCV charge

Since we are using the classical CCCV charging method as a benchmark for the designed charger we started the measurements by charging the battery according to this method. CCCV charging was achieved by setting the HP 414202A as current source. The charge current was set to 25mA and the voltage compliance of the source to 4.1V. This automatically implements both the Constant Current (CC) phases as well as the Constant Voltage (CV) phase.

Charging is commenced at a constant current of 25mA until the battery voltage hits the 4.1V. After this the current will gradually decrease since the voltage compliance limit is reached. The source will thus behave as a voltage source in this region. This will continue until the charge current has dropped below 2.5mA (10% of the initial charge current) after which charging was terminated by setting the output current of the source to 0A.

Every five seconds the battery voltage as well as the charge current were measured and stored. By integrating the charge current over time the SoC of the battery could be determined afterwards for each data point. We assumed that the battery current does not change significantly in between the 5 second periods so that integration becomes a simple summation of the current multiplied with the time interval.

To guarantee that charging started at 0% SoC the battery was discharged before each charge cycle. Furthermore, an additional sense wire was connected between the battery and the source. This guaranteed that the voltage measurement at the source were not influenced by any voltage drop over the connection leads or current sensor of the multimeter.

7-3-2 CC discharge

Discharging of the battery was carried out by setting the HP 414202A source to a current of -25mA. The battery was discharged with a constant current until the voltage dropped below 3V. Again the battery voltage and current were measured and stored every five seconds. This method was used both before and after charging of the battery with half an hour of relaxation time in between.

7-3-3 Hyperbolic tangent charge

After the CCCV charge and CC discharge are completed the prototype board was connected to the battery. The charge current and battery voltage were measured using the same measurement equipment. After the charge current had dropped below 2.5mA the battery was automatically switched back to the 414202A source. The current output of the source was set to 0A for half an hour afterwards the CC discharge phase, as described above, was started. The battery was also discharged before commencing the charge cycle to guarantee charging started from 0% SoC. The data from the charge and discharge cycle were used to calculate the battery charge efficiency and compared to the results of the regular CCCV charging method.

7-3-4 System efficiency measurements

To determine the power transfer efficiency of the inductive link and PCB, additional measurements were carried out. An oscilloscope and additional shunt resistor were used to monitor the voltage and current at both the input of the inductive link as well as at the input of the PCB. At all times a differential measurement between two probes was carried out. This needed to be done because the ground lead of the probes are connected to protective earth by the oscilloscope. Since also the battery ground was connected to the protective earth via the supply of the PCB we need to measure shunt voltages and coil voltages differentially.

Although we know from both the Matlab/Simulink system simulations and the Cadence circuit simulations that the power transfer efficiency is dependent on the battery's state of charge, we only measured the efficiency in the nominal region at about 50% SoC. Since there was no equipment available in the lab to measure all voltages and currents simultaneously we had to measure the various voltages one by one.

If we would measure at high or low SoC either the battery voltage or the charge current is changing by the minute so that comparing powers measured at different times cannot be used to calculate the power transfer efficiency outside the nominal region. Since we know that the battery charge current and battery voltage remains fairly constant around the 50% SoC, we can assume the power at the input of the inductive link has not changed by the time we are measuring the output power.

We also know from the simulation results that the duty cycle of the charge regulation switch has influence on the overall system efficiency. The higher the source amplitude the longer the charge regulation switch is closed degrading the system efficiency. We therefore lowered the source amplitude until the PWM generator saturated and the charge regulation switch was continuously open. We can now measure the best case system efficiency independent of the duty cycle but do have to keep in mind that the actual efficiency when the system is in use might be lower.

7-4 CCCV charge and CC discharge results

After the measurement data was collected the total energy that was charged and discharged could be calculated. We started by determining the state of charge of the battery for each data point by coulomb counting (integrating the charge current over time). The termination point of the CCCV charge was considered to be the 100% SoC point.

7-4-1 Charge and discharge time

After 5 hours and 45 minutes charging, the battery voltage has reached the 4.1V threshold and the CC phase of the charge cycle is completed. The battery has been charged to a SoC of 93% at this point and is continued to be charged further by the CV phase. The complete CCCV cycle finishes charging after 7 hours and 2 minutes.

Figure 7-8 shows the charge profile of the test battery while charging with the CCCV method. The switchover from CC to CV is clearly visible by the steep drop in charge current (dashed



Figure 7-7: Source unit and measurement equipment used for testing the prototype

green line). During the CV phase the battery voltage is increasing from 4.095V to 4.1V. This is due to the contact resistance of the clamps used to connect the battery. As the charge current drops also the voltage drop over the clamps reduces and the battery voltage becomes equal to the source voltage.

Discharging the battery is faster since the battery current is remained constant over the total discharge phase and takes 6 hours and 8 minutes to complete. Figure 7-9 shows the discharge profile of the battery. Note that the SoC starts at 100% and that the battery current is negative since we are discharging the battery instead of charging.

7-4-2 Battery charge efficiency

When we multiply the battery voltage and charge current for each data point and integrate the outcome over time we can calculate how much energy is delivered to the battery and how much can be extracted again. Working out the math we can show that a little over 600mWh is supplied to the battery during charge. 578mWh can be extracted from the battery using the constant current discharge.

Dividing the two numbers gives us a battery charge efficiency of 96.33%. The energy that is lost is dissipated in the internal impedance of the battery and any other resistance that is in-between the battery leads and the battery. In this situation also the additional protection circuit introduces some additional losses. However, since the resistance of the protection circuit is low ($50\text{m}\Omega$ [54]) the overpotential of the battery is the most important source of energy loss.

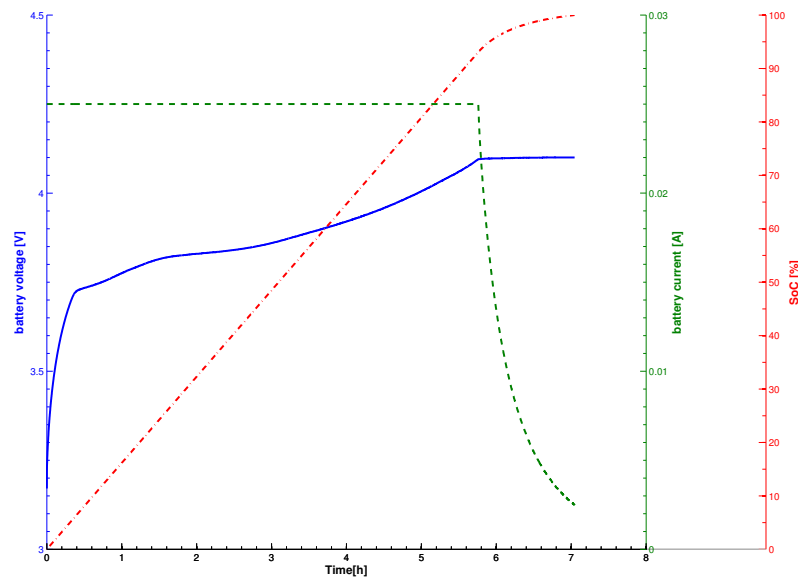


Figure 7-8: Charge profile of the test battery when charging according to the CCCV method. The solid blue line shows the battery voltage during charge versus the charge time. The green dashed line shows the charge current versus the charge time. The red dash-dotted line shows the State of Charge (SoC) of the battery versus the charge time.

7-5 Hyperbolic tangent charge and CC discharge results

The same procedure as was used to test the battery with the CCCV method was applied again but now with the prototype PCB as the charger instead of the HP 414202A source. Still the termination point of the CCCV method was used as a reference for a completely full (100% SoC) battery. Hereby we can easily see from the SoC that is obtained by the charger if the prototype is capable of completely charging the battery.

7-5-1 Charge and discharge time

The charge measurement was terminated by the HP Vee control software as soon as the charge current dropped below the 2.5mA, the same termination condition as for the CCCV charge cycle. This point was reached after 7 hours and 44 minutes. At this point the SoC of the battery has reached an value of 97.77%. The charger is thus slower compared to the CCCV charging and also terminates before the battery is fully charged.

The cause for the extended time, as well as the early charge termination, can be found when the curve of the charge current is examined. In Figure 7-10 the charge profile is plotted and the charge current is represented by the green dashed line. We can see from the graph that the maximum charge current is lower than the desired 25mA.

When the amplifier that reads the charge current was examined an offset in the measurement was found. Since the maximum charge current was lower compared to the CCCV charging

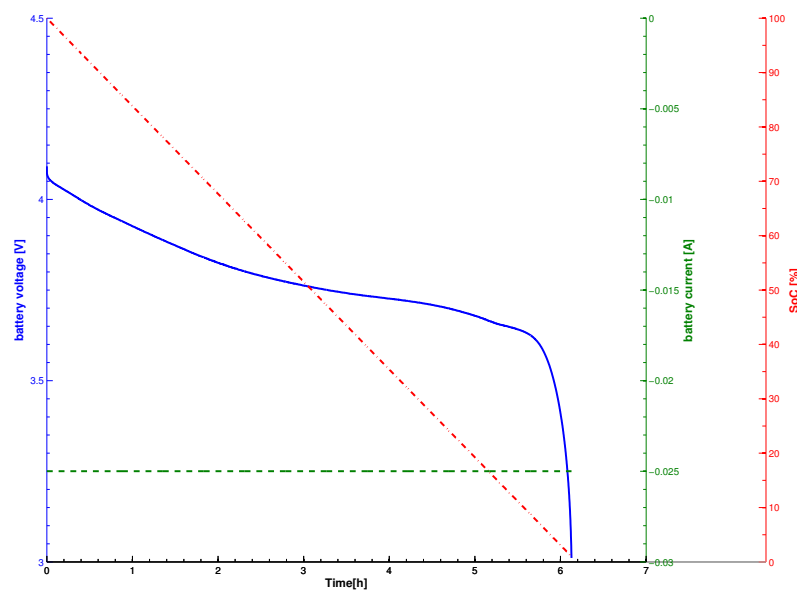


Figure 7-9: Discharge profile of the test battery when discharging with a constant current after CCCV charge. The solid blue line shows the battery voltage during discharge versus the time. The green dashed line shows the battery current versus time. The red dash-dotted line shows the State of Charge (SoC) of the battery versus time.

the charge time was extended. Also the charge termination condition was met too early so that the battery could not be fully charged. In Section 8-3-4 we will discuss how the current sensing could be improved.

7-5-2 Battery charge efficiency

Over the charge cycle, shown in Figure 7-10, 585mWh was supplied to the battery. A little more than 566mWh (96.75%) could be extracted again during the discharge shown in Figure 7-11. The prototype charger is thus slightly more efficient than the traditional CCCV charger. This could be a side-effect of the lowered charge current. After all, lower charge current results in lower voltage drop and lower losses in the parasitic resistances. To verify this the CCCV charge cycle was performed again but instead with a maximum charge current of 24mA.

Surprisingly the result of the second CCCV measurement was almost the same as the result of the first measurement. Although the time needed to complete the cycle was extended the total energy that was supplied and could be extracted remained the same. The increased battery charge efficiency is thus not the result of a lowered maximum charge current. Instead, it may be an effect of the difference in charge termination point.

Since charging is terminated a little earlier with the prototype charger, there is less energy supplied to a battery operating at high voltages. Due to the SoC dependent overpotential, most loss is concentrated at the high SoC region. Terminating charging earlier means that

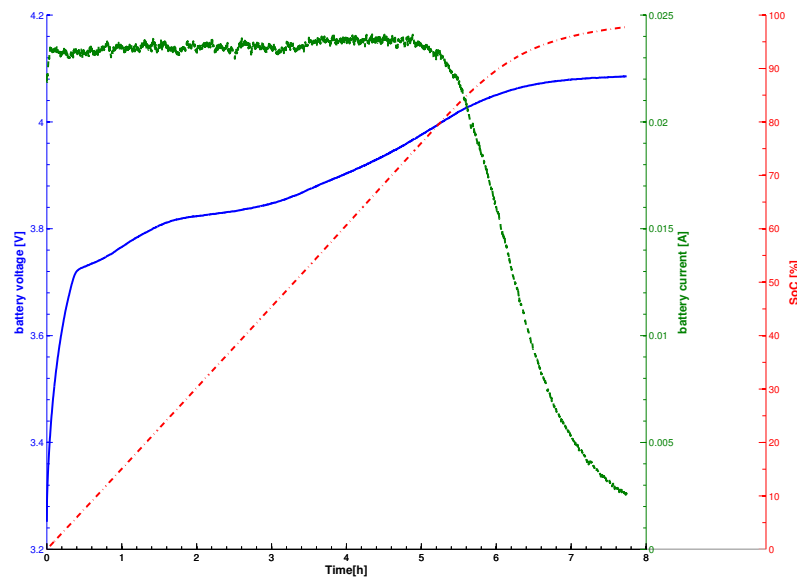


Figure 7-10: Charge profile of the test battery when charging with the prototype PCB. The solid blue line shows the battery voltage during charge versus the charge time. The green dashed line shows the charge current versus the charge time. The red dash-dotted line shows the State of Charge (SoC) of the battery versus the charge time.

this region is avoided and that the relative losses are reduced. Unfortunately also the amount of energy that can be discharged is reduced. It needs to be examined if the battery charge efficiency is still improved if the charge termination point is set to the correct SoC.

7-6 Overall system efficiency

The power transfer efficiency of the system has been split in two parts just as we did during the simulations. First we will discuss the efficiency of the inductive link that represents the power efficiency from the external source to the input of the charge circuit. Secondly the efficiency of the charger circuit in-between the inductive link and the battery is evaluated.

7-6-1 Link efficiency

To calculate the link power transfer efficiency we need to measure the power at the source side and at the PCB input. The source power was measured by first measuring the source voltage and measuring the source current via a shunt resistor afterward. The source power can be calculated by multiplying the RMS voltage by the RMS current. This calculation is only valid if the voltage and current are exactly in phase. One can imagine that since we are driving an inductive link that there may be a phase difference between the voltage and current. However if the system is operating at the resonance frequency the coil inductance is

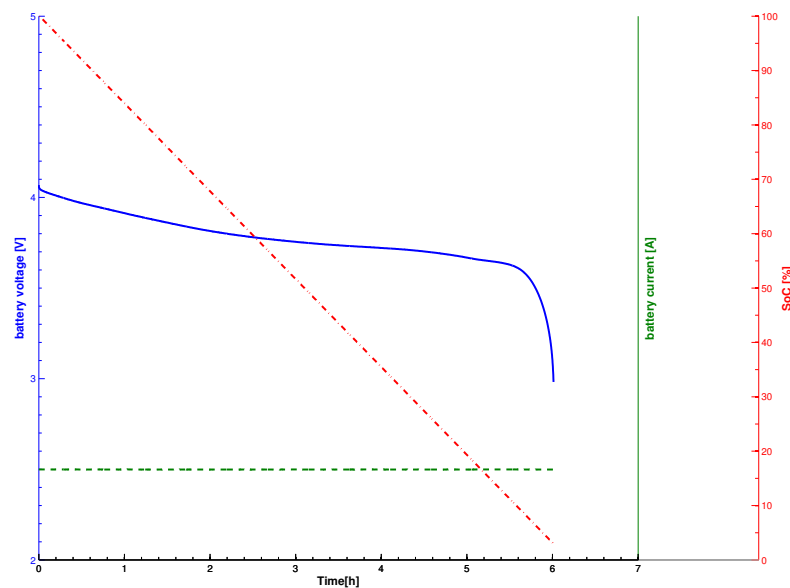


Figure 7-11: Discharge profile of the test battery when discharging with a constant current after charging with the prototype PCB. The solid blue line shows the battery voltage during discharge versus the time. The green dashed line shows the battery current versus time. The red dash-dotted line shows the State of Charge (SoC) of the battery versus time.

fully compensated and the loading of the source is purely resistive. Assuming that the voltage and current are in phase the source delivered 635mW while charging the battery.

The same measurement and calculation procedure were performed at the secondary side of the inductive link. Again the assumption was made that the voltage and current were in phase and that the power can be calculated by multiplying their RMS values. The inductive link supplies only 146mW to the control PCB. The power transfer efficiency of the inductive link is thus very poor and reaches a value of only 22.97%.

Poor link efficiency can be caused due to errors in the measurement of the inductance values of the antenna coils and deviations in the capacitor values. This causes the resonance frequency to deviate from the expected value. Other sources of error can be the parasitic capacitance and inductance of the rectifier diodes, PCB traces and battery that are connected in series with the resonant link. If the resonance frequencies of the primary and secondary side are not equal to each other nor the operating frequency the power transfer will be poor. Since the efficiency of the inductive link is not a primary goal of this thesis, the exact cause has not been investigated further.

7-6-2 Charger efficiency

To determine the power absorbed by the battery the output voltage and current of the PCB were measured. The output current was measured by probing the voltage across the shunt

resistor that is already present on the PCB. For the battery power we are interested only in the effective DC power. This means we are not using the RMS voltage and current for the calculation but use their mean values instead.

If we would use the RMS values we would incorrectly use a short negative charge current pulse as a effective charge current while it is actually discharging the battery. As we observed during circuit simulations (Section 6-9-2), negative charge currents can occur due to the time that the rectifier diodes need to switch from their conduction state to their blocking state.

By multiplying the mean output voltage with the mean output current we can show that the charger supplies 73mW to the battery. This means that only 50.19% of the power delivered to the PCB is effectively used for charging the battery. Multiple causes contribute to this poor efficiency.

First of all, the used rectifier was composed of diodes in a full bridge configuration. Although Schottky diodes were selected, still their voltage drop is about 400mV. Since at all times two diodes are conducting during charge a total voltage drop of 800mV can be found across the rectifier. Multiplying the voltage drop with the (RMS) output current of the PCB we can show that the rectifier is responsible for a loss of 29.6mW.

Secondly the used shunt resistor dissipates a substantial portion of the input power. Since the used amplifier required a relatively high input voltage the shunt resistor needed to have a relative high resistance value. A 5Ω shunt was used in this situation. The power dissipated by this resistor can be calculated by multiplying the resistor value with the square of the RMS output current. The shunt resistor is dissipating about 7mW meaning that there is a remaining difference of 36mW that cannot be explained using the two mentioned losses.

The final cause of the difference can be found by reviewing the power that the inductive link is supplying. During the calculations we assumed that the link voltage and current are exactly in phase. Since the voltage and current were measured separately the phase information is lost. However, the poor link efficiency already indicated that the inductive link is not operating at the resonance frequency.

If the operating frequency is not equal to the resonance frequency the link voltage and current will not be in phase. When we simply multiply the RMS voltage and current in this situation we are not calculating the real active power but are calculating the apparent power instead. This apparent power is the vector sum of the real power and the reactive power. Since we are comparing the input power with the DC output power we are only interested in the active power. To calculate the active input power we need to multiply the apparent power with a factor of $\cos(\phi)$ where ϕ is the phase angle between the voltage and current.

Assuming that the measurement of both the voltage and the current is triggered at the same phase we can align the two measurements and recover the phase information. By doing this we are able to show that there is indeed a phase difference between the voltage and current. Figure 7-12 shows a plot of the measured link output voltage and current in one graph. The peaks of the voltage and current do not align indicating that current slightly lags the voltage.

If we use the obtained phase information the active power of the link is actually lower than the power absorbed by the battery combined with the losses. However if we shift the current measurement data by just 12 nanoseconds (five samples) the numbers match up exactly. It is plausible that due to the scale difference in between the voltage signal and current signal the oscilloscope did not trigger at exactly the same phase.

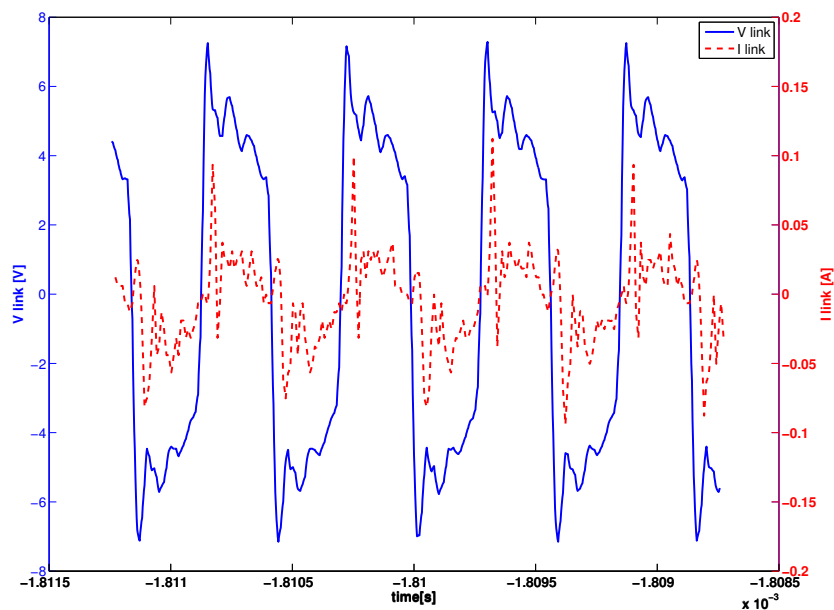


Figure 7-12: Measurement of link voltage and current. The delay between the peak of the voltage and the peak of the current indicate that the link is off resonance. The current measurement data has been shifted with 12 nanoseconds so that the active power equals the power delivered to the load plus all the losses in the system

If we use the corrected measurement data and recalculate the efficiency, the charger obtains a power transfer efficiency of 66.77%. A large portion (26.99%) of the input power is dissipated in the rectifier, the remaining 6.24% is dissipated by the shunt resistor. Although the results is not as good as the results of our simulation these numbers are in good correlation with our expectations. Due to the selected rectifier design we already expected a lower efficiency that was dominated by the diode voltage drop.

7-7 Conclusion

Since the used model to simulate a battery is not always sufficient to accurately predict the behavior of a battery we build and tested a prototype of the designed charger to verify correct operation. A 165mAh battery was charged with the prototype PCB as well as computer controlled sources that were programmed to charge according to the CCCV algorithm. Battery voltage and current were measured and logged so that the two chargers could be compared. Additional measurements were performed to determine the efficiency of the constructed prototype at nominal battery voltages.

The CCCV charging method completed in 7 hours and 2 minutes. After this period the battery was considered completely full and the SoC was set to 100%. A little over 600mWh is supplied to the battery during the charge period and 578mWh could be discharged again using

a CC discharge. Using the CCCV method 96.33% of the supplied energy is thus available for discharge.

When charging the battery with the prototype PCB that implemented the hyperbolic tangent charge curve more time was needed to complete the charge cycle. The charge termination point was reached after 7 hours and 44 minutes of charging where the battery was at a SoC of 97.77%. Due to an offset in the charge current measurement the maximum charge current was lower than the desired 25mA and the charge termination condition was met before the battery was fully charged. The amplifier that senses the shunt voltage needs to be improved in order to solve these problems.

Although less energy is supplied to the battery with the prototype charger, a larger portion of the supplied energy (96.75%) could be extracted again. The energy loss inside the battery due to the overpotential is dependent on the SoC and is larger at high SoC values. When charging is terminated earlier operation at high SoC is avoided increasing the battery charge efficiency. Unfortunately the absolute energy that can be extracted from the battery is reduced also. It needs to be examined if the battery charge efficiency remains as high if the charge termination point is set to 100% SoC.

The additional system efficiency measurements showed that the inductive link is operating at very poor efficiency of 22.97%. Probably the resonance frequency of the primary as well as the secondary circuit deviate from the expected values due to errors in the measured coil inductance value and specified capacitor value. Since a good link efficiency is not a primary goal of this thesis no further effort is done to improve the efficiency.

Just 73mW of the 146mW that is supplied to the PCB reaches the battery meaning that the remaining circuit reached a power transfer efficiency of 50.19%. There are three causes that can explain this rather disappointing result. First of all the constructed rectifier used diodes with a 400mV forward voltage drop. Since two diodes are in conduction at all times the combined voltage drop over the rectifier is 800mV. However, this can only explain a loss of 29.6mW.

A second contribution to the limited power transfer is found in the relative high value shunt resistor needed to sense the battery charge current. This 5 Ω resistor dissipates about 7mW. If we add the two losses together we still need to explain a difference of 36mW between the input power and combination of power absorbed by the battery and losses. The origin for this difference is found by reviewing the calculation of the input power.

By careful examination of the input we discovered that the measured voltage and current are not in phase with each other because the inductive link is not in resonance. The calculated power is not the real active power but instead the vector sum of both the active power and reactive power. Using the corrected input power we can show that 66.77% of the active input power reaches the battery. 26.99% is lost in the rectifier and 6.24% is lost in the shunt resistor. Just as expected the rectifier is thus limiting the power transfer efficiency.

Conclusion and Recommendations

In this final chapter the results and conclusion of the total project are summarized in the first section. In the second section we will evaluate if the project goals, that we set in the beginning, were achieved and what contribution was made in this project. In the final section we will give some recommendations for further research. These are not only possible improvements for the designed system but also some additional features that can be useful when the total stimulator system is to be designed.

8-1 Conclusion

Severe cases of Parkinson's Disease (PD), and various other neurological disorders, can be threatened by electrical stimulation of the Central Nervous System (CNS). An electrical pulse is supplied to specific targets inside the brain to modulate the activity of the neurons. Hereby the balance in neural activity of certain areas in the brain is restored and the symptoms are relieved. Although Deep Brain Stimulation (DBS) has proven to be an effective treatment, the used Implantable Pulse Generator (IPG) that generates the stimulation pulses is far from perfect.

Current IPGs need to be implanted in the chest due to their large volume and are connected to the electrode via an extension wire. The electrode and IPG are often placed during separate surgeries. Furthermore, the extension wire is an important source for device failure. In order to reduce the number of surgeries to the patient, the size of the device needs to be reduced so that it can completely fit in a human skull. We can then eliminate the need for an extension wire so that reliability is improved. It is important that the size reduction is achieved without compromising on the lifetime of the battery that powers the IPG.

The size of current devices is mostly determined by the size of the battery. We can reduce the volume of the battery, and thus of the total device, by switching from a non-rechargeable to a rechargeable battery. Although rechargeable batteries have lower energy densities, they can be recharged over and over again so that, over their total lifetime, they can provide more energy for the same size.

In circuit designs a battery is usually represented with a voltage source of a fixed value that represents the Electro Magnetic Force (EMF) of the battery. In reality the voltage is dependent on the State of Charge (SoC) of the battery. Furthermore a resistance that is also dependent on the SoC can be found in series with the voltage source. The internal resistance follows a U shaped curve meaning that it is high for SoC values below 20% and above 80% and low for the region in-between the 20% and 80%. Finally the dynamic behavior of a battery can be modeled by adding a capacitor in parallel with the output resistor.

To guarantee the lifetime of a Lithium Ion (Li-Ion) battery there are certain rules that need to be obeyed. First of all, a battery may never be charged above or discharged below certain voltage limits. Doing so results in permanent capacity loss and may even cause dangerous situations such as fire or explosion. Side reactions that deteriorate battery performances are more prominent at high temperatures and at high voltages. The Depth of Discharge (DoD) seems to have a more or less linear effect on the battery lifetime. If we would use only half the available battery capacity we can cycle the battery twice as often resulting in the same net energy processed by the battery. Taking this into account it is best to use the battery in the nominal region (between 20% and 80%) as much as possible and not push the battery to its limits. We hereby avoid operation at the extreme regions and keep the deterioration of the battery to a minimum.

Charging of the battery should be done with minimal interference of the daily routines of a patient. It is therefore desired that the charger is integrated with for example a headrest of a chair or a pillow. In this situation the IPG can be recharged automatically without any action from the patient. When this pillow based charge scenario is used, several hours are available to completely charge the battery. It is thus not necessary to use a fast charge algorithm.

Since the battery can only be replaced with a surgical procedure we do need an algorithm that can ensure long battery life. Furthermore the required circuit to implement the algorithm needs to be simple, small and low power so that it can be integrated on-chip together with the rest of the IPG. None of the investigated algorithms provided this simple control while keeping the non-linear behavior of the battery in mind. A potentially new algorithm is therefore proposed.

A novel charge algorithm that adapts the charge current to the changing impedance of the battery is proposed. When the battery is at low SoC and the impedance is high the charge current is low. While the battery is being charged and the impedance starts to decrease, the charge current can be increased. When the battery is approaching the end of charge voltage and the impedance starts to increase again, the charge current is reduced. Increasing and decreasing of the charge current follows the gradually changing impedance curve, hence we named this the smooth charging algorithm.

A Matlab/Simulink simulation of the proposed algorithm shows that we can reduce the overpotential of the battery, especially at the low SoC region, when we use the smooth charging algorithm. It also shows that, due to the reduced charge current, the time spent at the low SoC region and at the high SoC region is increased. The net energy loss in the battery due to the overpotential remains almost the same. Furthermore the total time to charge the battery is extended and a fairly complex circuit, with a high order polynomial transfer function, is required to implement the smooth charger. For this situation the classical Constant Current Constant Voltage (CCCV) charger remains the best available charge algorithm.

A special variation on the CCCV charger that combines the Constant Current (CC) and Constant Voltage (CV) phase into one single current-mode control loop is chosen for our implementation. The control loop has a hyperbolic tangent function that determines the appropriate charge current dependent on the battery voltage. Hereby safe battery charging with a simple and inherently stable circuit can be achieved.

The inductive coupling that provides the wireless energy transfer is reviewed. A series-series resonant link is selected since this topology can achieve better power transfer efficiencies than other topologies. The Series resonant output behaves like a current source so it fits the low-impedance load of a battery that is being charged better. With a series resonant input the used source can have a relative low voltage and the resonant capacitor value can be selected independent of the coupling factor and secondary side component values. If the resonant frequency is selected high enough the maximum link efficiency for this topology is only dependent on the load resistance and the secondary coil resistance.

The charge current is monitored and controlled to keep it at the desired value, even when the link properties change. When the current is above the desired value the link output is short-circuited for short periods to reduce the amount of current flowing through the battery. During the short circuit periods the excess energy is reflected back to the source instead of, what is usually the case, dissipated in a linear regulator. This improves the overall system efficiency.

Matlab/Simulink system simulations show that the inductive link does not achieve the theoretical maximum efficiency of 99.7%. Only a 64.7% average power transfer efficiency is reached due to the periods where the link is short circuited. During the short circuit period the output power is zero while there is still some input power that is dissipated in parasitic resistances of the antenna coils. The average power transfer efficiency is therefore lowered.

The charger circuit reaches an efficiency of 90.2% which is almost equal to previous reported values. The circuit does, however, include more functionality like AC to DC rectification. It is therefore expected that the total charger system exceeds the performance of existing implementations.

A Integrated Circuit (IC) design of the charger has been made for the AMS H18A4 technology. The antenna coils are not integrated and should be added off-chip. This is done so that the placement of the coils can be optimized for maximum coupling. Also the resonant capacitor should be added off-chip since it would require high voltage technology and a large chip area when integrated.

A rectifier that is partly constructed of MOS transistors and partly of Schottky diodes is used. The energy losses of the rectifier are hereby reduced compared with a full bridge diode rectifier. The two MOS transistors serve a double purpose and are also used for the current regulation switch. The diodes ensure that the battery is protected from discharging if there is no input power.

The control loop is implemented using sub threshold biased MOS transistors so that the circuit can also be implemented in IC technologies that do not offer bipolar devices. The designed circuit is simulated using the Cadence Virtuoso analog design environment. The results are in good correlation with the Matlab/Simulink simulations, although the absolute charger efficiency about 3% lower. Due to the finite switching time of the diodes and transistors, the

additional parasitic voltage drop and substrate injections the average power transfer efficiency of the charger is reduced to 87.36%.

To truly test the correct operation of the designed charger a prototype has been build using discrete and off the shelf components. The prototype was tested by wirelessly charging a 160mAh Li-Ion battery. Due to offset in the current sensing circuit the charge current was slightly below the designed value. This resulted in an increased charge time compared to the benchmark CCCV charge. Also the charge cycle was terminated premature due to the current sensor offset.

Premature ending of the charge cycle resulted that, compared to the benchmark, less energy was supplied to the battery. However, a larger portion of the supplied energy could be extracted by the discharge cycle. The high SoC region, where the impedance is higher, was avoided so that the battery efficiency was increased. The absolute energy that could be extracted was however still lower since the battery was not fully charged.

The constructed inductive link achieved a poor power transfer efficiency of only 22.97%. This is probably due to error in the measured coil inductance and mismatch in the selected capacitor values that cause the link to operate off resonance.

The Printed Circuit Board (PCB) transfers 66.77%, of the energy that is supplied to it, to the battery. 26.99% of the energy is lost in the rectifier since we used a full bridge diode rectifier for the prototype. The shunt resistor is responsible for the remaining 6.24% of energy loss. Just as we expected, the rectifier is the most important cause for the limited efficiency.

8-2 Project goals and contributions

To improve patient comfort and extend the lifetime of the IPG three main goals were introduced in the introduction of this thesis. The first goal was to prolong the battery life since the battery can only be replaced with surgery. This goal is achieved by selecting a charge algorithm that ensures that the battery is not overcharged. Also reducing the end of charge voltage can help in extending the cycle-life of the battery since side reactions that deteriorate the battery performance are more prominent at a high SoC.

The second goal was to make the total system energy efficient. This is important since the amount of available energy is limited due to regulations and medical safety concerns. It is thus desirable that most of the available energy can be used for charging and does not heat the surrounding tissue. This is first of all achieved by selecting a inductive link topology that is suitable for transferring energy to a low impedance load. Secondly the current regulation is done in a switched mode topology so that excess energy is not dissipated in a linear regulator but is reflected back to the source instead.

The third and final goal was to minimize the size of the charger system. Therefore we proposed an circuit design in the AMS H18A4 IC technology so it can be integrated on-chip with the rest of the IPG system. Since only medium voltage transistors and MOS devices are used it is expected that the charger can also be implemented in different technologies without too much design effort if that is required for other parts of the IPG.

Besides the proposed IC design we showed by means of a prototype that a flat spiral antenna coil with a diameter of 32mm is sufficient to power the charger. It is thus plausible that the charger can be constructed to fit in the small volume that is available in the human skull.

In summary, the following scientific contributions are made in this thesis:

- *A novel charge current control loop in a switched mode topology*
The separate control loop for CC and CV has been combined into one single hyperbolic tangent charge curve that controls the charge current in a switched mode topology. The stability problems between CC and CV switchover are hereby eliminated. The power efficiency compared to previously reported hyperbolic tangent chargers is improved by periodically short-circuiting the inductive link and reflecting excess energy back to the source.
- *Removed the need for additional regulators*
By dynamically controlling the duty cycle of the system, fluctuations in link properties can be compensated. There is thus no need for additional regulators that provide a stable output by dissipating excess energy.
- *Series-series topology inductive link should be used for charging*
The series-series resonant link is the best available inductive link for wireless battery charging systems. It has a current source like output that suits battery charging and has a power transfer efficiency that is only dependent on the load resistance and the secondary coil resistance.

8-3 Recommendations

Since the designed prototype charger is able to charge a Li-Ion battery up to a certain SoC we can consider the result quite successful. There are however several recommendations we can propose for future research. We subdivided the recommendations in four main topics, namely a) *additional features* that can be added to the system; b) *battery characteristics* that can be evaluated for an optimal system performance; c) *inductive link improvements* that can boost the link efficiency and finally d) *charger improvements* that increase the charge efficiency.

8-3-1 Additional features

- *Data communication* using the charge control switch.
The charger can communicate wireless to the outside world by controlling the charge control switch. In Figure 5-6 we showed that the power delivered by the external source decreases when the charge control switch is shorting the inductive link. Simple On-Off keying of the charge control switch could thus be used to transfer data to the external source. If this is used as a communication channel care must be taken that the average duty cycle is not changed since this may result in a charge current that is higher than the battery can handle.
- *Smart source* for optimal amplitude setting.
By detecting the duty cycle of the charger at the source side we can extract information about the desired charge current at that moment. If we provide the source with some additional control logic, making the source ‘smart’, we can automatically let the external source tune to the optimal amplitude. The transmitted energy now matches exactly with

the desired level so that the energy losses associated with the shorting of the link can be minimized.

8-3-2 Characteristics of the battery

- *Match Pulse-width Modulation (PWM) frequency* to the AC impedance of the battery. The 1KHz signal for the pulse width modulator has been selected arbitrary. Since a battery usually has an AC impedance that is changing over frequency it can be beneficial to select a different frequency where the battery impedance is lower. This can result in lower energy losses inside the battery.
- *Collaboration* with battery manufacturer to get accurate battery data. The battery manufacturer can help in providing detailed information about the battery such as the AC impedance. It may also be possible that the manufacturer has specified the end of charge voltage with a certain safety margin to prevent overcharging. If this is the case, reducing the end of charge voltage will not improve on the battery cycle life since operation at the extreme regions is already avoided. By collaborating with the manufacture a suitable end of charge voltage can be selected.

8-3-3 Inductive link improvements

- *Increase operation frequency* of the inductive link. We discovered from our simulations that the selected operating frequency of about 2MHz is too low to achieve an inductive link with maximum power transfer efficiency. Increasing the operating frequency may help in boosting the power transfer efficiency. We do have to redesign the two coils to prevent self-resonance. This can be done by for example adding a small gap in-between the windings so that the parasitic capacitance is reduced.
- *Side tap* in the resonant inductive link to power control circuit. Up till now the prototype needed to be supplied with power for the control circuit with an additional voltage source. When the system is implanted this voltage source is no longer available. It may be possible to tap the power needed for the control logic from the inductive link. The node that connects the resonance capacitor with the antenna coil may be used since the voltage swing at this node is fairly high. We do need to take care that the current drawn from this node is low, otherwise we are damping the resonance and deteriorate the power transfer.
- *Multi coil inductive link design* so that patients can move freely. For the developed prototype the two coils that form the inductive link were placed face to face to keep the alignment and power transfer stable. In reality, when the charger is implanted, it can be expected that the coils move around during charge and are no longer properly aligned. To guarantee that there is plenty energy available for charging the battery one may consider to use multiple coils at the transmitter side. The coils can be placed such so that at least one transmitter coil is optimally coupled to the charger at all times.

- *Litz wire* to reduce the skin effect of the coil windings.
The designed coils have a fairly large parasitic resistance compared to other coil designs that are, for example, described in [31]. Using a multi strand Litz wire for the secondary coil can help to reduce the skin effect so that the cross-sectional area of the used windings is used more effectively. We can hereby reduce the parasitic resistance of the secondary coil and, since the transfer efficiency is dependent on this resistor, boost the maximum link efficiency.
- *Check influence of tissue* on resonance frequency and coupling factor.
The designed inductive link was operated when it was surrounded by air only. The final design will have to be able to operate inside the human body. The RF power that is transmitted to the charger will thus have to penetrate at least the skin and probably a thin layer of fat and bone. How these materials influence the RF power needs to be considered since it is well known that, especially at higher frequencies, absorption of power by the skin and tissue plays a role.
- *Check regulation* for maximum RF power.
Linked with the influence of tissue on the RF power we need check if the designed system meets the regulations on medical safety and RF power. We need to take care that the skin and surrounding tissue is not heated too much by the transmitted RF power. Furthermore the maximum allowable field strength needs to be checked for the selected operating frequency.

8-3-4 Charger improvements

- *Use an instrumentation amplifier* for the charge current sensing circuit.
The current sensor used in the developed prototype suffered from offset errors. It is recommended to revise the used amplifier and use an instrumentation amplifier for the readout of the shunt resistor. These amplifiers have, in general, a very high input impedance. The input impedance of amplifier topology that is currently used relies on the value of the resistors in the feedback network. There may be some static leakage through the feedback network that discharges the battery that can be avoided when an instrumentation amplifier is used.
- *Integrate functions* with other parts of the IPG.
The proposed system is designed to operate completely independent of other functions that may be present in the total IPG. When the total IPG is designed it may be possible to combine certain functions and save power and chip area. For example the hyperbolic tangent control loop can be implemented in software using a lookup table if a microprocessor and memory are already required for different functions of the IPG.
- *Add trickle charge phase* for deeply discharged batteries.
Up till now we only designed and tested the charger for a battery voltage above the 3V. As explained in Section 2-6-1 deeply discharged batteries may be damaged and need to be recharged with special care. To be able to charge the IPG under any foreseeable condition a trickle charge phase may be required.

- *Zero current and zero voltage switching.*

The charge current control switch is now only controlled only by the PWM block. The PWM control signal and the input waveform are not synchronized. This means that the charge control switch can be closed or opened while it is conducting the full charge current or the full input voltage is across the switch. We know from switch mode power supply technology that the hard switching that is implemented now introduces high peak currents and causes additional switching losses. Synchronizing the PWM control signal with the input waveform so that the switch is only closed or opened at a zero crossing can reduce the switching loss and help to relax the peak current requirements for the switching devices.

Appendix A

Frequently used primary cells

This appendix describes the chemical reactions that take place during the discharge of 2 types of non-rechargeable (primary) lithium batteries. The goal of this appendix is to get a feeling of the typical values of battery voltage and capacity can be expected from batteries designed for medical implants. We will describe the Lithium-Manganese Dioxide batteries and the Lithium-Iodine batteries. We have selected these two types since both types of batteries are available from different manufacturers. Therefore we have different references to control the battery parameters.

In all batteries, an oxidation reaction at the anode (negative electrode) takes place that produces both electrons and ions. The electrons are collected at the negative electrode. If a load is connected these electrons can flow through the load to the cathode (positive electrode). At the cathode a reduction reaction takes place that consumes electrons and ions. To complete the electrical circuit the ions produced at the anode can flow through the electrolyte to the cathode.

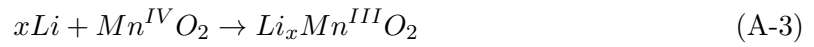
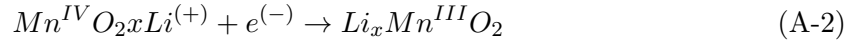
The total reaction is thus composed out of two half-reactions. One at the anode and one at the cathode. The reactions continue to take place until all material is consumed or until an equilibrium voltage is achieved. Each half-reaction has its own equilibrium potential. The difference between the two equilibrium potentials of the two half-reactions, is the equilibrium battery voltage. For both batteries discussed in this appendix we will show the two half-reactions and calculate the equilibrium potential.

A-1 Lithium-Manganese Dioxide (Li-MnO₂)

Lithium-Manganese Dioxide Li-MnO₂ is one of the first batteries that uses a solid cathode system and is today one of the most widely used primary batteries [55]. Examples of Lithium-Manganese based batteries that are medically used are the Litronik LiS3150M [30], the Litronik LiS3192R7 [56] and other cells manufactured by EaglePicher [14].

The anode of this type of battery is made out of Lithium. This Lithium is being oxidized to from a Lithium ion and a free electron via the reaction given in Equation A-1. The cathode is

contains a special heat-treated form of MnO_2 as the active material. The cathode reacts with the lithium ions and electrons according to Equation A-2. Combining the two half reactions results in the overall equation that is shown in Equation A-3.

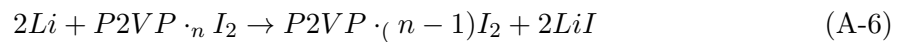


The equilibrium potential of the combined reaction is 3.5V. The open circuit voltage, however, is usually lower and typical about 3.3V for a new cell. This is due to a predischARGE that is usually performed to stabilize the cell. By lowering the open circuit voltage side reactions such as corrosion are reduced resulting in a longer shelf life.

A-2 Lithium-Iodine (Li-I2)

batteries based on Lithium-Iodine in general have a low self-discharge, high reliability and do not generate gas during discharge. This makes them very attractive for medical application however the internal resistance is quite high making them only usable for low power devices.

The Iodine is made conductive by the addition of an organic material. We consider the case where a polymer called poly-2-vinylpyridine (P2VP) is used for this purpose. At the anode the regular oxidation of lithium takes place according to Equation A-4. Both Iodine and the P2VP polymer are involved with the reduction reaction at the cathode that is shown in Equation A-5. The overall reaction follows Equation A-6. $Li-I_2$ Li-(Poly-2-vinyl pyridine)In



The equilibrium cell potential is near the 2.8V and stays nearly the same over the service life of the cell. The discharge curve is not as flat as may be expected but shows a gradual decaying voltage over a discharge. This is caused by the relative high internal impedance that increases when the battery is discharged.

Type	Open circuit voltage	Nominal voltage	Wh/l	discharge rate
Li-MnO ₂	3.3	3.2	710 - 960	High
Li-I ₂	2.8	2.8	890 - 950	Low

Table A-1: Data of primary lithium cells

A-3 Comparison

In Table A-1 the different properties of the two cells are summarized. The lithium manganese battery has a higher working voltage and can handle higher discharge current than the lithium iodine type. On the other hand the lithium iodine has a long service life and a fairly stable working voltage as long as the discharge current is low.

We can conclude that each device requires a specific battery. If, for example, high (pulse) currents are required a lithium manganese battery may be the optimal choice. For a device that requires only a small amount of power but has to remain operating for many years a lithium iodine battery might be the best choice. The optimum battery for the specific application might be even a different type, for example a lithium/carbon monofluoride, that is not taken into account in this appendix.

Appendix B

Frequently used secondary cells

Secondary or rechargeable Lithium batteries basically operate in a similar manner as their non-rechargeable counterparts. Both are composed of an anode, a cathode and an electrolyte in between. The difference is that the chemical reactions occurring in a rechargeable battery can be reversed by simply reversing the flow of electrons with an external power source. When the flow of electrons is reversed, also the movement of ions is reversed. Since lithium ions can move back and forth between the electrodes, rechargeable batteries are sometimes referred to as rocking-chair batteries.

Lithium batteries basically outperform any other rechargeable battery on any criteria. They offer high voltages, high energy densities and high power capabilities. Furthermore, they do not suffer from memory effect, do not require maintenance, operate in a broad temperature range and can be cycled for many times.

A disadvantage of lithium batteries is the capacity loss or even fire and explosions when overcharged. Discharging a battery too deeply also results in permanent damage. These problems can be solved by adding protection circuits that guarantee proper use of the battery. Today, lithium batteries are used in many applications and dominate the market. That is why this thesis focuses on lithium batteries alone.

The exact composition of rechargeable lithium batteries that are suitable for medical applications was not specified in the data sheets that we had available. Therefore, we will only discuss a lithium cobalt oxide battery, which is one of the rechargeable batteries most used today. We will show the two half-reactions that occur inside the battery while in use and compare the performance with the non-rechargeable batteries discussed in Appendix A.

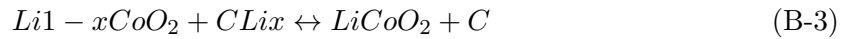
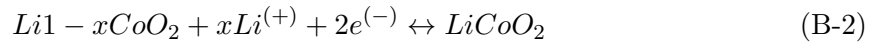
B-1 Lithium cobalt oxide (Li-CoO₂)

Besides lithium and cobalt oxide, carbon is also present in the Li-CoO₂ battery. A carbon material is used for the anode since an anode composed of lithium metal results in unsafe batteries that suffer from thermal runaway, fire and often explosions [16].

Maximum Voltage	Nominal voltage	Wh/l	number of cycles
4.2	3.7	560	1200

Table B-1: Data of secondary lithium cobalt oxide cell

The chemical reaction taking place at the anode is given by Equation B-1. During discharge the reaction takes place from left to right. During charge the direction is reversed and takes place from right to left. At the positive electrode, or cathode, the cobalt oxide reacts with lithium according to Equations B-2. Again, during discharge the equation is followed from left to right and during charge from right to left. The overall battery reaction follows Equation B-3 with again the same arrow conventions for the charge and discharge directions.



B-2 Comparison

In Table B-1 the typical characteristics of the Lithium cobalt oxide battery are listed. Although the nominal battery voltage is higher than the voltage of the non-rechargeable batteries discussed in Appendix A, the energy density is far lower. When a non-rechargeable and rechargeable battery of the same volumes are discharged with the same current the non rechargeable battery will be able to supply the current far longer. After deletion the secondary cell can be recharged many times while the primary cell will have to be replaced and discarded.

We can conclude that secondary batteries can provide more energy per volume than a primary battery if we consider the total lifetime. For small power hungry devices rechargeable batteries are thus preferred over non rechargeable. The battery can be recharged many times without consuming too much volume or weight.

Extreme low power devices that for example are usually switched off or in standby, should still use primary cells since the self-discharge of secondary batteries is usually higher. This would mean that regular recharging would be necessary even though the device has not used any power. In these situations a primary cell that is always ready for use may be beneficial.

Bibliography

- [1] B. Ford, *Deep Brain Stimulation for Parkinson's Disease*. Parkinson's Disease Foundation, 3th ed., 2008. [Online; <http://www.pdf.org/pdf/DBS2008.pdf> accessed 3-July-2012].
- [2] R. S. Shah, S. Y. Chang, H. K. Min, Z. H. Cho, C. D. Blaha, and K. H. Lee, "Deep brain stimulation: technology at the cutting edge," *J Clin Neurol*, vol. 6, pp. 167 – 182, Dec 2010.
- [3] N. Lipsman, M. Ellis, and A. M. Lozano, "Current and future indications for deep brain stimulation in pediatric populations," *Neurosurg Focus*, vol. 29, p. E2, Aug 2010.
- [4] ANS, *Eon - handleiding voor de arts*. Advanced Neuromodulation Systems, INC, 2005. Manual of ANS Eon Neuromodulation System.
- [5] M. F. Bear, B. W. Connors, and M. A. Paradiso, *Neuroscience, Exploring the Brain*. Lippincott Williams & Wilkins, 2007.
- [6] S. Patel, C. Mancinelli, R. Hughes, A. Dalton, L. Shih, and P. Bonato, "Optimizing deep brain stimulation settings using wearable sensing technology," in *Neural Engineering, 2009. NER '09. 4th International IEEE/EMBS Conference on*, pp. 6 – 9, May 2009.
- [7] S. A. Factor and W. J. Weiner, *Parkinson's Disease, Diagnosis and Clinical Management*. Demos Medical Publishing, 2008.
- [8] B. van den Berg, "De ziekte van parkinson en parkinsonisme in nederland - een schatting van de prevalentie en incidentie op basis van data uit het dbc informatie systeem," 2010. [Online; www.parkinson-vereniging.nl accessed 9-August-2012].
- [9] R. Pahwa and K. E. Lyons, eds., *Handbook of Parkinson's Disease*. infroma healthcare, 4th ed., 2007.
- [10] A. M. Lozano, P. L. Gildenberg, and R. R. Tasker, eds., *Textbook of Stereotactic and Functional Neurosurgery*. Springer, 2009.

- [11] Medtronic inc., *Activa PC Multi-program neurostimulator - implant manual*, 2008.
- [12] Medtronic inc., *Activa RC Multi-program rechargeable neurostimulator - implant manual*, 2008.
- [13] A. M. Harries, S. Major, M. Sandhu, and C. R. Honey, “Rechargeable internal neural stimulators – is there a problem with efficacy?,” *Neuromodulation: Technology at the Neural Interface*, 2011.
- [14] Eaglepicher, *Product And Service Catalog*, 2010. [Online; <http://www.eaglepicher.com/images/stories/EaglePicher%20Medical%20Brochure%202010.pdf> accessed 3-July-2012].
- [15] E. Gatti, “Alessandro volta’s profile,” in *Power Electronics Specialists Conference, 1996. PESC '96 Record., 27th Annual IEEE*, vol. 1, pp. 3 – 6 vol.1, jun 1996.
- [16] K. Matsuki and K. Ozawa, “General concepts,” in *Lithium Ion Rechargeable Batteries* (K. Ozawa, ed.), WILEY-VCH Verlag GmbH & Co, 2009.
- [17] Wikipedia, “Alessandro volta — wikipedia, the free encyclopedia,” 2011. [Online; en.wikipedia.org accessed 23-June-2011].
- [18] D. Linden, “Basic concepts,” in *Handbook of Batteries* (D. Linden and T. B. Reddy, eds.), McGraw-Hill Companies, Inc., 2002.
- [19] W. van Schalkwijk and B. Scrosati, “Introduction,” in *Advances in Lithium-Ion Batteries* (W. van Schalkwijk and B. Scrosati, eds.), Springer US, 2002.
- [20] T. B. Reddy and S. Hossain, “Rechargeable lithium batteries (ambient temperature),” in *Handbook of Batteries* (F. Toolenaar and T. B. Reddy, eds.), McGraw-Hill Companies, Inc., 2002.
- [21] L. Gao, S. Liu, and R. A. Dougal, “Dynamic lithium-ion battery model for system simulation,” *Components and Packaging Technologies, IEEE Transactions on*, vol. 25, pp. 495 – 505, sep 2002.
- [22] J. Vetter, P. Novák, M. R. Wagner, C. Veit, K. C. Möller, J. O. Besenhard, M. Winter, M. Wohlfahrt-Mehrens, C. Vogler, and A. Hammouche, “Ageing mechanisms in lithium-ion batteries,” *Journal of Power Sources*, vol. 147, no. 1 – 2, pp. 269 – 281, 2005.
- [23] L. W. Yao and J. A. Aziz, “Modeling of lithium ion battery with nonlinear transfer resistance,” in *Applied Power Electronics Colloquium (IAPEC), 2011 IEEE*, pp. 104 – 109, april 2011.
- [24] S. F. Bender, J. W. Cretzmeyer, and T. F. Reise, “Zinc/Air Batteries-Button Configuration,” in *Handbook of Batteries* (D. Linden and T. B. Reddy, eds.), McGraw-Hill Companies, Inc., 2002.
- [25] P. Arora, R. E. White, and M. Doyle, “Capacity fade mechanisms and side reactions in lithium-ion batteries,” *Journal of The Electrochemical Society*, vol. 145, no. 10, pp. 3647 – 3667, 1998.

-
- [26] M. Broussely, P. Biensan, F. Bonhomme, P. Blanchard, S. Herreyre, K. Nechev, and R. Staniewicz, "Main aging mechanisms in li ion batteries," *Journal of Power Sources*, vol. 146, no. 1 – 2, pp. 90 – 96, 2005.
- [27] H. Maleki and J. N. Howard, "Effects of overdischarge on performance and thermal stability of a li-ion cell," *Journal of Power Sources*, vol. 160, no. 2, pp. 1395 – 1402, 2006.
- [28] M. Broussely, "Aging mechanisms and calendar-life predictions in lithium-ion batteries," in *Advances in Lithium-Ion Batteries* (W. van Schalkwijk and B. Scrosati, eds.), Springer US, 2002.
- [29] M. N. van Dongen, "A versatile output stage for implantable neural stimulators," Master's thesis, TU-Delft faculty of Electrical Engineering, Mathematics and Computer Science, 2009.
- [30] Litronik an MST company, *LiS 3150 M LITRONIK Li-Manganese Dioxide Medium Rate Battery*, 2010.
- [31] N. S. Artan, H. Vanjani, G. Vashist, Z. Fu, S. Bhakthavatsala, N. Ludvig, G. Medveczky, and H. J. Chao, "A high-performance transcutaneous battery charger for medical implants," in *Engineering in Medicine and Biology Society (EMBC), 2010 Annual International Conference of the IEEE*, pp. 1581 – 1584, 31 2010-sept. 4 2010.
- [32] C. Lin, H. Huang, and K. Chen, "Built-in resistance compensation (BRC) technique for fast charging li-ion battery charger," in *Custom Integrated Circuits Conference, 2008. CICC 2008. IEEE*, pp. 33 – 36, sept. 2008.
- [33] Y. Sun, X. Wu, and M. Zhao, "Li-ion battery charger with smooth-switch-over four-stage control," in *Integrated Circuits, ISIC '09. Proceedings of the 2009 12th International Symposium on*, pp. 49 – 52, dec. 2009.
- [34] Y. H. Liu, C. H. Hsieh, and Y. F. Luo, "Search for an optimal five-step charging pattern for li-ion batteries using consecutive orthogonal arrays," *Energy Conversion, IEEE Transactions on*, vol. 26, pp. 654 – 661, june 2011.
- [35] Dallas semiconductor Maxim, "Engineering journal volume forty-six," 2003. [Online; <http://pdfserv.maxim-ic.com/en/ej/EJ46.pdf> accessed 6-July-2011].
- [36] S. Eaves and D. Shaffer, "Lithium-ion batteries for telecom applications," in *Telecommunications Energy Conference, 2007. INTELEC 2007. 29th International*, pp. 708 – 712, 30 2007-oct. 4 2007.
- [37] W. A. van Schalkwijk, "Charging, monitoring, and control," in *Advances in Lithium-Ion Batteries* (W. van Schalkwijk and B. Scrosati, eds.), Springer US, 2002.
- [38] V. Sukumar, M. Alahmad, K. Buck, H. Hess, H. Li, D. Cox, F. N. Zghoul, M. Mojaradi, W. C. West, and J. F. Whitacre, "Nano current charging algorithms for thin film lithium microbatteries," in *11th NASA Symposium On The VLSI Design, Coeur d'Alene, Idaho*, pp. 258 – 29, May 2003.

- [39] P. H. L. Notten, J. H. G. Op het Veld, and J. R. G. van Beek, "Boostcharging li-ion batteries: A challenging new charging concept," *Journal of Power Sources*, vol. 145, pp. 89 – 94, 2005.
- [40] V. Pop, H. Bergveld, D. Danilov, P. P. L. Regtien, and P. H. L. Notten, "Methods for measuring and modelling a battery's overpotential," in *Battery Management Systems, Accurate State-of-Charge Indication for Battery-Powered Applications* (V. Pop, H. Bergveld, D. Danilov, P. P. L. Regtien, and P. H. L. Notten, eds.), Springer Science+Business Media B.V., 2008.
- [41] B. Do Valle, C. T. Wentz, and R. Sarpeshkar, "An area and power-efficient analog li-ion battery charger circuit," *Biomedical Circuits and Systems, IEEE Transactions on*, vol. 5, pp. 131 – 137, april 2011.
- [42] M. Chen and G. A. Rincon-Mora, "Accurate, compact, and power-efficient li-ion battery charger circuit," *Circuits and Systems II: Express Briefs, IEEE Transactions on*, vol. 53, pp. 1180 – 1184, nov. 2006.
- [43] S. Chopra, "Contactless power transfer for electric vehicle charging application," Master's thesis, TU-Delft faculty of Electrical Engineering, Mathematics and Computer Science, 2011.
- [44] K. van Schuylenbergh and R. Puers, *Inductive Powering, Basic Theory and Application to Biomedical Systems*. Springer Science + Business Media B.V, 2009.
- [45] P. Li and R. Bashirullah, "A wireless power interface for rechargeable battery operated medical implants," *Circuits and Systems II: Express Briefs, IEEE Transactions on*, vol. 54, pp. 912 – 916, oct. 2007.
- [46] S. Dearborn, "Charging Li-ion Batteries for Maximum Run Times," *Power Electronics Technology*, pp. 40 – 49, Apr 2005.
- [47] N. S. Artan, H. Vanjani, G. Vashist, Z. Fu, S. Bhakthavatsala, N. Ludvig, G. Medveczky, and H. Chao, "A high-performance transcutaneous battery charger for medical implants," in *Engineering in Medicine and Biology Society (EMBC), 2010 Annual International Conference of the IEEE*, pp. 1581 – 1584, 31 2010-sept. 4 2010.
- [48] A. Ghahary and B. H. Cho, "Design of a transcutaneous energy transmission system using a series resonant converter," in *Power Electronics Specialists Conference, 1990. PESC '90 Record., 21st Annual IEEE*, pp. 1 – 8, 0-0 1990.
- [49] B. Gilbert, "The multi-tanh principle: a tutorial overview," *Solid-State Circuits, IEEE Journal of*, vol. 33, pp. 2 – 17, jan 1998.
- [50] R. Sarpeshkar, *Ultra Low Power Bioelectronics - Fundamentals, Biomedical Applications, and Bio-Inspired Systems*. Cambridge University Press, 2010.
- [51] S. Ziegler, R. C. Woodward, H. H. C. Iu, and L. J. Borle, "Current sensing techniques: A review," *Sensors Journal, IEEE*, vol. 9, pp. 354 – 376, april 2009.
- [52] H. Lavric and R. Fiser, "Lossless current sensing technique on mosfet rds(on) with improved accuracy," *Electronics Letters*, vol. 46, pp. 370 – 371, 4 2010.

- [53] Greatbatch Medical, *Xcellion Rechargeable Batteries*, 2009. [Online; <http://www.greatbatchmedical.com/assets/products/Xcellion%20Rechargeable%20Batteries.pdf> accessed 19-Nov-2012].
- [54] BAK, *Specification of Li-polymer Rechargeable Battery, Model No.: LP-402025-1S-3*, 2012. [Online; <http://www.farnell.com/datasheets/1666646.pdf> accessed 28-Nov-2012].
- [55] D. Linden and T. B. Reddy, "Lithium batteries," in *Handbook of Batteries* (D. Linden and T. B. Reddy, eds.), McGraw-Hill Companies, Inc., 2002.
- [56] Litronik an MST company, *LiS 3192 R7 LITRONIK Li-Manganese Dioxide High Power Battery*, 2010.

Glossary

List of Acronyms

Ah	Ampere Hour
BJT	Bipolar Junction Transistor
BRC	Build-in Resistance Compensated
CC	Constant Current
CCCV	Constant Current Constant Voltage
CNS	Central Nervous System
CV	Constant Voltage
DBS	Deep Brain Stimulation
DoD	Depth of Discharge
EMF	Electro Magnetic Force
IC	Integrated Circuit
IPG	Implantable Pulse Generator
Li-Ion	Lithium Ion
PCB	Printed Circuit Board
PD	Parkinson's Disease
PWM	Pulse-width Modulation
SEI	Solid Electrolyte Interphase
SoC	State of Charge
SoH	State of Health
UPDRS	Unified Parkinson's Disease Rating Scale

List of Symbols

κ	capacitive divider ratio
V_t	thermal voltage
A	ampere
C	capacity unit
k	Boltzmann constant
q	Elementary charge
T	absolute temperature
V	volt

Index

	A		Current regulation switch.....60	
Ah	7		Cycle life.....9	
	B		D	
Battery		DoD.....9		
aging effects	14		E	
model	12		Efficiency	
non rechargeable	10		Cadence simulations.....67	
rechargeable	11		measurements.....82	
	C		Simulink simulations.....51	
C rate.....8			I	
Cells			Inductive link	
primary	10		design	58
secondary	11		selection.....46	
cells			P	
primary			Parkinson.....1	
Li-I ₂	102		R	
Li-MnO ₂	101		Rectifier.....60	
secondary	105		S	
Li-CoO ₂	105		Shelf life.....9	
Charging			SoC.....8	
algorithm selection	33		SoH.....9	
boost.....	29		System overview.....45	
burp.....	29		U	
CCCV.....	23		Use scenario	
float.....	27		charge.....21	
multi-stage	25		discharge.....19	
pulse.....	28			
relaxation	29			
Smooth Charging.....	34			
Control loop				
design	62			
transfer function.....	50			